A landscape approach to forecasting climate change impacts on geographic ranges and phenologies of plants in the Washington Cascades

Ian K. Breckheimer

A dissertation
submitted in partial fulfillment of the
requirements for the degree of

Doctor of Philosophy

University of Washington

2017

Reading Committee:

Janneke Hille Ris Lambers, Chair

Abigail Swann

Benjamin Kerr

Program Authorized to Offer Degree:
Biology

University of Washington

Abstract

A landscape approach to forecasting climate change impacts on
geographic ranges and phenologies of plants in the Washington Cascades

Ian K. Breckheimer

Chair of the Supervisory Committee:
Professor Janneke Hille Ris Lambers
Department of Biology

As the pace of environmental change accelerates, biologists are transforming the discipline of ecology from a fundamentally descriptive science to one that can be used to generate skillful forecasts. Although important progress is being made, this work is stymied by (1) our limited understanding of the physical and biological processes involved, (2) our limited knowledge of how those processes vary across space, and (3) our ignorance of the feedbacks between ecological change and human society. In this work, we aim to contribute new process understanding, conceptual frameworks, and quantitative tools that help to alleviate these three limitations and advance our ability to forecast the impacts of climate change on plants in the Cascade Range (Washington, USA), where rapidly changing climate and hydrology pose unique risks to features of ecosystems that are economically and culturally important. Chapter one concerns the fundamental ecological processes that maintain the geographic range limits of plants, focusing on the role of climate and disturbance in setting contemporary range limits and mediating the response of those ranges to a warmer climate. As a study system, we used two species of yellow monkeyflower (*Erythranthe* spp.) that have similar habitat requirements, but strikingly different elevation ranges in Mt. Rainier National Park. We combined data from a large-scale transplant experiment and a multi-year observational study using a spatial population model. We found that the ranges of these two

closely related and ecological similar species responded very differently to changes in climate, and we forecast that ranges will shift downhill for one species under some scenarios. This work illustrates the importance of accounting for landscape-scale processes in generating skillful forecasts of species range shifts. Chapter two focuses on forecasting how climate change will affect the landscape patterns of reproductive synchrony (landscape flowering phenology) in plants across networks of habitat patches. In this work, we use previously estimated relationships between climate and flowering time, as well as spatially extensive datasets on species distributions and microclimates, to predict spatial patterns of landscape phenology across Mt. Rainier throughout the growing seasons of 2009 - 2015. We found that unusually early snow melt in low elevation meadows in 2015 caused many species to bloom out of sync across their elevation ranges, decreasing the potential for pollen dispersal between meadows. Because 2015 conditions were similar to those expected by the late 21st century under unabated climate change (early low-elevation snow melt, warm spring temperatures), this raises the possibility that climate change could be an agent of population fragmentation in this system. Finally, chapter three considers how warming climates affect the relationships between ecosystems and their social and management context. Specifically, we use thousands of geolocated photos uploaded to the social media platform Flickr to track interactions between recreational visitors and the plant phenology of subalpine and alpine ecosystems in the Washington Cascades, where spectacular wildflower displays draw millions of visitors each year, and generate tens of millions of dollars of economic activity. We found that the timing of recreational visits to subalpine ecosystems at Mt. Rainier National Park was substantially less sensitive to variation in climate than the timing of wildflower displays. This led to pronounced mismatches between visitor and wildflower activity in the climate-change analog conditions experienced in 2015 at our sites. Overall, this work illustrates how a landscape approach can help to overcome the challenges associated with forecasting ecological responses to environmental change.

TABLE OF CONTENTS

LIST OF FIGURES

LIST OF TABLES

ACKNOWLEDGMENTS

This work, and indeed any research project large enough to shake a stick at, is the product of a multitude of people and institutions. I am tremendously fortunate to have benefited from enthusiastic field assistants and volunteers, including C. Fagan, J. Lucas, C. Jenkins, D. Jenkins, R. Theobald, S. Theobald, J. Woltzen, M. Piper, C. Ray, A. O'Brien, D. Chen, K. Kurfurst, J. Marcus, N. Lozanoff, L. Fitzgerald, K. Burns, J. Levy, J. Laudenberger, E. Loggers, C. Chen, C. Budd, K. Olsen, H. Weisener, G. Siegmund, L. Felker, D. Lyons, H. Bessoh, L. Sebastian, A. Hampton, C. Fagan, A. Wall, T. Ota, S. Martine-Blangy, A. Kinne, T. Rautu, E. Pletcher, T. O'Mara, C. Kim, M. Kovenoch, W. Cosgswell, and L. Vachon, as well as the more than 100 volunteers who contributed to our MeadoWatch citizen science program. Past and present members of the Hille Ris Lambers lab provided critical data, advice, and logistical support, especially A. Ettinger, K. Ford, E. Theobald, C. Chang, S. Kroiss, M. Harsch, and M. L. Sethi. Numerous collaborators provided data, computational tools, and valuable critical feedback, including J. Lundquist, N. Cristea, M. Raleigh, R. Rochefort, E. Lia, and T. Rautu. I am deeply indebted to the dedicated staff of the National Park Service, including L. Whiteaker, B. Samora, J. Drown, A. Peterson, T. Chestnut, B. Wright, K. Bacher, and J. Drown. Institutional support at the University of Washington was provided by M. Heringer, D. Ewing, J. Milne, and N. Kurashige. I received invaluable outside feedback on portions of this work from M. Velland, B. Miller, A. Angert, and several anonymous reviewers. I have been extremely fortunate to have the support of an a stellar advisory committee including. H. D. Bradshaw, L. Buckley, A. Swann, B. Kerr, and L. Hauser. My advisor J. Hille Ris Lambers was critical to the success of these projects, and provided sage mentorship throughout my PhD program. This work was financially supported by nu-

merous sources, including a Northwest Climate Science Center fellowship and NSF Doctoral Dissertation Improvement Grant to I. Breckheimer (NSFDGE-1600605). I. Breckheimer also received funds from the Biology Department at the University of Washington including the Giles and Experimental Field Ecology Awards. This work was partially supported by a NASA Biodiversity and Ecosystem Functioning award (NASA NNX14AC34G), and an NSF Career grant (NSF DEB-1054012) to J. Hille Ris Lambers. Collection of additional data used in this work was supported by the Mazamas, the American Alpine Club, and the National Science Foundation (NSFDGE-1256082).

DEDICATION

To R.T. Paine, who showed me the power of experiments, and to my dear wife, Lizza, who reminds me of the power of poetry.

Chapter 1

CLIMATE CHANGE AND DISTURBANCE INTERACT TO CAUSE DOWNHILL RANGE SHIFTS

1.1 Abstract

Long-term studies which measure changes in species distributions with climate change have revealed a surprising diversity of responses. Although a majority of species distributions have tracked climates which are shifting upslope and higher in latitude, the ranges of many species have failed to closely track climate, and range limits of some species have moved downhill or south, counter to the expected direction. The dominant factors driving these counter-gradient range shifts are unclear, but many have suggested that they reflect the imprint of ecological interactions, novel physiological responses, or past biogeographical events in defining contemporary range limits. Here we suggest that climate's influence on disturbance regimes and metapopulation dynamics —broad scale patterns of colonization and persistence across networks of habitat patches —play an under appreciated role in determining the response of species ranges to climate change, and may explain some of the diversity of climate-driven range shifts observed in nature. To make this case, we marshal evidence from a field study of two ecologically similar riparian plant species (common yellow monkeyflower, *Erythranthe guttata*, and mountain monkeyflower, *E. caespitosa*) in Mt. Rainier National Park, WA, USA. We combined detailed demographic data collected from individuals growing in experimental populations across the range limits of both species with four years of comprehensive census data from wild populations. We then used these data to parameterize a spatial population model that incorporates the effects of climate and other habitat attributes on local demographic performance, as well as on colonization and local extinction

processes. Simulating range dynamics at Mt. Rainier under a variety of climate change and disturbance scenarios, we found that both the magnitude and direction of predicted elevation range shifts differed dramatically between species and were extremely sensitive to changes in the disturbance regime. Increases in flood disturbance, predicted in the region by the late 21st century, caused the upper range limit of *E. guttata*, the low-elevation species, to move up in elevation twice as far as in a scenario assuming no change to the disturbance regime. Under current levels of flood disturbance, or if disturbance becomes less frequent, models projected downhill shifts in the low-elevation limit of *E. caespitosa* in scenarios assuming considerable warming. Overall, simulated range shifts were considerably more sensitive to climate impacts on colonization and disturbance processes than impacts on local demography for both species, indicating that neglecting these important processes might lead to misleading predictions about range shifts in response to changes in climate. Our results highlight the importance of interactions between climate, local demography, disturbance, and colonization processes in determining the response of species ranges to environmental change. We suspect that these interactions are important in many systems where populations are patchy near range limits, and that understanding their role will bolster efforts to forecast the impacts of climate change on species distributions.

1.2 Introduction

Climate plays a fundamental role in setting the limits of species geographic ranges, and anthropogenic climate change has caused many species to shift their ranges to track warming climates over the last century. This has resulted in pronounced northerly and uphill shifts to range limits (pro-gradient range shifts) across taxa as diverse as mammals [125], insects [116], and pelagic fish[135], a clear biological fingerprint of accelerating climate change[31]. However, broad-scale patterns of range-shifts also include a surprising amount of species-level variation, with a large proportion of species shifting their limits downhill or towards more southerly latitudes, which is usually counter to the movement direction of temperature isotherms[107, 31]). These shifts are important because they demonstrate how biolog-

ical complexity confounds our ability to forecast how climate change influences extinction risks[171], as well as the future potential distributions of important taxa like timber trees[35], agricultural crops[134], and pathogens[13]. Counter-gradient range shifts are especially common in plants, with several recent studies demonstrating counter-gradient shifts in the ranges of temperate trees[63], and even some regional floras[40, 80].

Despite their critical importance and significant research effort over the past two decades, the ecological drivers of these counter-gradient range shifts are still unclear. Several authors have suggested that the ranges of plants respond more directly to shifts in aridity than to temperature[63], a view bolstered by ecophysiologial studies[5]. Others have suggested that counter-gradient range shifts could reflect transient effects of past species distributions, as species invade suitable habitats where they were previously excluded by biogeographic barriers or human land-use[75]. Species interactions could also be important drivers of some counter-gradient range shifts, particularly at low-latitude and low-elevation limits[109]. Finally, some plants face demographic lags and dispersal limitations that could prevent them from tracking suitable climates[52], issues that are especially critical for long-lived organisms such as trees [50].

Many of these explanations rest on the fundamental assumption that climate change will always cause pro-gradient range shifts if climate directly reduces population performance towards range limits. As suitable climates shift uphill and up in latitude, population growth rates increase at the leading edge of species distributions and decline at the trailing edge, causing distributions to track climate[49] (Fig. 1.1A). Counter-gradient shifts, then, would require some other set of processes (e.g. novel ecological interactions), to overwhelm the direct effects of climate on demographic performance at range limits. However, it is also possible that complex interactions between climate and disturbance that influence colonization and extinction dynamics of metapopulations could also be responsible for creating stable geographic range limits along climatic gradients, even if apparent local-scale population growth rates do not decline towards range limits[88, 6, 70]. We argue that these dynamics might also be responsible for counter-gradient range shifts. For example, if climate change increases

local population growth rates at range limits, but also decreases population persistence by increasing rates of population-replacing disturbance (Fig. 1.1E), then the overall pattern of habitat occupancy that defines that limit could shift in a pro-gradient or counter-gradient direction with warming, depending on the interactive effects of these metapopulation processes and local population growth rates (Fig. 1.1F).

Could these interactions between climate, local demographic performance, and metapopulation dynamics be responsible for some of the counter-gradient range shifts observed over the past century? Detailed, simultaneous examinations of local demographic performance and metapopulation dynamics across range limits are rare in the literature, but recent syntheses[79, 106] provide some tantalizing clues that these complex dynamics might be widespread. Pironon et al.[136], for example, recently found that patterns of habitat occupancy, the proportion of suitable habitat where a species is present, declines much more reliably along environmental gradients towards range limits than local abundance or demographic performance in occupied habitat patches. This suggests that factors affecting colonization or population persistence might play a role in reducing occupancy at range limits. Further, a synthesis of experimental studies of local population growth rates indicated that, for plants, nearly 25% of studies showed increases in local demographic performance at or beyond climatic range limits[106]. Although suggestive, this evidence is indirect. Rather than revealing the role of colonization and disturbance, a lack of decline in local population performance towards range limits, for example, might instead be indicative of dispersal limitations or transient range limits set by past biogeographic events[155].

In this study, we provide the first detailed examination of how climate's effects on local demography and disturbance interact to produce stable range boundaries across climatic gradients, as well as the potential for complex range-shift dynamics under climate change scenarios, including counter-gradient range shifts. We focus on the elevation range boundaries of two closely-related perennial plants (yellow monkeyflowers, *Erythranthe spp.*) with similar fine-scale habitat requirements but dramatically different elevation ranges. Our work combines detailed data on patch-scale demography of these two species from a transplant

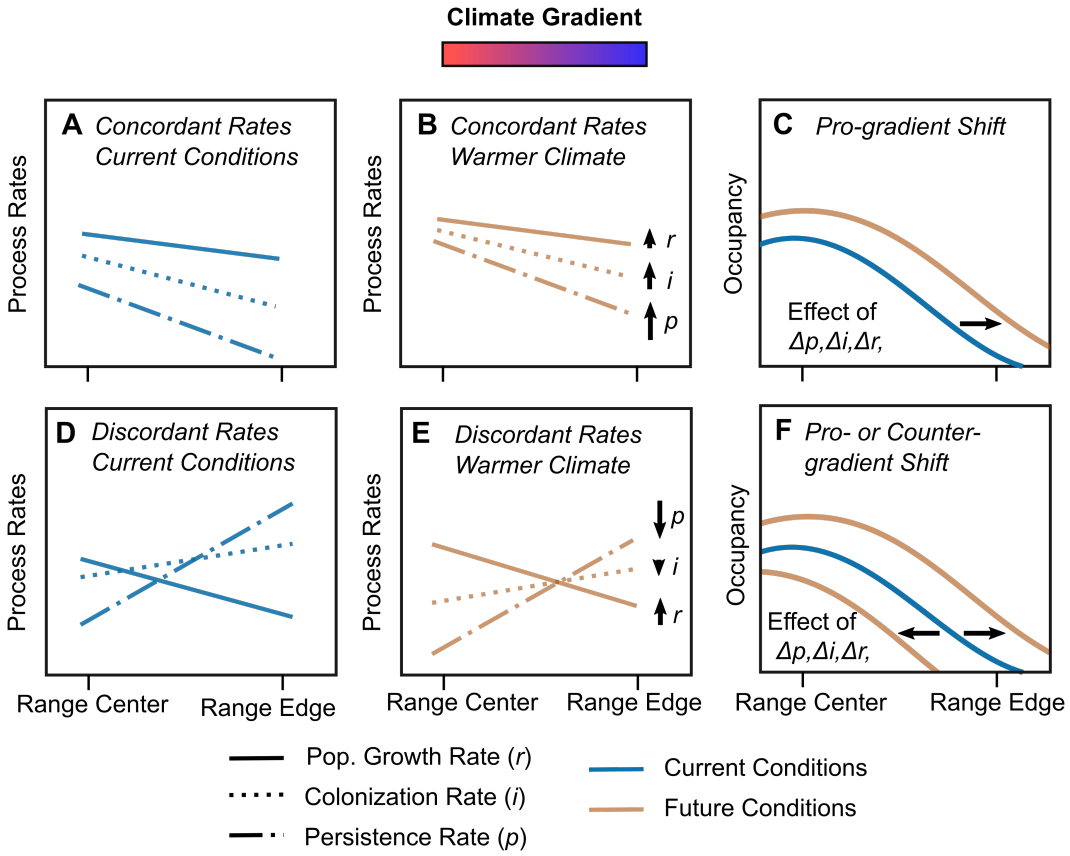

Figure 1.1: Metapopulation dynamics can cause pro-gradient (uphill, higher-latitude) or counter-gradient (downhill, lower-latitude) range shifts under climate change depending on the interactive effects of climate on different processes at range limits. If local population growth (r, solid lines), patch-scale persistence (p, dot-dashed lines), and colonization rates (i, dotted lines), all decline along a climatic gradient from range centers to range edges ("concordant rates", **A**), then these rates will increase under climate change (**B**), and range limits will expand as climates become more suitable at current range edges (**C**). In contrast, if some of these rates increase towards range limits ("discordant rates", **D**) then the rates of some processes will decline under climate change (**E**). This could drive either along-gradient or counter-gradient range shifts (**F**), depending on the interactive effects of climate on local demography and metapopulation processes.

experiment with extensive surveys of abundance and metapopulation dynamics of wild populations across their range limits at Mt. Rainier National Park (Washington, USA). To examine the integrated effects of climate on local demography, metapopulation processes, and range shift dynamics, we combine this experimental and observational data using a simple spatial population model, and use that model to project changes to habitat occupancy and elevation range limits under a variety of plausible scenarios that incorporate warming climates and altered disturbance regimes. Our work addresses the following sets of specific questions:

1. How does climate influence the performance of local populations of the two focal species (*E. guttata* and *E. caespitosa*) at and beyond their elevation range limits? Does local demographic performance decline towards range limits because of the influence of climate?

2. How do climate, disturbance, and other habitat characteristics affect metapopulation dynamics (patterns of colonization and extinction) of these two species across their ranges?

3. What are the interactive effects of these processes on elevation range shifts under climate change scenarios? Which sets of processes (climate effects on local demographic performance or metapopulation processes) have the greatest influence over the magnitude and direction of range shifts under climate change?

1.3 Methods

1.3.1 Overview

We examined the interplay of climate, disturbance, local demography, and metapopulation dynamics across the ranges of our two focal species by combining data from a transplant experiment with censuses of wild populations using a spatial population model. Our transplant experiment, established at two sites, allowed us to link local demographic performance

to climate. Four years of population monitoring across the range limits of both species allowed us to link population persistence and colonization rates to climate and other habitat attributes. By combining these two sources of data with a spatial population model, we were able to assess how these factors interact to drive the maintenance of range limits and the magnitude and direction of range shifts under climate change. Below, we describe our study sites, experimental methods, monitoring protocols, and modeling choices in more detail.

1.3.2 Study System

Our work focuses on the elevation ranges of two closely-related species of yellow monkeyflower (*Erythranthe*, section *Simeola*, formerly *Mimulus*[11]), inhabiting riparian environments in Mt. Rainier National Park. Mt. Rainier National Park, located in the Cascade Range of Western North America (Fig. 1.2A), is a 95,660 ha natural area centered on the 4392 m stratovolcano Mt. Rainier. The mountain has been volcanically quiescent in historic times, and low-elevation slopes are cloaked in old-growth coniferous forest interrupted by the courses of large streams that drain the Park's steep topography and heavily glaciated volcanic cone (Fig. 1.2B). Main-stem rivers at Mt. Rainier (largest drainage area 17,780 ha) as well as some smaller streams, are subject to regular flooding and debris flow events that keep riparian areas largely free of large trees and lead to complex and dynamic braided channels that migrate across valley bottoms on annual and sometimes sub-annual timescales[6, 32]. The climate of Mt. Rainier National Park is typical of the Cascade Range, with warm, dry summers and cool, wet winters characterized by Pacific storms that lead to large snowpack accumulations at high elevations and large Fall and early Spring stream flows. The growing season at high elevations is strongly limited by the large snowpack, which often persists into July in the subalpine zone[69]. Riparian vegetation along low-elevation streams is sparse, and is dominated by red alder (*Alnus rubra*) and *Salix spp.* Smaller-order streams at higher elevations have channels that are less dynamic, and riparian zones are characterized by dense herbaceous subalpine vegetation. Substrates of most streams at Mt. Rainier consist of andesite and basalt cobbles mixed with finer volcanic-derived glacial sediments[32].

Both focal plant species are short-lived, primarily outcrossing perennials with showy yellow flowers pollinated primarily by bees (data not shown). Plants overwinter either as fleshy rhizomes (*E. guttata*) or thickened stems on the soil surface (*E. caespitosa*[147]), and are found in sunny or partly shaded, perennially moist environments along permanent waterways and seeps. Common yellow monkeyflower (*E. guttata*) is ubiquitous in low and mid-elevation riparian environments (<500 - 1500 m) at Mount Rainier National Park, inhabiting both forested streams and main-stem rivers (Fig. 1.2C). *E. guttata* is also found throughout northwestern North America, and although it's taxonomy is complex and controversial[64], plants in Mt. Rainier National Park have been ascribed to *E. guttata* (G. Nesom, *pers. comm.*). Subalpine Monkeyflower, *E. caespitosa*, (formerly *Mimulus Tilingii var. caespitosus* A.L. Grant) is a mat-forming species restricted to the Cascade Range from Oregon to southern British Columbia[129]. In Mt. Rainier National Park *E. caespitosa* is most common along streams in the subalpine and alpine ecological zone (1400 - 2300 m elevation), but also co-occurs with *E. guttata* at mid-elevations (600 - 1400 m), where it is restricted to sunny environments along larger streams (Fig. 1.2C). Despite their similar floral morphology, sympatric distributions, and recent evolutionary divergence, the two species are separated by strong post-zygotic reproductive barriers[72] and can be readily distinguished at field sites because of large differences in plant stature, leaf size, and the presence of a distinctive red band on the proximal end of the corolla tube in *E. guttata* (Fig. 1.2D).

1.3.3 Transplant Experiment

To isolate the impact of changes in climate on local demographic performance across range limits of our focal species, we grew 336 individuals of both species in a standardized semi-natural setting at two transplant sites located at different elevations. One site, Nisqually Vista (46.7843°N, -121.7482°W), is a previously disturbed subalpine meadow along Dead Horse Creek in Mt. Rainier National Park at an elevation of 1540 m, near the center of the elevation range of *E. caespitosa*, but at the range limit of *E. guttata*. The low-elevation site, Tahoma Woods (46.7584°N, -122.1239°W), is located approximately 15 km West of Mt.

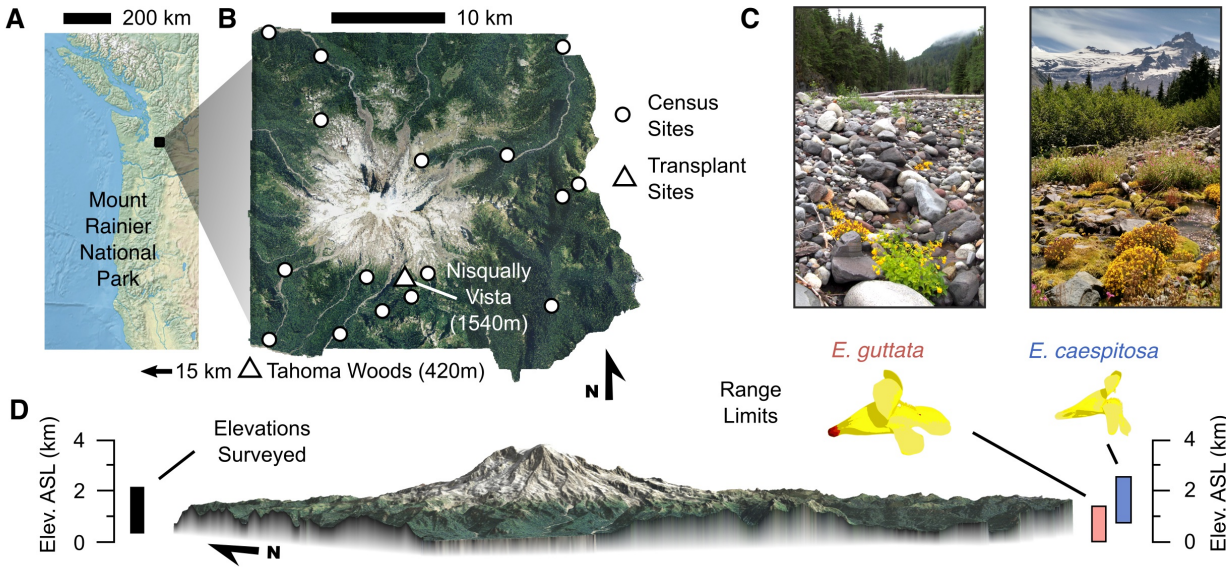

Figure 1.2: Monkeyflower study system, located in Mt. Rainier National Park, Washington, USA (**A**). Population census sites (**B**) were located along 16 sections of stream totaling approximately 12 km (white circles). Two transplant experiment sites (white triangles) were located at 1540 m (Nisqually Vista), and 430 m elevation (Tahoma Woods). The Tahoma Woods site was located approximately 15 km west of the park boundary near the town of Ashford. Larger, low-elevation streams in the park (**C**, left photo) are characterized by frequent flood scouring, with populations of both common yellow monkeyflower (*Erythranthe guttata*, foreground) and subalpine monkeyflower (*Erythranthe caespitosa*, background). High elevation streams (**C**, right photo) in the subalpine and alpine ecological zones experience less scouring and channel migration, and support populations of *E. caespitosa*. Range limits of the two species (**D**) differ markedly, with *E. guttata* uncommon (<5% occupancy) above 1500 m elevation and *E. caespitosa* uncommon below 700 m. The low-elevation limit of *E. guttata* occurs outside of the park boundary, and was not monitored, and the high-elevation boundary of *E. caespitosa* occurs in difficult-to-access glacial environments that were also not monitored.

Rainier National Park near the town of Ashford, WA. The Tahoma Woods site was located in a field near the National Park Service greenhouse facility, on the floodplain of the Nisqually River at an elevation of 430 m, below the low-elevation range boundary of *E. caespitosa*. The sites were matched for slope (<5%), canopy cover (10-20%), and insolation time, but differed in elevation by approximately 1100 m, and were thus exposed to very different climates. We measured climates at each site and each experiment block by installing air temperature sensors (Onset HOBO pendant loggers) below 10 cm diameter white plastic funnels hung at 4 m elevation in adjacent conifer trees. To measure soil temperatures and snow duration, we buried 8 HOBO loggers adjacent to all of the the transplant blocks. For each species in each site, we monitored germination and early seedling survival as well as adult survival and total seed production for three growing seasons. Additional details of the experimental design, including site photographs and information about seed sources, can be found in Appendix A.1.

To estimate vital rates for each species at each site, we used Bayesian generalized linear mixed-effects models implemented in the `stan_glmer` and `stan_glmer.nb` functions in the *R* package `rstanarm`. Each vital rate was estimated jointly across the study, with fixed effects representing Species, Site, and their interaction. Models also included random intercepts of source population, experiment block, and maternal family. Error distributions were Bernoulli (adult survival), Binomial (seedling survival), and Negative Binomial (seed production). The `rstanarm` functions estimate parameters via Hamiltonian Monte-Carlo implemented in the software *Stan*(http://mc-stan.org)[26]. We fit models using four chains, each with 5000 iterations, discarding the first 2500 iterations to yield 10000 posterior samples. We assessed convergence with visual inspection of the chains, as well as the $\hat{R}$ statistic. To propagate uncertainty in vital rates forward to our assessment of population growth rates, we used the `posterior_linpred` function in `rstanarm` to generate 10000 posterior samples of each vital rate for each site and species. Estimates were not conditioned on the random effects (i.e. they represented estimates of the population mean). To synthesize these vital rates into an aggregate estimate of the population growth rate at each site, we used a simple stage-based

matrix population model[28] with three adult stages (1st, 2nd, and 3rd-year plants) and no seed bank. We implemented the model using the `pop.projection` function in the *R* package `popbio`[161], and measured the average rate of population growth over 5 years using a starting size of 100 1st-year plants. We assessed uncertainty in population growth rates between species and sites by implementing the population model once for each of the 10000 posterior samples of the estimated vital rates.

1.3.4 Population Census

We examined the population structure and metapopulation dynamics of our focal species across their elevation range limits using an extensive field study. We censused every living individual of both species in 16 representative sections of riparian habitat in Mt. Rainier National Park from 2013 to 2016, encompassing approximately 10 linear km of stream. The study sites, located at elevations from 490 m to 1900 m, spanned the readily accessible riparian environments at Mt. Rainier, including 8 sites along main-stem rivers and 8 sites along smaller streams in the forest and subalpine zones. Upstream and downstream borders of the sites were bounded by stable and recognizable landmarks such as bridges or rock outcrops. Each site was visited once per growing season near the peak of local flowering for both focal species (early July - early September, depending on the elevation of the site). The showy flowers and habitat specificity of these species allowed us to be confident that each census was comprehensive. At each site we recorded the size and phenological status of each rosette of each species, and geolocated it to an accuracy <5 m using a commercial smartphone (Motorola XT-1056, XT-1095) with a modern Global Positioning Satellite System that accesses both GPS and GLONASS satellites. The collection of tens of thousands of geographic coordinates was enabled by an electronic data management system (Open Data Kit[22]), and positioning track logs were recorded using the smartphone application My Tracks (Google Inc.). For analysis, each study site was split into 27 m resolution grid cells in a Geographic Information System (NAD83 UTM grid, Zone 10N). All individuals falling in each spatial grid were aggregated to yield an estimate of the population size for that grid cell for that

year. The dataset used for further analysis, then, included population size estimates for 2135 grid cells over four years of study, a total survey area of 155.6 ha in each year.

1.3.5 Climate and Habitat Covariates

We used climatic and habitat covariates derived from a variety of sources as potential predictors of population and metapopulation dynamics. We derived plant-relevant microclimate variables (e.g. growing season air temperature, snow duration) for each 27 meter grid cell each year of the study from a microclimate model (see Appendix A.2) parameterized from extensive data collected within the study system. We extracted canopy cover, slope, and topographic roughness covariates from 1 m resolution digital elevation models and canopy surface models derived from a LiDAR dataset collected at Mt. Rainier National Park in 2007-2008[159]. To identify saturated-soil environments suitable for monkeyflowers, we developed a 1 m resolution binary habitat classification using Object-based Image Analysis (OBIA), implemented in *eCognition* software (Trimble Corp.). This habitat classification operated on a raster stack integrating high-resolution 4-band aerial photography collected in 2011 as part of the National Areal Imagery Program, as well as topographic and infrared return intensity information from LiDAR. For each 27 m grid cell, we used this binary habitat classification to compute the proportion of the cell that was classified as wetland or stream. As an index of flood disturbance potential for each site in each survey year, we extracted 99th percentile maximum stream flows for each water year (Oct. - Sept.) from the nearest downstream USGS stream gauge in each river basin (Carbon River at Fairfax, Nisqually River at National, White River at Buckley, Cowlitz River at Packwood). Dividing this value by the basin area gave a drainage-area standardized index of peak flow. We then multiplied this value by a flow accumulation raster derived from the 3 m resolution DEM using the function `r.watershed` in *GRASS GIS*[130](https://grass.osgeo.org/), and took the maximum value in each 27 m grid cell covered by the population survey. The resulting index has high values for sites on main-stem rivers, and for basins and water years with large peak flow events. Smaller-order streams have both lower typical values, and smaller amounts of year-

to-year variability in flooding potential. To determine which climatic and habitat covariates have influences on metapopulation dynamics, and thus should be included in the spatial population model, we first performed separate statistical analyses of rates of occupancy, year-to-year persistence, and colonization using Generalized Additive Mixed-effects Models (GAMM) implemented in the *R* package `GAMM4`[184] with survey site and year random intercepts. Covariates were included in the final analysis if they had a coefficient significantly different from zero, and polynomial terms were included if a spline smoother on that term in the GAMM showed significant non-linearity. Climatic and habitat covariates that were selected for the final analysis were mean growing-season air temperature, current water-year flooding potential, canopy cover, and logit-transformed proportion of stream habitat. All selected predictors were weakly co-varying (Pearson correlation coefficient <0.5).

1.3.6 Dynamic Range Model

To understand the combined effects of climate, disturbance and other habitat characteristics on the maintenance of range limits in our focal species, we used our field data to parameterize a simple spatially explicit population model incorporating the effects of climate and other habitat characteristics on patch-level demography as well as on dispersal and disturbance processes. A detailed description of the model structure can be found in the supplemental material (Appendix A.3), but we provide an abbreviated description here. The model is a discrete-space, discrete-time representation of metapopulation dynamics, and is derived from the Gompertz-logistic open population approach of Hostetler and Chandler[90], but it extends this model in two key ways. First, our formulation incorporates discrete disturbance events that cause local extirpations that would be otherwise unlikely given demographic stochasticity. This is important in our system, where flood disturbance regularly scours riparian habitats, frequently extirpating otherwise healthy populations. Second, we incorporate a spatially explicit colonization process that allows local dispersal between habitat patches (27 m grid cells in our analysis) driven by their proximity. The effects of time-varying climatic and static habitat covariates are implemented in regression equations linking the

covariates to rates of local population growth, colonization, and catastrophe in each cell in each year. The model includes an extremely simple representation of patch-level demography appropriate for short-lived species, like ours, that achieve reproductive maturity in their first year. The simple representation of patch-level demography allows the model to remain tractable when incorporating non-equilibrium processes such as disturbance and colonization, and allows all the model parameters to be fit simultaneously using data from our field population survey. We fit the model in a Bayesian state-space framework[149] that allowed us to propagate uncertainty in the model parameters to our predictions of geographic range limits, account for unmeasured environmental heterogeneity via site-level random effects, and incorporate evidence from the transplant experiment via informative priors on the demographic parameters. We validated the model by verifying that statistical distributions of predicted population sizes closely matched observations, and that the model reproduced the broad-scale patterns of occupancy and abundance across the ranges of both species (Appendix A.4).

1.3.7 Simulating Range Dynamics

After validating the model, we used posterior samples of the model's parameters derived from Markov Chain Monte-Carlo estimation to forecast range dynamics in a variety of plausible scenarios of changes to climate and flood-driven disturbance regimes for our field sites at Mt. Rainier, accounting for uncertainty in the model's parameters. Climate change forecasts for the Cascade Range predict growing season warming of up to 6.1°C[117] and increases in winter 20-year return flows of up to 80%[166], but different emissions scenarios, models of atmospheric dynamics, and downscaling techniques paint diverging pictures of late-21st century climates in the Cascades, including Mt. Rainier National Park. Because our goal is to demonstrate how climate interacts with metapopulation processes to affect climate-driven range-shifts, rather than produce specific forecasts of future geographic distributions of our focal species at Mt. Rainier, we implemented model simulations using 54 possible climate and disturbance scenarios for each species, which range from a uniform warming across the

elevation gradient of Mt. Rainier of 2.7°C to a cooling of 0.9°C, and a 1.5σ increase or 1.5σ decrease in the flood disturbance index. In each scenario, climatic covariates were input at their observed values for the first 16 years of the simulation, and then nudged to the scenario mean on year 17. The simulation was then run out for 100 years so that geographic distributions could stabilize at quasi-equilibrium, and we extracted predicted patterns of habitat occupancy for each of the 2135 grid cells in the field study for the last 50 years of the simulation. To measure the impact of these climate and disturbance scenarios on elevation range limits, we regressed predicted occupancy by elevation in each of the last 50 years of the simulation using a generalized linear model with a quadratic functional form and logit link. The resulting parameters for each simulation year were then averaged to represent the elevation-occupancy relationship for that model scenario and posterior parameter combination. We then found the lowest (*E. caespitosa*), and highest (*E. guttata*) elevations with a predicted occupancy greater than 2%, which we considered the elevation range limit, as well as the average prevalence of each species across all sites, and the elevation with the maximum predicted occupancy. This procedure was repeated for each of 1000 joint posterior samples of the model parameters for each scenario. This analysis was quite computationally intensive, and took approximately 5250 processor-hours to complete on an Amazon Elastic Compute Cloud (C8xlarge instance, 36 cores, 64 GB RAM). Code for the model and simulation procedure is available on GitHub (https://github.com/ibreckhe/MORA_monkeyflower_metapop).

1.3.8 Estimating Range-shift Sensitivities

Finally, to understand which processes have the largest amount of leverage over climate-driven range shifts for each species, we determined which parameter combinations in our dynamic range model were most strongly associated with large changes in geographic range limits in our climate and disturbance change scenarios. We used the *R* function `cor` to compute the Pearson correlation between the value of each parameter in our model and the magnitude of range limit shifts in simulations of our most extreme climate and disturbance scenarios ($+1.5\sigma$). Strong correlations indicate either that the process represented by the

parameter has a strong influence on range shift dynamics or that it is strongly correlated with a parameter that does have this influence, a possibility that we checked for by examining a correlation matrix of posterior samples of all of the model's parameters. Because the posterior samples of the parameters are considered equally probable given the data and priors, correlations between these samples and the magnitude of range shifts represent the influence of variation in biologically plausible parameter values. We refer to these correlations as range shift sensitivities in the Results and Discussion.

1.4 Results

1.4.1 Patch-scale Demographic Responses to Climate

Our two focal species showed dramatically different patch-scale demographic responses to climate across their range limits in experimental populations that we established in standardized semi-natural settings (Fig. 1.3). For both species, we found dramatic reductions in seed production at high-elevation transplant sites located at Nisqually Vista (1540 m ASL) compared to low-elevation sites located at Tahoma Woods (430 m, Fig. 1.3B). These reductions were more pronounced for *E. guttata* individuals, which produced a total of 5162 (95 %CI 2391 to 11329) seeds on average during years 1 and 2 of the experiment at the low elevation site, compared to just 183 (95% CI 82 to 420) seeds at the high-elevation site. Seed production was also lower (194 seeds, 95% CI 92.9 to 416) for *E. caespitosa* at the high-elevation site, compared to 487 seeds (95% CI 218 to 1057) at the low-elevation site, but overwinter survival and seed-to-1st-year-seedling survival were slightly higher (Fig. 1.3A). Summarizing differences in adult survival, seed production, and seedling survival using a simple matrix population model, we found that local population growth rates (r) declined dramatically at the high-elevation range limit of *E. guttata*, but did not decline beyond the low-elevation limit of *E. caespitosa* (Fig. 1.3D). This was true both for asymptotic population growth rates (which assume a stable stage distribution), as well as in simulations of initial population growth rates over four years initiated from seed. Elasticity values, which

measure the proportional sensitivity of population growth rates to variation in individual vital rates, suggest that second year seed production was the most important driver of variation in population growth rates for both species, followed by first-year survival. Despite strong species-specific differences, population growth rates at both sites were well above replacement level for both species, reflecting the experimental conditions in which flood scouring risks were eliminated, competition from nearby plants was suppressed, and seed germination and early seedling survival was assessed in ideal conditions (i.e. irrigated mineral soil).

1.4.2 Occupancy and Metapopulation Dynamics Across Range Limits

Our population survey revealed dramatic, and contrasting patterns of occupancy, abundance, colonization, and persistence across the lower-elevation range boundary of *E. caespitosa* and the upper-elevation boundary of *E. guttata* in Mt. Rainier National Park (Fig. 1.4). As predicted, occupancy declined for both species towards their range limits, with less than 2% of stream-side habitat patches occupied below 600 m for *E. caespitosa* and less than 2% occupied above 1800 m for *E. guttata* (Fig. 1.4A). Abundance, as measured by the average number of rosettes in occupied habitat patches, also declined dramatically towards the lower-elevation range limit of *E. caespitosa*. In contrast, abundance in occupied habitats did not decline towards the upper range limit of *E. guttata*, but instead increased slightly, from an average of 3.2 rosettes per grid cell at 600 m elevation, to 7.5 rosettes per grid at 1800 m. The two species also showed dramatic differences in year-to-year population persistence across the elevation gradient at Mt. Rainier (Fig. 1.4B), with persistence significantly higher along high-elevation streams for both species. This pattern was especially dramatic for *E. caespitosa*, with high persistence probability along high-elevation streams (probability 0.74 at 1900 m), and extremely low persistence probability along low-elevation streams (0.06 at 600 m). Differences in the rates of colonization of unoccupied habitat patches across the elevation gradient (Fig. 1.4C) were not significant for *E. caespitosa*, but decreased dramatically towards the high-elevation range limit of *E. guttata*. After accounting for other habitat covariates such as canopy cover and stream drainage area using GLMMs, we found

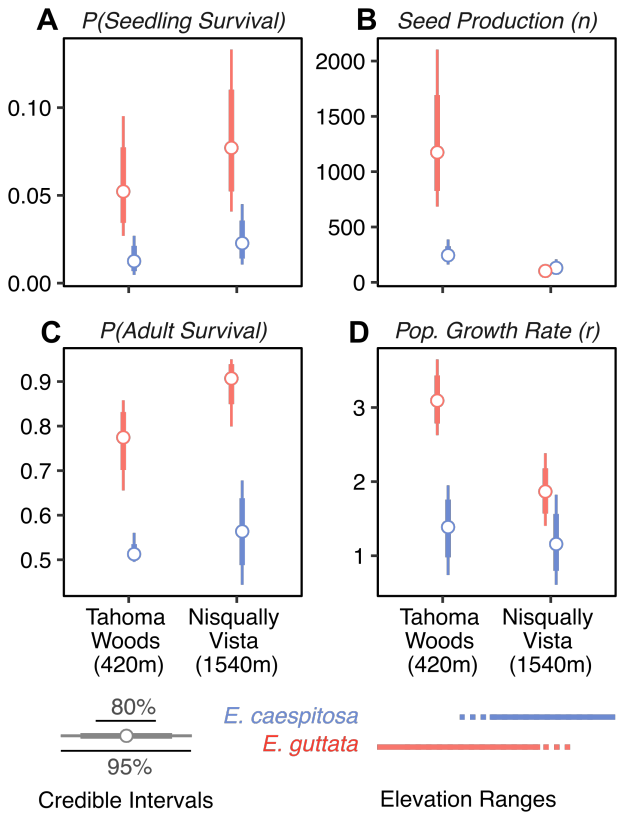

Figure 1.3: Vital rates and local demographic performance of *E. caespitosa* and *E. guttata* individuals tracked for 3 years at two transplant sites. The Tahoma Woods site is located below the low-elevation range limit of *E. caespitosa* (420 m ASL), and the Nisqually Vista site is located near the upper range limit of *E. guttata* (1540 m). Germinant survival at 1 year (**A**) was lower at the low-elevation site for both species, as was average adult survival over years 2 and 3 (**C**), but this was compensated for by much higher average annual seed production at the low elevation site (**B**), especially for *E. guttata*, which produced nearly 10 times the number of seeds at the low elevation site as at the site located near its elevation range limit. Summarizing the effects of these differences in vital rates, population growth rates (**D**) declined dramatically at range limits for *E. guttata*, but did not decrease significantly beyond range limits for *E. caespitosa*.

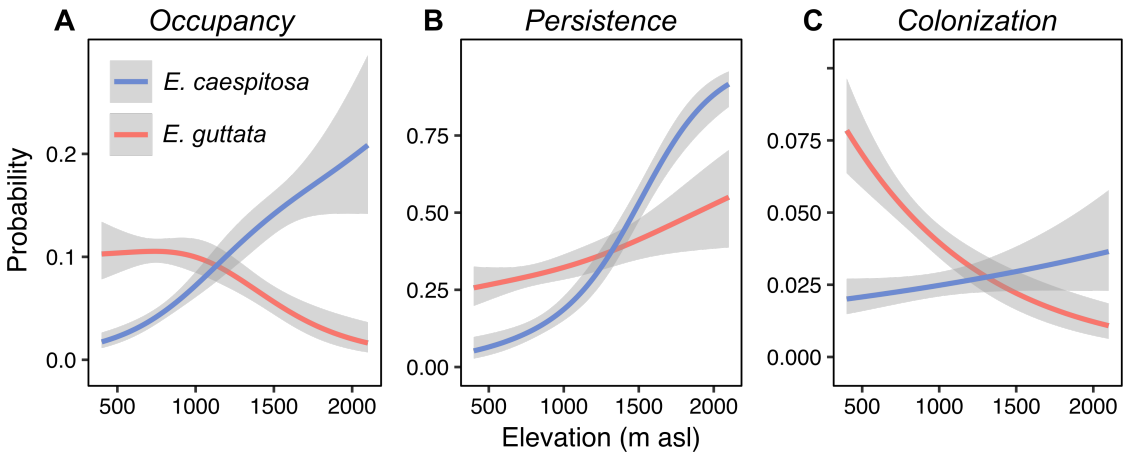

Figure 1.4: Patterns of occupancy and metapopulation dynamics across the low-elevation range limit of *Erythranthe caespitosa* (blue) and the high-elevation range limit of *Erythranthe guttata* (red) along streams in Mt. Rainier National Park that were surveyed in 2013 - 2016. Probabilities represent mean rates of occupancy (**A**), persistence (**B**), and colonization (**C**) across all patches of stream habitat surveyed, divided into 27 m grid cells (see methods). Lines and shading represent the mean and 95% confidence intervals, respectively, from a generalized additive mixed model fit with a Bernoulli error distribution and incorporating stream and year as random intercepts. Occupancy probabilities decline towards range limits for both species, but more steeply for *E. guttata*. Persistence probabilities increase for both species from low elevations to high elevations, but more dramatically for *E. caespitosa*. Colonization probabilities decline precipitously across the high elevation range limit of *E. guttata*, but do not differ between low and high elevations for *E. caespitosa*.

strong support for the influence of climate on metapopulation dynamics in this system. Statistical models which included growing-season average air temperature were preferred over those with only non-climatic covariates for rates of colonization (likelihood ratio test, $\chi^2 = 8.42, p = 0.0148$) and persistence ($\chi^2 = 8.54, p = 0.0140$) in *E. guttata*, and persistence ($\chi^2 = 7.36, p = 0.0252$) in *E. caespitosa*. Colonization rates also co-varied with climate in *E. caespitosa*, but climate effects were marginally non-significant in a model incorporating other habitat covariates ($\chi^2 = 4.37, p = 0.1124$).

1.4.3 Dynamic Range Model Validation

We found that our dynamic range model fit the data well for both focal species, and faithfully reproduce important statistical, spatial, and temporal patterns of occupancy and abundance in our population survey data. Abundance of both species shows a large amount of skew and extreme zero-inflation in our study, with approximately 92% of patches unoccupied in given year. Further, the model shows predicted elevation distributions that are similar to the observed distribution of occupancy and abundance across the elevation gradient at Mt. Rainier (Appendix A, Fig. A.3), as well as the spatial patterns of colonization and persistence across ranges depicted in Fig. 1.4 (Appendix A, Fig. A.3). We did find that average quasi-equilibrium occupancy over 100 years of simulation was somewhat lower than that of the real data for both species. This could reflect bias in the model, but could also be an artifact of study site selection, as all population survey sites were initially selected to contain at least one individual of one of the two study species, which might lead to an overestimation of long-term of occupancy.

1.4.4 Range Shifts under Climate Change Scenarios

In our simulations of range change under different scenarios of altered climate and flood disturbance, we observed a diverse set of range dynamics including pronounced pro-gradient and counter-gradient range shifts (Fig. 1.5). Warmed growing-season air temperatures drove large uphill range shifts for the low elevation species, *E. guttata*, with predicted uphill shifts to both the range optimum (the elevation of maximum average occupancy) and the high-elevation range limit (the highest elevation with occupancy of suitable habitat of at least 2%). For growing-season warming of 2.7°C, in line with median expected climate change in vicinity of Mt. Rainier by the 2060s under a moderate emissions scenario (RCP 4.5)[117], *E. guttata* increased in average prevalence (Fig. 1.5A), while it's range optimum was expected to move uphill by approximately 311m (80% posterior credible intervals 165 to 358m), and it's upper-elevation limit was forecast to move uphill by approximately 529m (80% CI 209 to

634m) in the absence of changes to the disturbance regime. Increases in flood disturbance on the magnitude of those expected by the late 21st century, caused more dramatic uphill range shifts of 346 to 864m when combined with warming (Fig. 1.5B,C). In contrast, we found that *E. caespitosa*'s lower-elevation range limit was projected to move downhill approximately 97m (80% CI 29 to 351m) with 2.7°C of warming, assuming no change to the disturbance regime, and by 234m (80% CI 45 to 689m) if flooding decreases by 1.5σ (Fig. 1.5F). We also found that the overall prevalence and range optimum of *E. caespitosa* was relatively insensitive to changes in both climate and disturbance (Fig. 1.5D,E).

1.4.5 Drivers of Range Shift Dynamics

What explains the widely divergent range-shift dynamics of these two species in our model simulations? The values of the parameters representing how different population and metapopulation processes are affected by environmental change, and how closely these parameters are associated with variation in the amount of range shift (Range Shift Sensitivities, Table 1.1), give us some clues about which processes might be important. Consistent with the results from our common-garden experiment, warmer growing season temperatures boost patch-scale population growth rates in *E. guttata*, but have little influence on population growth rates in *E. caespitosa*. Higher flooding potential is negatively associated with local population growth rates and positively associated with rates of colonization for both species. Further, an interaction between temperature and flood frequency affects both colonization and the probability of catastrophe in *E. guttata*, with flooding more likely to drive colonization and less likely to extirpate populations in warmer climatic conditions. This suggests that the response of *E. guttata*'s range limit to altered climate and disturbance regimes is jointly controlled by the direct effects of climate and flooding on local demography, colonization, and catastrophe. The situation is somewhat simpler for *E. caespitosa*, where climate has little effect on local population growth. Instead, warmer temperatures have a small positive influence on colonization rates, which lead to counter-gradient range shifts under warmer conditions in the absence of increases in flood disturbance. Our post-hoc analysis

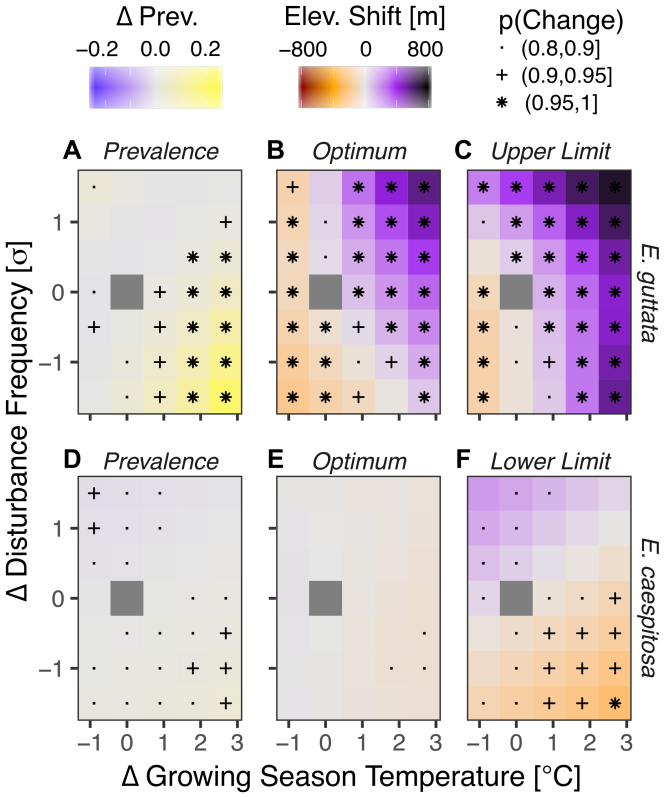

Figure 1.5: Changes in quasi-equilibrium prevalence (mean occupancy probability) and elevation ranges of common yellow monkeyflower (*E. guttata*) and subalpine monkeyflower (*E. caespitosa*) as a function of different climate and disturbance scenarios relative to the gray box, which represents current conditions. *E. guttata* increases in prevalence more dramatically (**A**) with increases in growing season temperature when flood disturbance decreases in frequency. The elevation of maximum occupancy (optimum, **B**) and lower range limit (**C**) shift up in elevation more dramatically with increases in flood disturbance. In contrast, *E. caespitosa* prevalence does not change dramatically in the climate and disturbance scenarios modeled (**D**), and neither does it's range optimum (**E**), but it's lower-elevation range boundary (**F**) shifts downhill with warming, and more dramatically with decreases in flood disturbance. The low-elevation range limit of *E. guttata* and the high-elevation limit of *E. caespitosa* are outside of the elevation range of the study, and results are not shown. Symbols represent the posterior probability of range shifts being different from 0 for each scenario, with asterisks (*) corresponding to scenarios with greater than 95% probability of a shift in prevalence or range position, plus symbols (+) represent a 90 to 95% probability of shift, and dots (.) represent 80 to 90% probability.

of the range shifts predicted for each posterior sample of the model's parameters gives us important clues about the relative importance of these drivers. For both species, elevation range shifts driven by both warming and disturbance were much more sensitive to variation in parameters influencing rates of colonization, than to parameters influencing rates of catastrophe or local population growth (Table 1.1).

1.5 Discussion

Our work provides strong support for the hypothesis that climate's influence on metapopulation processes can drive complex range shift dynamics, including counter-gradient range shifts. We found that climate strongly influenced demographic performance of our two focal species, but did not always decrease performance towards range limits. We also found that focal species differed in colonization and extinction dynamics across their elevation ranges, driven both by gradients in climate and other habitat attributes. As a consequence, climate and it's effects on population and metapopulation processes were critical to understanding current distributions and projected range shifts under climate change. More broadly, we argue that counter-gradient range shifts may be a common consequence of climate change if climate drives divergent changes in local population growth and metapopulation processes such as colonization and extirpation rates. Below, we explain these points in more detail.

Consistent with many recent studies, we found evidence that climatic conditions reduce patch-scale demographic performance towards some, but not all range limits. In particular the colder conditions at the high-elevation transplant sites, characterized by lower growing-season temperatures, large winter snowpack, and a short growing season, dramatically reduced growth and seed production of our low-elevation focal species*E. guttata* at transplant sites near it's high-elevation range limit. Higher adult survival and slightly (although not significantly) higher seed-to-seedling survival of *E. guttata* at the high-elevation site was insufficient to compensate for reductions in fecundity, driving much lower estimated population growth rates. The situation was somewhat different across the low-elevation limit of *E. caespitosa*, where lower year-two survival and slightly (but not significantly) lower

Type	Parameter	*E. guttata* est. (95% CI)	DS	CS	*E. caespitosa* est. (95% CI)	DS	CS
Init. Abund. (λ)	λ_0	**-2.106** (-3.513, -0.802)	0.10	0.08	**-2.450** (-3.601, -1.496)	0.18	0.12
	λ_{Clim}	-0.429 (-1.657, 0.897)	0.13	0.08	**-1.**452 (-2.97, -0.591)	0.06	0.10
	λ_{Dist}	**1.229** (0.545, 1.908)	0.02	0.03	0.020 (-0.567, 0.595)	0.13	0.04
	λ_{Stream}	**1.143** (0.794, 1.51)	0.01	0.17	**1.271** (0.886, 1.661)	0.17	0.10
	λ_{Stream^2}	**-0.429** (-0.822, -0.033)	0.04	0.08	-0.399 (-0.868, 0.054)	0.01	0.03
	λ_{Canopy}	-0.239 (-0.6, 0.123)	0.06	0.04	**-0.572** (-0.995, -0.152)	0.02	0.06
	λ_{Canopy^2}	**-1.215** (-1.689, -0.764)	0.04	0.01	-0.130 (-0.665, 0.331)	0.15	0.19
	$\lambda_{Clim:Dist}$	0.460 (-0.439,1.365)	0.11	0.07	0.406 (-0.281, 1.156)	0.10	0.07
Colonization (ι)	ι_0	**-1.371** (-2.281, -0.619)	0.51	0.10	**-2.757** (-3.357, -2.142)	0.46	0.17
	ι_{Clim}	-0.065 (-0.758, 0.553)	0.41	0.77	**0.341** (0.106,0.836)	0.87	0.43
	ι_{Dist}	**0.437** (0.14, 0.719)	0.37	0.77	**0.331** (0.078, 0.623)	0.41	0.78
	ι_{Stream}	**1.236** (1.074, 1.406)	0.20	0.10	**0.937** (0.746, 1.128)	0.04	0.21
	ι_{Stream^2}	**-0.463** (-0.63, -0.297)	0.00	0.08	-0.137 (-0.342, 0.073)	0.16	0.16
	ι_{Canopy}	0.096 (-0.061, 0.261)	0.09	0.21	**-0.534** (-0.767, -0.313)	0.01	0.12
	ι_{Canopy^2}	**-0.811** (-1.007, -0.614)	0.13	0.09	**-1.059** (-1.309, -0.819)	0.11	0.01
	$\iota_{Neighbor}$	**0.709** (0.597, 0.825)	0.01	0.10	**1.041** (0.905, 1.192)	0.03	0.19
	$\iota_{Clim:Dist}$	**-0.953** (-1.328, -0.568)	0.30	0.82	0.003 (-0.524, 0.532)	0.08	0.09
Catastrophe (ϕ)	ϕ_0	**-5.555** (-10.024, -2.587)	0.01	0.00	**-4.63** (-8.356, -2.158)	0.06	0.04
	ϕ_{Clim}	2.67 (-2.476, 7.269)	0.00	0.21	1.426 (1.16, 4.783)	0.01	0.10
	ϕ_{Dist}	-2.348 (-6.293, 1.668)	0.1	0.01	0.101 (-2.907, 3.857)	0.01	0.02
	$\phi_{Clim:Dist}$	**-5.763** (-11.425, -0.935)	0.03	0.06	**2.083** (0.301, 4.209)	0.029	0.30
Pop. Growth (r)	r_0	0.022 (-0.423, 0.515)	0.26	0.11	**-0.963** (-1.622, -0.33)	0.05	0.06
	r_{Clim}	**0.406** (0.074, 0.742)	0.10	0.03	0.081 (-0.242, 0.411)	0.15	0.10
	r_{Dist}	**-0.918** (-1.5, -0.349)	0.11	0.04	**-1.26** (-1.962, -0.641)	0.04	0.04
	r_{Canopy}	0.343 (-0.174, 0.89)	0.03	0.08	-0.183 (-0.706, 0.325)	0.12	0.04
	r_{Stream}	-0.263 (-0.787, 0.259)	0.07	0.00	-0.003 (-0.521, 0.489)	0.13	0.19
Other	κ	**197.615** (124.715, 268.841)	0.01	0.10	**199.309** (123.981, 270.52)	0.18	0.01
	α	**0.136** (0.121, 0.153)	0.29	0.29	**0.166** (0.144, 0.192)	0.04	0.19
	α_{init}	**0.075** (0.059, 0.093)	0.00	0.01	**0.051** (0.041, 0.063)	0.08	0.25

Table 1.1: Parameter estimates and range limit sensitivities for the spatial population model. Bold values are credibly different from zero. Parameter values are grouped by which regression equation they fall into, initial abundance (λ), colonization (ι), catastrophe (phi), and local population growth (r). The abbreviations DS and CS refer to disturbance sensitivities and climate sensitivities, a measure of how strongly each parameter is associated with changes in elevation ranges in the most extreme climate and disturbance scenarios (+2.7°Cand +1.5σ flood index).

seed-to-seedling survival was compensated by increased fecundity at the low-elevation site, located approximately 100 m below it's low-elevation range limit (Fig. 1.3). This resulted in no significant differences to aggregate population growth rates between transplant sites that differed in elevation by more than 1000 m. This general pattern, where lower survival is partially or totally compensated for by higher seed production in lower-elevation or lower-latitude sites, is common across the ranges of many organisms [49, 173, 156]. Unfortunately, because many different aspects of climate co-vary across Mt. Rainier's elevation gradient, our study design does not allow us to directly measure which climatic factors are responsible for differences in vital rates or aggregate demographic performance. Nonetheless, the experimental work does support a role of climate in maintaining the range limit of one of our two focal species via it's effects on individual-scale performance.

In our study system, the effects of climate on individual-scale demographic performance only partially explain the patterns of occupancy and abundance across the range limits of the two focal species that we tracked in this study. Instead, we found strong evidence that populations of the low-elevation species, *E. guttata*, have a high-elevation range limit that is jointly controlled by the influence of climate and flooding on both individual-scale demographic performance and patch-scale colonization and extinction dynamics. This is evident in the large reduction in population growth rates of *E. guttata* that we observed in transplant sites located near it's high-elevation range limit (Fig. 1.3), as well as our integrated analysis of metapopulation dynamics, which suggests that *E. guttata* is restricted to low-elevation sites both because local populations grow more slowly in cooler conditions, and the species is less likely to colonize high-elevation streams that are subject to low rates of flood disturbance (Fig. 1.4, Table 1.1). In contrast, our transplant experiment provides evidence that *E. caespitosa* individuals perform well in warm conditions outside of the species' climatic range, and our integrated analysis suggests that *E. caespitosa* is restricted to high-elevation habitats because local populations persist poorly in warmer environments, and environments that are subject to greater flood scouring (Fig. 1.4B). Studies of many plant species, including monkeyflowers[7] have shown that abundance and local demographic performance

vary idiosyncratically across species ranges, suggesting that larger-scale processes, like the metapopulation dynamics we observed in our study, likely drive the consistent reductions in habitat occupancy that define many range limits[136].

We speculate that the dramatic differences in the environmental responses of these two closely-related species is driven, at least in part, by differences in key life-history traits. In particular, the overwintering behavior of these two species is starkly different, with *E. guttata* forming extensive underground rhizomes that extend up to 30cm below the soil surface, while *E. caespitosa* overwinters with thickened leaves and stems at the soil surface, forming only fibrous roots underground. This means that *E. guttata* rosettes are substantially protected from freeze damage, and can effectively re-sprout through flood deposited sediments (*pers. obs.*). These traits are potentially adaptive along low-elevation streams where winter snow cover is intermittent, minimum soil surface temperatures can drop to -10°C during extreme cold events, and winter flooding and sediment redistribution is especially common. The overwintering strategy of *E. caespitosa* is appropriate for high-elevation, stream-side habitats where large winter snowpack typically prevents freezing at the soil surface[69], and channel morphology is less dynamic. These same traits could expose overwintering stems to damaging freeze events at lower elevations. We suspect that this effect may be responsible for extremely low overwinter survival of *E. caespitosa* at our low-elevation transplant site in year 2 of the transplant experiment, where minimum soil temperatures dropped to -6°C. Experimental evaluations of freezing tolerance could help to test this idea.

Our analysis of the effects of population and metapopulation processes on range limits integrates extensive data from a multi-year field experiment with large-scale population surveys across a large environmental gradient, and we provide some of the first indications that metapopulation dynamics might drive counter-gradient range shifts of plants under climate change. Like any modeling study, however, our results also partly reflect the structure of the model itself, which formally encodes our understanding of the processes involved. There are some processes that are likely important in this system, however, that were not explicitly included. The effects of unobserved environmental variation, for example, was accounted for

by site-level random effects that affect initial abundance and colonization rates, but we could not incorporate site-level random effects on catastrophe or local population growth rates, because such models failed to converge. Our analysis also does not explicitly incorporate biotic interactions, including competitive or facilitative interactions between the two focal species. Or initial analysis of prevalence and occupancy dynamics did not reveal strong evidence for interspecific competition or facilitation between our two focal species, but these interactions may become more important if, as we predict, *E. guttata* shifts its range uphill into subalpine environments where *E. caespitosa* is more common. Moreover, our model includes local, but not long-distance feedbacks between local demographic performance, dispersal, and colonization. This lack long-distance feedbacks between abundance and colonization could potentially cause us to underestimate the effects of changing local demography on range shifts. Long-distance dispersal is notoriously difficult to measure directly[167] but we may be able to indirectly estimate some of these parameters in future work using genetic data[16].

Our study is one of the first to assess how climate's effects on individual performance interact with it's effects on metapopulation dynamics to shape species range shifts under climate change, and we are not aware of any studies that directly evaluate the individual-scale and patch-scale effects of climate on range limits and range shifts in a field system (but see[88] for a theoretical treatment). In our simulations of quasi-equilibrium range change under different climate and disturbance scenarios, the positive effects of warming on rates of colonization in *E. caespitosa* drive modest counter-gradient (downhill) range shifts. These shifts became more pronounced with decreases in flood disturbance, which increases population persistence along lower-elevation streams that are more vulnerable to flooding. An altered disturbance regime also affects the magnitude of uphill range shifts in *E. guttata*. Although some previous work explores the importance of dispersal and disturbance dynamics for forecasting changes to communities and geographic ranges under climate change[167] these studies are uncommon compared to work that focuses on links between climate and local population performance. Further, the few studies that do incorporate both population

and metapopulation processes into range shift predictions often structure models so that climate affects only local demography or habitat suitability[6, 70]. Without the potential for divergent effects of climate on population-scale and metapopulation-scale processes (Fig. 1.1D), these models do not generate counter-gradient range shifts.

The complex roles of climate in driving population-scale and metapopulation-scale dynamics that we found in this system are potentially quite common, and could be important drivers of some of the counter-gradient range shifts that have been observed in nature over the past century of climate change. Although our focal species are short-lived, and inhabit particularly disturbance-prone environments, there is no reason to dismiss the possibility that similar dynamics might operate over larger spatial and temporal scales for longer-lived organisms, especially near the boundaries of species ranges, where populations tend to be patchy[136]. Warming climates are changing both equilibrium population dynamics of many species as well as altering the frequencies of extreme events that extirpate populations or push them out of demographic equilibrium, such as drought[3], wildfire[2], or pathogen outbreaks[38]. If changes in climate alter the frequencies or severities of these events at range limits, then understanding their role in mediating range shift dynamics will be critical to forecasting future changes to geographic distributions[189, 144]. This potentially poses a challenge to ongoing efforts to predict species range-shifts under climate change by upscaling plot-level measurements of demographic rates, and using traits and shared phylogenetic history to predict demographic responses to climate across many species[60]. If these plot-level measurements are collected at spatial and temporal scales that are too small to capture metapopulation processes, then forecasts of range change based on these approaches might be misleading.

We believe that our study provides a template for future work that integrates the effects of environmental change on population and metapopulation processes at multiple spatial scales to forecast the impacts of climate change on species distributions. For most organisms, it is not possible to directly measure how environmental variability and change impact both individual performance and colonization and extinction dynamics across large landscapes.

We contend that the general approach of this study–using field experiments to evaluate climate effects on demographic performance and integrating this information into spatial models of metapopulation dynamics fit to field data–is particularly promising. This effort will be aided considerably by new classes of probabilistic population models, like the one we used here, that integrate individual-level and patch-level processes (see also[162, 21, 100]). Moreover, new types of observations from drones[41, 27], hyperspectral imagery [29, 115], eDNA [104], and citizen scientists[24] make it increasingly feasible to monitor the spatial distribution and abundance of organisms over large landscapes. Our work suggests that these new types of observations and computational tools may be critical in generating skillful forecasts[47] of the impacts of accelerating climate change on species ranges and ecological communities.

Chapter 2

WARMER WINTERS CAUSE FRAGMENTATION OF MOUNTAIN MEADOW ECOSYSTEMS VIA INTRASPECIFIC PHENOLOGICAL MISMATCH

2.1 Abstract

Landscape phenology, or the spatial pattern of the timing of biological events like leafing and flowering, has strong influences on the demography, population structure, and evolution of organisms. These patterns are particularly important for non-mobile groups, such as plants, in environments where the cues that trigger phenological events vary across small spatial scales. In these systems, mismatches in reproductive timing between adjacent patches of habitat driven by fine-scale environmental variation can create temporal barriers to reproduction, a phenomenon we call intraspecific phenological mismatch. In addition to having fundamental ecological and evolutionary consequences, intraspecific phenological mismatch could exacerbate the negative impacts of climate change on plants by reducing connectivity between nearby populations. This can occur if climate change increases spatial heterogeneity in flowering time, decreasing the time intervals over which individuals can interact via pollen dispersal. Here we use unprecedented high resolution (3 m) landscape-scale estimates of flowering phenology to examine how annual variation in climate drives changes in intraspecific mismatch, and hence population connectivity, for 16 animal-pollinated plant species across a large network of alpine and subalpine meadows in Mt. Rainier National Park, Washington, USA. Our results indicate that small-scale spatial variation in climate produces pronounced intraspecific phenological mismatch in flowering in our landscape. Further, in years with early snow melt, overall predicted pollen dispersal across the network of meadows decreased by 5-15% across species, driven by increasing heterogeneity in snow disappearance dates be-

tween nearby meadows. The reductions in reproductive connectivity were much larger (up to 75%) in relatively poorly connected populations near the climatic boundaries of the meadow ecological zone, meadows that are already negatively impacted by tree encroachment and other factors. We also show that the negative effects of early snow melt on connectivity are enhanced for species that shorten their flowering period when snow disappears early. Our study is one of the first to demonstrate direct effects of climate on the reproductive synchrony and connectivity of plant populations. Our results likely apply to many montane systems where climate change is driving upward movement of the rain/snow transition zone, generating increasing differences in snowpack and snow duration between the high-elevation and low-elevation boundaries of subalpine and alpine ecosystems.

2.2 Introduction

Organisms live in heterogeneous environments, which makes it challenging to synchronize important life events like reproduction and dispersal between habitat patches. Spatial patterns of reproductive phenology determine the structure and effective size of populations [84, 114], the spatial and temporal distribution of their interactions with other organisms [87, 123], and their relative exposure to risky climatic events like frost and drought [93, 30]. Despite its fundamental importance, landscape reproductive phenology is poorly studied, at least in part because repeated direct measurements of reproductive life stages are often difficult or impossible to collect across large landscapes. The numerous studies that examine the environmental controls on the timing of angiosperm flowering almost exclusively rely on observations of individuals, small study plots, or area searches [37, 48, 182] without explicitly considering how the timing of those events vary across space.

Landscape reproductive phenology is particularly important in landscapes where the climatic drivers of phenology are heterogeneous at small spatial scales [96, 69, 138, 164]. This means that nearby plant populations can be cued to flower at very different times, with the differences in flower timing governed by differences in climatic drivers across the landscape. When this asynchronous timing occurs in adjacent populations, we call this phenomenon

"intraspecific phenological mismatch": reductions in reproductive opportunity driven by differences in the timing of reproduction between conspecific individuals or populations (Fig. 2.1). This contrasts with "interspecific phenological mismatch", which concerns reductions in interactions between species, for example predators and their prey or plants and their animal pollinators. While interspecific mismatch has been the subject of considerable research effort, particularly regarding potential climate change impacts [51, 141, 71], there has been little previous work that examines spatial or taxonomic patterns of intraspecific mismatch or its consequences[121, 158]

The consequences of intraspecific phenological mismatch could be significant. For example, when individuals bloom asynchronously the flowering period at landscape scales lengthens relative to the individual scale, with potential consequences for interacting organisms such as pollinators[87]. Intraspecific mismatch might also be a powerful driver of assortative mating, potentially allowing adaptations to the local environment to persist in the face of homogenizing gene flow [140, 103]. Further, asynchronous phenology could also allow plants to escape from competitive interactions with conspecifics, as well as other negative interactions [158, 67]. Perhaps most importantly, however, intraspecific mismatch also reduces effective population sizes [74] and increases fragmentation of populations, with potentially negative demographic consequences, especially for small populations with restricted distributions in patchy landscapes[101], or for populations near the edges of geographic ranges. The extensive literature on fragmentation suggests that these poorly connected populations could be more vulnerable to environmental change, including the effects of climate change, but direct evidence of these interactive effects is lacking [77].

Climate change could increase intraspecific phenological mismatch, and thus fragment populations, if it increases the spatial heterogeneity in environmental controls on phenology. This issue is particularly relevant in temperate mountainous regions with large winter snowpack, where the timing of seasonal snowpack disappearance is the most important environmental control on subalpine and alpine plant phenology [105, 98]. Snowpack is much more sensitive to increases in winter temperature at the low elevation boundary of subalpine

ecosystems than it is at higher elevations [126, 160, 45]. Consequently, as winter temperatures warm, 21st century changes in the date of seasonal snowpack disappearance in the Western USA are forecast to be more than twice as rapid at mid-elevation (1000 to 2000 m) than they are at high elevations as the elevation of the rain-snow transition increases [151] (Fig. 2.1A). This accelerated seasonal snow disappearance at low elevations (Fig. 2.1B) could drive more pronounced intraspecific phenological mismatch in montane ecosystems that are currently above the rain/snow transition zone for most of the accumulation season (Fig. 2.1C). The size of climate effects on intraspecific mismatch in mountain environments depends on how climate and other aspects of the environment shape species' geographic distributions as well as the landscape pattern of flowering across mountain slopes and local microtopography. Specifically, the degree to which accelerated snow disappearance at low elevations causes intraspecific phenological mismatch between subalpine and alpine plant populations depends on 1) how species elevation ranges overlap with the zone of most rapid changes to environmental drivers of phenology, 2) how small-scale patterns of abundance vary with respect to climate and microtopography, and 3) the duration of flowering at small scales and how flowering duration is modified by changes in climate.

In this work, we developed the first direct estimates of the extent to which climate drives intraspecific phenological mismatch in montane ecosystems. We harnessed high-resolution environmental data and well-validated models of environmental controls on species distributions and phenologies to reconstruct landscape flowering phenology for a suite of 16 animal pollinated wildflower species across 4723 ha of subalpine and alpine meadows at Mt. Rainier National Park (MORA), WA from 2009 to 2015. We then used a simple model of pollinator dispersal to examine how intraspecific phenological mismatch reduces reproductive connectivity across populations of our focal species. Finally, we explored how connectivity within species and meadows responds to annual variation in climate, including a climate change analog year, 2015, which had dramatically reduced low-elevation snowpack at Mt. Rainier and throughout the Cascade Range [127]. In doing this work, we also tested three specific predictions regarding climate and intraspecific phenological mismatch 1) that intraspecific

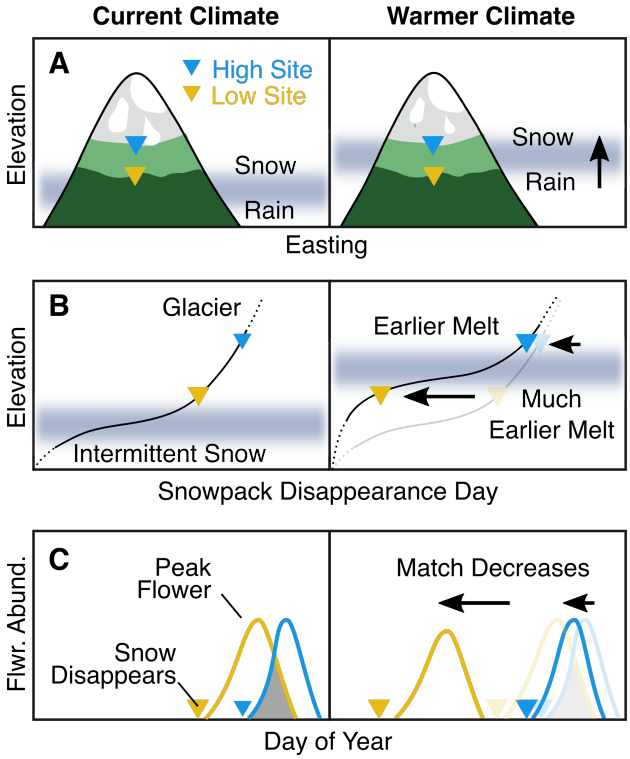

Figure 2.1: One mechanism by which climate change could drive intraspecific phenological mismatch. As warmer winter temperatures cause uphill movement of the rain-snow transition zone (**A**), low-elevation sites (orange triangles) are likely to experience larger changes in the date of snowpack disappearance than high elevation sites (blue triangles, **B**). If snow is an important control on reproductive phenology, this increasing variation in snowmelt timing across the elevation gradient could cause phenological events like flowering in low-elevation sites to become mismatched in time from events at higher elevations(**C**).

.

mismatch would be exacerbated in years with larger differences in snow melt timing between low-elevation and high-elevation meadows, 2) that species which are distributed across a smaller range of elevations and a larger range of microhabitats will show less pronounced and less variable patterns of intraspecific mismatch, at least in part because their entire distribution is not likely to be interrupted by the rain-snow transition, and 3) that species with shorter flowering duration and meadows near the climatic extremes of the meadow elevation zone would experience larger year-to-year variability and larger decreases in connectivity under climate-change analog conditions.

2.3 Methods

2.3.1 Methods Overview

We produced high-resolution (3m) maps of the topography, vegetation structure and microclimate of Mt. Rainier's subalpine and alpine vegetation zones by synthesizing data from LiDAR and a dense network of weather stations and microclimate sensors (Fig. 2.2A) using geostatistical techniques. We then trained a machine learning model with these maps in combination with data from an extensive structured vegetation survey to predict the fine-scale geographic distributions of 16 montane perennial wildflower species across Mt. Rainier's meadow zone (Fig. 2.2B). To estimate landscape flowering phenology for each species, we combined the maps of species predicted prevalence with maps of their flowering phenology derived from a well-validated phenology model trained on extensive local field observations. This process produced high-resolution maps of the landscape patterns of flowering for each species in each day of the growing season from April 2009 to September 2015, a time interval that included among the coolest, latest-snow melt (2011), and the warmest, earliest-melt (2015) years in the historical climate record at Mt. Rainier. After summarizing the resulting maps to estimate the abundance and temporal progression of flowering for each species in each meadow in each year, we validated these meadow-scale estimates using independent data from a citizen-science program. After validation, we computed the intraspecific pheno-

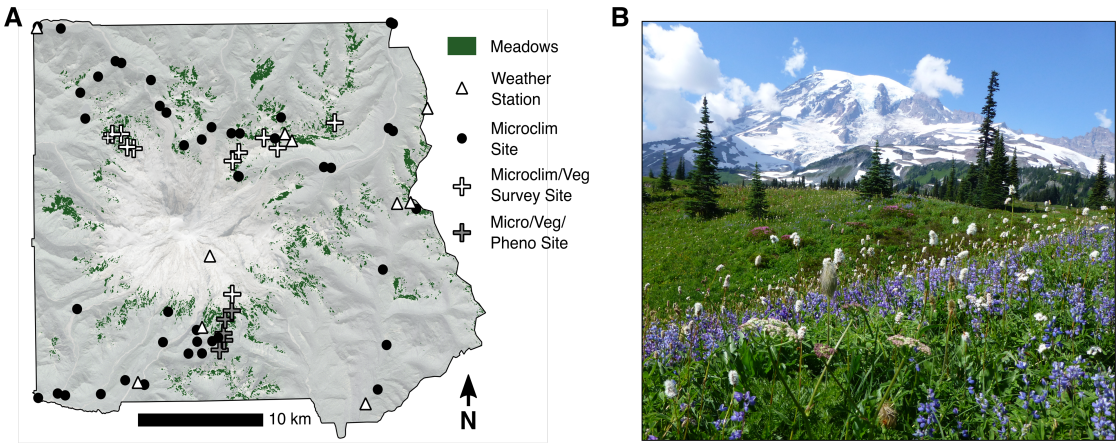

Figure 2.2: **A**. Distribution of subalpine meadow ecosystems at Mt. Rainier National Park in relation to weather stations (triangles), microclimate sensor sites (circles), microclimate and vegetation survey sites (white crosses), and sites where microclimate, vegetation composition and weekly phenology was monitored (gray crosses). **B**. The short growing season drives synchronous blooming of many species including arctic lupine (*Lupinus arcticus*, purple), Gray's lovage (*Ligusticum grayi*, white umbels in foreground), and American Bistort (*Polygonum bistortoides*, white spikes). Photo: E. Theobald.

logical match for each pair of meadows using a numerical integration technique. Finally, we modeled connectivity via animal-vectored pollen dispersal for each species in each meadow in each year using a graph representation of the meadow network and a simple dispersal model. We then summarized the results of this model by species and year, as well as an abundance-weighted average for each meadow in each year. For each species-year combination, we examined the sensitivity of our results to different parameter choices in the pollen dispersal model.

2.3.2 Study Areas

We examined how climate affects landscape flowering phenology and reproductive connectivity across subalpine and alpine meadows in Mt. Rainier National Park (Washington, USA). Mt. Rainier, located in the Cascade Range of Western North America, is a 4392 m stratovolcano with a broad zone of subalpine and alpine vegetation from 1400 to 2200 m

elevation. This zone is characterized by broken-canopy coniferous forest at low elevations and sparse clumps of krummholz conifers interspersed with alpine and subalpine meadows at higher elevations[83, 148]. Climatically, these environments have dry summers and cool, wet winters with large seasonal snow accumulation. Seasonal snowpack typically persists into the summer (June - August) thus the presence of snow substantially shortens the growing season for low-growing vegetation. The dominant non-conifer vegetation in the subalpine and alpine zones consists of short-stature deciduous shrubs and geophytes (Fig. 2.2B). The brief growing season contributes to spectacular seasonal displays of animal-pollinated wildflowers in these environments, a major draw of human visitors to Mt. Rainier National Park. Microtopography and the volcanic cone of Mt. Rainier produce significant climatic and ecological heterogeneity in the subalpine and alpine zones. Meadows on the eastern slopes receive approximately one-third less snow than meadows on the north and west slopes, which also receive more summer precipitation[43]. At the low-elevation boundary of the subalpine zone, snow melts approximately 3 weeks earlier than it does at the high-elevation boundary of the zone, and roughly 5 days earlier on the east slope of Mt. Rainier than on the west slope. However, the small-scale heterogeneity of snow disappearance timing is high, with approximately as much variation in last snow dates within meadows as between them in years with typical climate conditions[69]. We mapped subalpine and alpine meadow environments at Mt. Rainier using vegetation structural and spectral information from a high-density discrete return LiDAR dataset collected at Mt. Rainier in 2007 and 2008[159]. Details of the meadow mapping procedure can be found in Appendix B.1.

2.3.3 Interpolating Climate Drivers

Because climate drives both species distributions and phenology, we needed to accurately estimate the spatial distribution of plant-relevant climatic variables (snow and air temperature) across subalpine meadows at Mt. Rainier. Using geostatistical techniques, we interpolated small-scale spatial patterns in the climatic drivers of species distributions and phenologies using observations from weather stations and an extensive network of microclimate sensors.

Our approach produced 3 m resolution grids of the date of seasonal snowpack disappearance, as well as daily average air temperatures, and we combined these maps to produce high resolution gridded estimates of mean annual temperature (MAT) as well as warmth accumulation (growing degree-days) in the 50 days after snowmelt. The point observations driving our gridded geostatistical estimates are taken from an extensive network of microclimate sensors (520 snow sites, 111 air temperature sites) that we have maintained at Mt. Rainier since 2009, as well as 8 weather stations maintained by the National Park Service, US Department of Agriculture, NWS Cooperative Observer Network, and the Northwest Avalanche Center (Fig. 2.2A). Because we suspected that our results were sensitive to patterns of spatial autocorrelation in environmental drivers as well as the mean conditions, we used a variety of techniques to ensure that our predicted maps of microclimate are unbiased and reproduce patterns of spatial dependence that are seen in the observations, including comparisons against independent data, conditional Gaussian simulations, and Bayesian Kriging. The techniques we used to measure and geostatistically model snow disappearance and air temperature are described in detail in Appendix B.2, and B.3.

2.3.4 Predicting Species Geographic Distributions

We estimated the spatial distribution (i.e. probability of presence) of 16 common plant species across our landscape using data from a large structured vegetation survey and boosted regression trees (BRT)[56] . We selected focal species that were common (i.e. represented in vegetation surveys at more than 10% of vegetation survey sites), are animal pollinated, and found predominantly or exclusively in subalpine or alpine meadow environments at Mt. Rainier[15]. We derived binary (presence/absence) training data for species distribution modeling from vegetation inventories performed in 2011, 2012, and 2013 at network of 200 study plots (1 m^2) distributed in subalpine and alpine meadows in three areas of Mt. Rainier National Park (Fig. 2.2A): Paradise (100 plots), Sunrise (50 plots) and Spray Park (50 plots). In each area, 5 representative sites were selected across the elevation range of subalpine and alpine meadows. Within each site, 12 - 16 plots were established in a stratified

design spanning the range of local topography, with an equal number of plots placed near microtopographic ridges, midslopes, and depressions. This design ensured that sampling captured the range of habitat heterogeneity and vegetation composition at each site, as well as larger-scale variation across Mt. Rainier's elevation gradient (see [69] for a more detailed description of the survey design). Plot locations were recorded with a global positioning satellite system (Garmin GPSMap 62S) and manually adjusted to 3m accuracy by overlaying points on orthophotography and a high resolution digital elevation model. Potential predictors of species distributions, including microclimate measures (summer precipitation, mean annual temperature, mean date of snow disappearance, Appendix B.2, B.3), as well as vegetation structure (canopy cover, canopy height, near-infrared reflectance), and microtopography (elevation, topographic wetness) were extracted for each survey plot point using bilinear interpolation. For each focal species, we used the resulting data to train a predictive model using generalized BRT, a machine-learning technique that has been shown to work well for species distribution modeling using relatively small presence-absence datasets [181]. We fit the BRT models using the `gbm.step` function in the *R* package `dismo` [85] using a tree complexity of 10, a learning rate of 0.001, and a bag fraction of 0.5. Response functions were restricted to be monotonic to further reduce the potential for overfitting [55]. We assessed the predicted accuracy of each model using K-fold cross validation, and selected focal species that were represented in at least 10 plots, and had an average cross-validation AUC >0.75 for further consideration. After using the fit BRT models to predict species prevalence across subalpine meadows at Mt. Rainier, we visually assessed the predictions to ensure that the predicted distributions aligned with our field experience. In two cases (*L. arcticus* and *P. bistortoides*), this assessment identified problems with models that were remedied by removing problematic predictors, producing a simpler model with slightly lower cross-validation performance, but greater alignment with observed qualitative patterns of prevalence at Mt. Rainier.

2.3.5 Estimating Phenological Responses to Climate

To predict landscape patterns of flowering, we rely on a previously published [164] model of flowering phenology for each focal species that relates the daily presence or absence of flowering at a 1 m^2 study plot to day of year (DOY) using a non-linear function. The model was trained with 29,420 weekly observations of flowering presence and absence in a subset of 70 vegetation plots described in the previous section from 2009 to 2015. The model treats the presence or absence of flowering of a particular species i on a particular day j at a particular plot k as a Bernoulli-distributed random variable with a mean probability, α. This probability of flowering was allowed to vary by DOY according to a logit-quadratic function

$$logit(\alpha_{ijk}) = w_{jk} * (o_{jk} - DOY_{jk})^2 + h_{jk} \tag{2.1}$$

where the parameters w, h, and o control the width, height, and timing of peak flower, respectively, and we made each of these parameters linear (for h and o) or exponential (for w) functions of three climatic covariates: snow disappearance day (SDD), snow-free growing degree days (GDD) and soil moisture duration. The model was fit in a hierarchical Bayesian framework that allowed us to incorporate plot-level random effects and allowed estimates for rare species to borrow strength for more common species. Assessment against 10% of the observations withheld for testing indicated that the model performed well (AUC >0.88 for all focal species, mean 0.94), and we judged that it could be used to reliably extrapolate phenology to to the landscape scale. Although we lacked spatially comprehensive data on one climatic covariate, soil moisture duration, this climate driver has a significant influence on the phenology of only 5 of our 16 focal species, and the standardized effect sizes were small relative to the influence of the snowmelt and growing degree days[164]. In our projections of landscape phenology, we held this covariate at it's median value recorded at the phenology plots in each year. This allows year-to-year variation, but not spatial variation in soil moisture to contribute to predictions of landscape phenology. Additional detail about

the model structure, fitting procedure, and performance evaluation can be found in [164].

2.3.6 Mapping Landscape Phenology

We combined estimates of presence and flowering probabilities to predict the aerial extent of flowering for each focal species in each meadow in each day of the growing season from April 1st 2009 to November 1st 2015. Our predictions took advantage of spatially varying habitat heterogeneity that affects floristic composition as well as spatially and temporally varying estimates of key environmental drivers of phenology described above. Specifically, to derive daily maps of flower prevalence, we combined 3 m resolution gridded estimates of species probability of presence and their probability of flowering given presence using the following relation.

$$p(Flwr, Pres)_{ijk} = p(Pres)_{ik} * p(Flwr \mid Pres)_{ijk} \tag{2.2}$$

The resulting estimates of joint presence and flowering probabilities for each grid cell for each species on each day (a total of 1.44×10^{11} pixels), were summarized by adding flowering probabilities for each meadow polygon for each species on each day. Assuming that the estimates of presence and flowering probability are unbiased, this procedure yields estimates of the total area of meadow habitat that was occupied by at least one open flower of each focal species across the flowering season. These meadow-scale estimates of the progression of flowering account for the heterogeneity in the climate drivers of phenology within and between meadows, as well as differences in species abundances between meadows and between microhabitats within meadows. Because of the computational demands of this analysis, it was not feasible to propagate error forward from the fit phenology models to the landscape-scale estimates, but we verified that this error was small relative to differences between species. The full raster predictions required approximately 385 processor-hours to generate, and we performed the computation in *R* using the `raster` and `gdalUtils` packages on an Amazon Elastic Compute Cloud (EC2) instance (instance type c4.8xlarge, 32-core, 40 GB

RAM). We validated our meadow-scale predictions of flowering phenology by comparing them to independent observations of flowering taken by volunteer observers as part of our citizen science program, MeadoWatch (http://meadowatch.org), which we have operated at Mt. Rainier National Park since 2013. Details of this validation procedure can be found in Appendix B.4.

2.3.7 Measuring Intraspecific Phenological Mismatch

We computed the intraspecific phenological mismatch between focal species populations in all pairs of meadows within a minimum 5 km perimeter distance for each year of the study. Our measure of intraspecific mismatch was the proportional overlap in meadow-scale progressions of flowering area for each nearby meadow pair. Because meadows differ in total area and the relative abundance of focal species, meadow-scale progressions of flowering in all meadows pairs were normalized to have a summed area of 1 before comparison. The intraspecific match coefficient M a representative meadow pair (meadow indices $m = 1$ and $m = 2$) was then computed as

$$M_{1,2} = \frac{\sum_{j=60}^{305} \min(R_{j,m=1}, R_{j,m=2})}{\sum_{j=60}^{305} \max(R_{j,m=1}, R_{j,m=2})} \tag{2.3}$$

where normalized areas of flowering on day j in meadows $m = 1$ and $m = 2$ are $R_{j,m=1}$ and $R_{j,m=2}$, respectively. To reduce the computational demands, this value is only computed for days between March 1 (day 60), and November 1st (Day 305). This procedure yields an estimate of overlap for each pair of meadows that varies between 1 for populations that are completely phenologically matched and 0 for populations that are completely mismatched. Pairs of meadows with a minimum perimeter distance greater than 5 km were not assessed, because these distances exceed the maximum typical dispersal distances observed for insect pollinators. Computation for this stage of the analysis was done in *R* using the packages `dplyr` and `foreach`.

2.3.8 Modeling Connectivity

We used a simple pollen dispersal model to estimate the effects of intraspecific phenological mismatch on reproductive connectivity for focal species in our landscape. Our preliminary data suggest that functionally important generalist pollinators of common subalpine and alpine plant species at Mt. Rainier include bumblebees (genus *Bombus*), small solitary bees of many different genera, and flies in the orders *Syrphidae*, and *Muscidae*, with smaller contributions from lepidopterans, ants, and hummingbirds. Because our analysis considers many focal plant species that are known to be visited by diverse communities of pollinators, and our goal was simply to determine whether intraspecific phenological mismatch between nearby meadows has potential functional consequences, we used a simple, generic model of pollen dispersal. Our approach was similar to that of Lonsdorf et al.[108] in that it used a simple negative exponential dispersal kernel to represent pollinator movement, but in this case we also penalized dispersal by the phenological matching coefficient, M, described previously. To make this analysis computationally feasible, we created a simplified graph representation of the landscape [122] with meadows as nodes, and edges connecting all meadows within 5 km by minimum perimeter distance (1.1×10^6 connections per species).

As a measure of reproductive connectivity, we estimated total pollen influx for each species in each meadow in each year. Our pollen dispersal model calculates potential pollen influx, F, to meadow m from n other meadows for each species as

$$F_{m=1} = \sum_{m=2}^{n} A_m e^{-\beta D_{1,m}(1/M_{1,m})} \tag{2.4}$$

where A_m is the area of flowering for meadow m across the whole season, β is a parameter that affects how quickly dispersal decays with distance, $D_{1,m}$ is the minimum perimeter distance between the focal meadow and all other meadows m, and finally $M_{1,m}$ is the phenological matching coefficient between the focal meadow and another meadow m. Because we lack data on the absolute magnitude of pollen provision or removal rates across species, our estimates of pollen influx are on an area-weighted basis, with a single square meter of

predicted flowering area in an adjacent meadow ($D = 0$) contributing a single unit of influx. This means that the units of influx contributed by a given meadow are strictly proportional to the prevalence of flowering, and presumably represent different amounts of pollen for different species. Despite this limitation, these estimates are comparable across meadows and years within species, which allows us to infer the effects of climate on the relative, but not absolute magnitudes of pollen influx. Additionally, because the units of influx are on a common scale across species (square meters) they also allowed us to combine species-specific estimates of dispersal to derive overall measures of functional connectivity for each meadow. We did this by computing a weighted average pollen influx for each meadow across all focal species, with the weights corresponding to the estimated prevalence of each species in each meadow. We assessed the sensitivity of our results to assumptions about pollinator dispersal behavior by repeating the analysis using three different values for the parameter, β, that correspond to 95% of dispersal occurring within 500 m, 1000 m, and 3000 m, respectively. Computation for this stage of the analysis was done in *R* and *GrapHab* version 1.2.3[68]

2.4 Results

2.4.1 Validating Landscape Phenology

We found that meadow-scale estimates of patterns of landscape flowering phenology driven by climate closely corresponded to independent observations of phenology recorded by MeadoWatch volunteer citizen scientists (Fig. B.3). From 2013 to 2015, the years for which we have both landscape scale predictions of flowering and volunteer observations, 96.1% of volunteer observations fell within the predicted flowering interval for nearby meadows (those within 300 m). Correspondence was high for volunteer observations both in the vicinity of Mazama Ridge (95.5%), and near Glacier Basin (99.4%), but did vary by species (range 89.2% to 99.1%) and year (range 94.9% to 99.7%). We also detected a small early flowering bias in the meadow-scale predictions of approximately 4.3 days across species and years, but since volunteer observations are restricted to existing trails, this may be due to limitations of

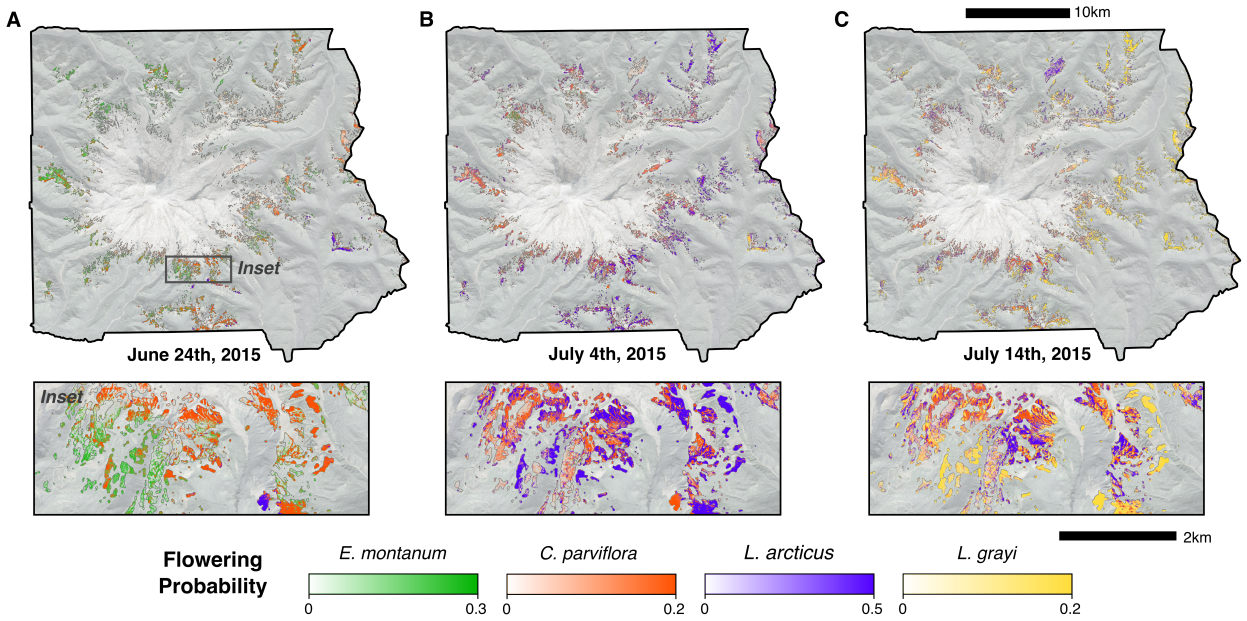

Figure 2.3: Estimated spatial and temporal patterns of flowering for four focal species, *Erythronium montanum* (green), *Castilleja parviflora* (red), *Lupinus arcticus* (blue), and *Ligusticum grayi* (yellow), highlighting spatial variation in flowering in 2015. Maps represent joint probabilities of presence and flowering across Mt. Rainier National park on June 24th (**A**), July 4th (**B**), and July 14th (**A**), 2015. Inset maps show patterns of flowering in the vicinity of Paradise.

the citizen science sampling design. Despite these limitations, we judged that our landscape phenology predictions were accurate enough to represent broad-scale variation in landscape patterns of flowering across Mt. Rainier National Park.

2.4.2 Landscape Phenology and Climate

We found that patterns of landscape flowering phenology at Mt. Rainier were extremely variable both over space and through time for our 16 focal species. At the meadow scale, seasonal peak flowering varied by an average of 51.7 days between the earliest-flowering (*Erythronium montanum*) and the latest-flowering (*Gentiana calycosa*) focal species in the community. Within species, peak flowering between meadows varied by as many as 57.5

days (*G. calycosa*), and standard deviations of peak flower timing among meadows varied between 15.7 and 19.8 days across species. The average duration of flowering at plot scales varied between 11.0 and 22.3 days across focal species, but these patterns were relatively poor predictors of average meadow-scale ($n = 16$, $R^2 = 0.274$, $T = 2.748$, $p = 0.0124$) and landscape-scale durations of flowering ($R^2 = 0.0143$, $T = 0.539$, $p = 0.596$). This was because species had unique geographic distributions, and large-scale patterns of flowering duration depended more strongly on the range of environments over which a species was distributed.

In 2015, a record low-snowpack year that closely mimicked expected typical climatic conditions at Mt. Rainier under unabated climate change[1], we observed unusual patterns of landscape phenology (Fig. 2.3). This year was characterized by extremely early landscape-scale peak flowering (average of 42.1 days earlier than normal all focal species), new patterns of co-flowering on plot scales ("phenological reassembly", detailed in[164]), and large differences in flower timing across Mt. Rainier's elevation gradient driven by extremely early snow disappearance near the lower elevation boundary of the subalpine zone. We estimated that average peak flowering anomalies were 47.3 days (SD 11.5 days) early at low elevation meadows (between 1400 - 1600m) in 2015, compared to 29.0 (SD 10.3) days early at the high elevation boundary of the meadow zone (between 2000 - 2200 m, Fig. 2.4B). We also observed larger than normal differences in snow disappearance and flowering between east and west slopes of Mt. Rainier in 2015 (mean 9.46 days, compared to 5.18 for 2009 - 2014). These effects were moderated somewhat by cool spring temperatures after snow melt, which caused the peak community flowering (the day on which the largest area of a meadow is in bloom) to be delayed by an average of 7.89 days relative to snow melt in 2015.

2.4.3 Intraspecific Phenological Mismatch

Heterogeneous patterns of landscape flowering phenology at Mt. Rainier produced intraspecific phenological mismatch between nearby meadows (Fig. 2.4). In years with typical climates (2009 - 2014), plant populations in meadows separated by distances of less than

200 m had an average phenological matching coefficient of just 0.461 (SD 0.0664 across focal species). For all focal species, phenological mismatch between meadows increased with geographic distances from 200 m to approximately 2000 m, before stabilizing at greater distances (Fig. 2.4C). Phenological mismatch increased most steeply between 0-2000 m, which are similar distances to the average geographic distance between the lowest-elevation and the highest-elevation meadows on the slopes of Mt. Rainier. This indicates that the declines are mainly due to differences in phenology across Mt. Rainier's elevation gradient. Phenological mismatch also increased more rapidly with distance in 2015 than in years with more typical climates, driven by increased heterogeneity in the climatic drivers of phenology (Fig. 2.4C), as well as species-specific responses of flowering duration to altered climatic conditions (see below).

2.4.4 Species-specific Patterns of Vulnerability to Fragmentation

Overall, we found that intraspecific phenological mismatch in typical climatic conditions experienced at Mt. Rainier from 2009 to 2014 decreased reproductive connectivity of populations of our 16 focal plant species by 37.3 to 53.1% (mean 44.8%, SD 4.81 %) relative to a hypothetical scenario where phenology is perfectly matched across all pairs of meadows (Fig. 2.5A). This decrease in connectivity was strongly related to the degree to which climatic heterogeneity decreases the average phenological match between nearby meadows ($n = 16$, $R^2 = 0.95$, $T = 16.9$,$p < 0.001$), and was also strongly negatively related to year-to-year variability in estimated pollen flux across species ($R^2 = 0.98$, $T = -37.7$, $p < 0.001$), Fig. 2.5B). Further, we found that early snow disappearance conditions in 2015 reduced phenological matching and connectivity compared to years with typical climates for 13 of 16 focal species (Fig. 2.5C), a result that was robust to large variations in our assumptions about pollinator dispersal distances. Mismatch had a stronger influence on connectivity for species that were restricted to moist microsites ($R^2 = 0.440$, $T = -3.31$, $p = 0.00511$, Fig. 2.5D). Species-specific patterns of vulnerability to further fragmentation in 2015 were unrelated to year-to-year variability in connectivity ($R^2 = 0.0176$, $T = -0.500$, $p = 0.624$, Fig. 2.5B)

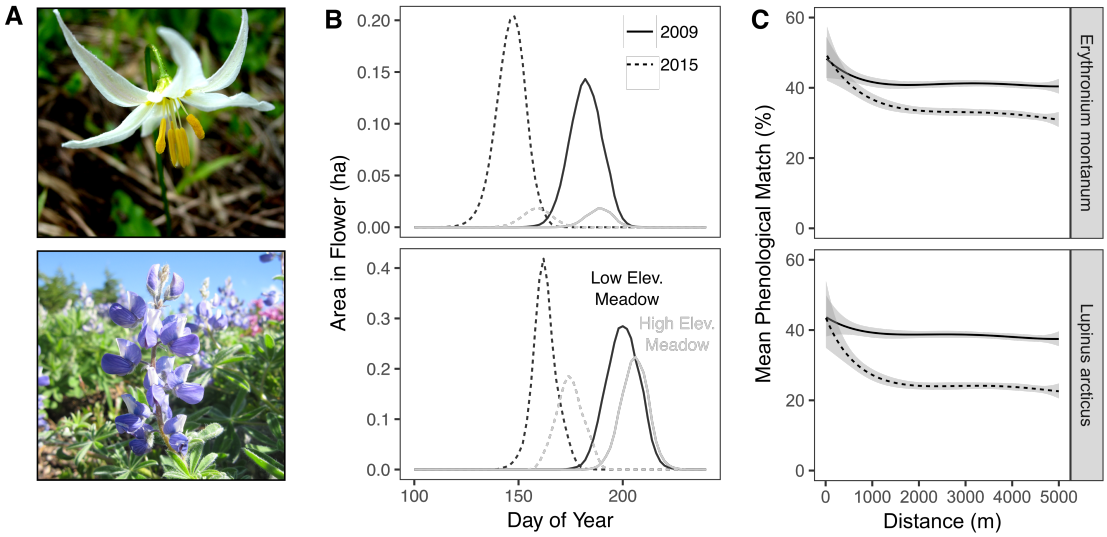

Figure 2.4: **A**. Flowering phenophases of two focal species, avalanche lily (*Erythronium montanum*) and arctic lupine (*Lupinus arcticus*). **B**. Meadow-scale progressions of flowering for these two focal species in two representative meadows in the vicinity of Glacier Basin. This pair of meadows, which differ in elevation by approximately 600 m, have different species compositions and phenologies and are exposed to different amounts of change in climatic drivers of phenology leading to heterogeneous responses of meadow-scale flowering in 2015, an early snow melt year, compared to 2009, an average snow melt year. **C**. Average phenological match across a sample of 100,000 pairs of meadows as a function of geographic distance for the two focal species in 2009 and 2015. Different species distributions and phenological responses to climate drive larger decreases in phenological match for arctic lupine than for avalanche lily.

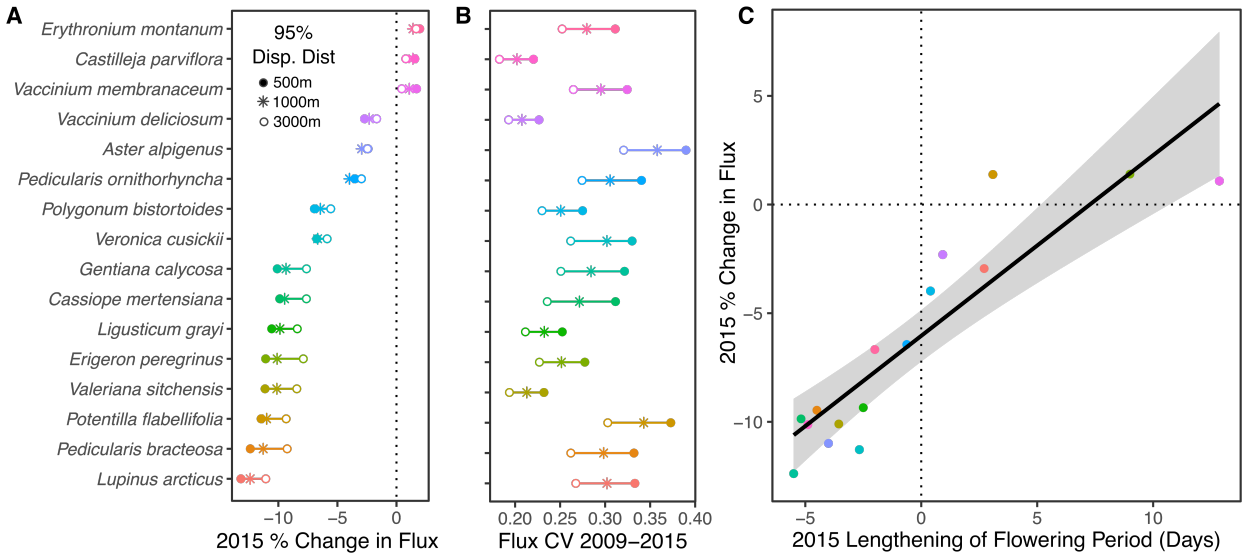

Figure 2.5: Species-specific patterns of vulnerability to decreased reproductive connectivity in a changing climate. **A**. Average decrease in pollen influx in 2015 compared to years with typical climates (from 2009 to 2014). Symbols represent different modeled dispersal kernels with 95% of pollen flux occurring within 500 m (asterisks), 1000 m (filled circles), and 3000 m (open circles). **B**. Coefficient of variation (SD/mean) in pollen influx from 2009 to 2015. Symbols are identical to A. **C**. Estimated decrease in pollen flux in 2015, an early snow melt year, compared to average annual influx from in 2009 to 2014. **D**. Relationship between moist-site specificity and average decrease in pollen flux due to phenological mismatch. **E** 2015 decrease in pollen flux as a function of species-specific changes in the plot scale duration of flowering in 2015 compared to the mean of typical years (2009 2014) assuming 1000 m dispersal distances.

and were only weakly related to plot-scale durations of flowering ($R^2 = 0.265$, $T = -2.25$, $p = 0.0413$), but were highly sensitive to how early snow melt conditions in 2015 affected the duration of flowering ($R^2 = 0.81$, $T = -7.64$, $p < 0.001$). This response varied considerably across focal species, with most species shortening their flowering period in 2015 in response to the early snow melt and lower soil moisture, however, 5 species lengthened their average flowering period (Fig. 2.5E). The species with shorter flowering duration in 2015 showed greater decreases in connectivity (mean 9.67%) than the 5 species that lengthened flowering duration (mean 0.892%). Just three species, *Erythronium montanum*, *Vaccinium membranaceum*, and *Castilleja parviflora*, showed increases in connectivity in 2015 relative to typical (2009 - 2014) climatic conditions. The results reported above assume 1000 m maximum dispersal distances, but the qualitative patterns described here are robust to this assumption.

2.4.5 Meadow-scale Patterns of Vulnerability

Spatial and temporal patterns of overall functional connectivity, estimated by computing the weighted average pollen influx for each meadow in each year across all focal species, showed distinct geographic patterns of vulnerability to fragmentation driven by intraspecific phenological mismatch between nearby meadows (Fig. 2.6). Climatically marginal meadows near the low and high-elevation boundaries of the meadow zone were, on average, less than half as well connected as meadows near the center of their elevation range (Fig 2.6A). We also found that meadow complexes that attract the most visitors due to their wildflower displays, including meadows in the vicinity of Paradise and Sunrise, are particularly well connected, whereas smaller and more geographically isolated meadow complexes are considerably less well connected by pollen dispersal (Fig. 2.6B). These isolated meadows also show much larger year-to-year variability in overall connectivity. Assuming that 95% of pollen flux occurs over distances less than 1 km, meadows located at 1400 m and 2200 m, had a coefficient of variation (CV) in pollen flux (annual SD / mean) of approximately 1.4, whereas connectivity was much more stable from year to year for meadows located at 1800 m (CV 0.33, Fig.

2.6C). Overall, we estimated that early snow melt conditions in 2015 reduced weighted average pollen flux between meadows by approximately 8.3% compared to years with more typical climatic conditions. These decreases were much larger (mean -17.0 %) in climatically marginal meadows (1400 - 1500 m and 2100 - 2200 m) than in meadows near the center of the meadow zone (Fig. 2.6E).

2.5 Discussion

Our study provides the first landscape-scale assessment of intraspecific phenological mismatch driven by climate and its implications for the functional connectivity of plant populations. Patterns of flowering across subalpine and alpine meadows at Mt. Rainier National Park were extremely heterogeneous both spatially and temporally (Fig. 2.3), and were characterized by intraspecific phenological mismatch between populations in nearby meadows (Fig. 2.4). For example, a typical plant population in a typical meadow in our study was only 46% phenologically matched with populations in closely neighboring meadows, those less than 200 m distant, and this match declined to an average of 34% at distances greater than 2 km. Using a simple model of pollinator dispersal, we estimated that intraspecific phenological mismatch in our landscape decreases the potential flux of pollen between meadows by approximately 45% in typical climatic conditions, a result that was robust to widely different assumptions about pollinator behavior. Further, we found that climate change analog conditions experienced at Mt. Rainier in 2015 radically shifted the landscape-level progression of flowering and decreased predicted pollen dispersal compared to years with more typical climatic conditions (Fig. 2.5). Phenological responses to early snow melt and species geographic distributions both contributed to species-level variation in intraspecific phenological mismatch and vulnerability to further fragmentation under climate change. Specifically, species that were restricted to moist microsites and species that shortened their flowering duration in response to early snow melt conditions showed increased intraspecific mismatch and reduced connectivity relative to other species (Fig. 2.5).

Overall, we found strong support for some, but not all, of our *a priori* predictions regard-

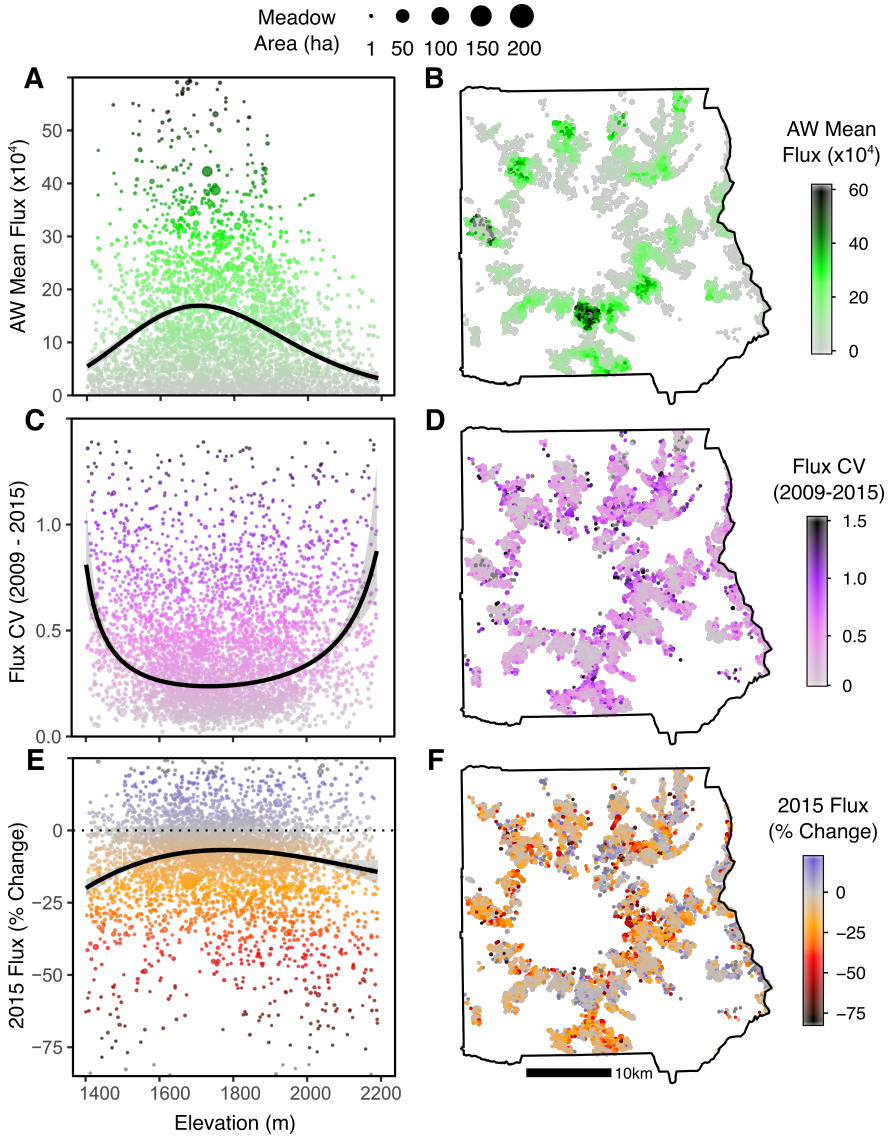

Figure 2.6: Geographic patterns of meadow-scale pollen flux as an abundance-weighted average across all focal species, assuming 1000 m maximum dispersal distances. Symbol size is proportional to meadow area in all panels. **A**. Mean 2009 to 2015 area-weighted flux across the elevation gradient of subalpine meadows at Mt. Rainier. Black line represents a cubic polynomial fit. **B**. Map of pollen flux depicted in A. **C**. Coefficient of variation (SD / mean) area-weighted pollen flux from 2009 to 2015 across the meadow elevation gradient. Black line represents a cubic polynomial fit **D**. Map of quantities depicted in B. **E** Percent change in pollen flux in 2015 compared to the 2009 2014 average. Black line represents a cubic polynomial fit. **F** Map of quantities depicted in E.

ing intraspecific phenological mismatch. In accordance with our expectations, we found that intraspecific mismatch was sensitive to year-to-year variation in the spatial heterogeneity of important climatic drivers of phenology, and was particularly sensitive to differences in snow melt dates across the elevation range of our study sites. We also found limited support for the notion that species that were distributed across smaller ranges of elevations and larger ranges of microhabitats were less vulnerable to increasing intraspecific mismatch in a warming climate. The small size of our suite of focal species (16) considerably limits our statistical power in detecting species-specific drivers of vulnerability, however. Surprisingly, the plot-scale duration of flowering in typical climate conditions was a poor predictor of species vulnerability to mismatch in our system, contrary to our *a priori* expectation. This was because flowering durations at the scale of individual plots were only weakly related to average flowering durations at the scale of whole meadows and hence the opportunity for mismatch between them. Instead, idiosyncratic fine-scale species distributions with respect to snow duration, micro-topography, and hydrology exposed species to different amounts of spatial and temporal heterogeneity in the climatic drivers of phenology. Although this issue has been raised elsewhere [53, 91], few studies explicitly assess how fine-scale species distributions affect their exposure to microclimate variability and change, and incorporating this small-scale heterogeneity into models of species responses to climate change is a major ongoing challenge [124, 153, 170].

The steep climatic gradient, rugged microtopography, and dramatic rain and snow shadow provided by Mt. Rainier's volcanic cone are likely the major drivers of spatial heterogeneity in flowering in our study. Meadow plants at low elevations and on Mt. Rainier's drier eastern slopes flowered as much as 6 weeks earlier than normal in 2015, experiencing the largest decreases in average connectivity during that year (by 15 to 70%). These ecologically marginal meadows were already poorly connected by pollen dispersal in typical climatic conditions, and they also experienced relatively large year-to-year variations in connectivity driven by climate variation (Fig. 2.6). It is likely that intraspecific phenological mismatch is less dramatic in regions with more moderate topography and less variable microclimates,

but these patterns should not be unusual in montane landscapes, and our results point to the under-appreciated importance of environmental heterogeneity in mediating responses of species and ecosystems to climate[172, 112]. We estimated that the average pollen influx to meadows near the margins of species elevation ranges were less than half as large as near range centers, driven by a combination of increasing geographic isolation and increasing phenological mismatch between range centers and range edges. Although beyond the scope of this study, this result supports the notion that phenology could play a role in maintaining species range limits [34, 86, 102].

Relatively few previous studies provide a basis for comparison with our work. A handful of studies across temperate, tropical, and alpine systems have found marked intraspecific differences in flowering phenology at sites in different positions along elevation[188, 73] and other climatic gradients[178], but other studies [143, 176] have found little evidence for asynchronous flowering of populations in different environments. Flowering synchrony is thought to be adaptive for most plants[92, 59](but see[177]), a view supported by evidence from temperate and tropical shrubs [10, 17], and wind-pollinated trees[99], but we are not aware of any previous work that assesses how climate impacts landscape patterns of flowering, or the effects of resulting changes in flowering synchrony on pollen dispersal potential. Our study, with a taxonomic and geographic scope that spans the elevation ranges of many species, provides unique insights into how species distributions and phenologies interact with climate to drive variation in flowering synchrony and intraspecific phenological mismatch at landscape scales.

The ultimate consequences of the reduced connectivity we found for meadow plant populations in warming climatic conditions are difficult to predict without further work. Existing literature suggests that decreasing demographic connectivity in networks of populations that are currently linked by dispersal could leave them more vulnerable to environmental change[78, 97]. The impacts of habitat fragmentation, another mechanism that can decrease demographic connectivity, have been shown to reduce effective population sizes[186], evolutionary potential[4], and the resilience of populations to disturbance[174, 57]. We suspect

that intraspecific phenological mismatch could play a similar role, although our efforts to quantify these effects are ongoing. Moreover, numerous studies emphasize the importance of outcrossing in plant populations, and decreases in pollen flux between meadows could reduce breeding distances and heterozygosity[19, 33]. Reduced dispersal, especially at the "trailing edge" of species distributions, also has important evolutionary consequences. It may improve the effectiveness of climate as an agent of selection if it reduces swamping gene-flow, thus increasing the potential for evolutionary processes to buffer the negative effects of climate change[14]. This is possible in some systems, but it depends on the existence of substantial standing variation in heritable traits linked to performance in a warming climate and effective population sizes that are large enough for selection to be effective in the face of genetic drift[157, 25].

We suspect that our analysis underestimates the potential for climate change to drive reductions in pollen dispersal in this system. For a minority of our focal species (5 of 16), the relatively cool air temperatures that followed snow melt in 2015 delayed floral development and lengthened flowering in low-elevation meadows where seasonal snow pack disappeared before the onset of climatological summer. This lengthening of flowering reduced the potential for intraspecific phenological mismatch between nearby populations, and caused our estimates of between-meadow pollen dispersal to be less dramatically reduced than we would expect if both snowpack and spring temperatures in 2015 tracked conditions forecast for the late 21st-century [117]. Moreover, whether lengthened early-season flowering increases dispersal depends on the assumption that pollinator services are equally abundant throughout the year, an assumption that is unlikely to be valid, especially since the activity and pollination performance of the most common generalist pollinators in our landscape, bumblebees and syrphid flies, almost certainly is reduced at cooler temperatures [110, 150], and only bumblebee queens are actively foraging during the early season in temperate subalpine environments [139]. Unfortunately, we currently have insufficient data on the phenology of pollinator activity in this system, or a detailed understanding of pollinator behavior that would allow us to represent animal-vectored pollen dispersal in a more sophisticated way

[131]. Our simple model, based on existing literature [108], is computationally efficient enough to apply across a large landscape like Mt. Rainier, but follow-up studies are necessary to tease apart how intraspecific phenological mismatch interacts with floral resources and pollinator abundance, activity, and behavior.

Although not our main objective in this study, our work also highlights how small-scale spatial heterogeneity in species' prevalence and phenology affects the duration of flowering across spatial scales. The average flowering period of a typical focal species at the scale of a 1 m^2 quadrat was approximately 17 days in length, but this lengthened to an average of 24 days at the scale of whole meadows, and was approximately 71 days across the entirety of the subalpine ecosystem in Mt. Rainier National Park. This scale-dependence in the durations of phenological phases has been mentioned elsewhere[8], but this study gives us the first quantitative estimates of the magnitude of this effect in plant reproduction. Scale-dependence in landscape phenology means that both intraspecific and interspecific phenological mismatch are also scale-dependent phenomena in heterogeneous landscapes, an issue that is rarely addressed in field studies (but see [87]). In the future, we hope to use the maps of landscape-scale phenology described in this work to examine the spatial scaling of flowering phenology in detail. If general scaling relationships [146, 12] between the duration of flowering and environmental heterogeneity emerge, then these relationships could be used to quantitatively link different kinds of observations, for example, structured field surveys and herbarium specimens, collected at different implicit spatial grains.

This study adds to the large and growing literature on how phenology and climate interact to affect ecological, evolutionary, and biogeochemical processes that will have important consequences for ecosystems and human society as climate change accelerates. We demonstrated that climate plays a key role in mediating the amount and spatial structure of pollen dispersal in plant communities, and that climatic conditions similar to those expected in the late 21st century under unabated climate change cause reductions in reproductive connectivity across a diverse suite of perennial montane plant species. The mountain meadow ecosystems that these species inhabit are already existentially threated by global change,

including rapid alteration of hydrology[61], tree line advance [81], and atmospheric nitrogen deposition[18, 118]. Our study suggests that rapidly changing climates may also reshape spatial patterns of plant reproduction and pollen dispersal, a key ecological process. Although our study area is unique in many ways, we suspect that the dynamics and vulnerabilities we describe at Mt. Rainier are common throughout montane ecosystems with snow-dominated climates. Anthropogenic warming is raising rain/snow transition elevations worldwide[76], driving increasing differences in hydroclimate and snow duration between the low-elevation and high-elevation boundaries of subalpine ecosystems. We show that these changes in climate drivers may increase the potential for intraspecific phenological mismatch, especially in plant populations on mountain slopes that are close to the rain-snow transition zone. These slopes harbor a significant fraction of the temperate zone's biological diversity, and understanding the consequences of altered connectivity in these systems will improve our ability to forecast the ecological impacts of climate change.

Chapter 3

CROWD-SOURCED DATA REVEALS PHENOLOGICAL MISMATCH BETWEEN SOCIAL AND ECOLOGICAL SYSTEMS DRIVEN BY CLIMATE

3.1 Abstract

As climate change accelerates, it is critical for scientists and policymakers to understand how climate influences the links between ecosystems and their social context. Surprisingly, despite increased attention to coupled analyses of social-ecological systems, there have been few studies that simultaneously measure how changes in climate drive changes in the temporal distribution of natural resources and the people that use those resources. Here we measure how climate influences the spatial and temporal match between human visitors and seasonal displays of subalpine wildflowers at Mt. Rainier National Park, where wildflower blooms are a key visitor draw. We use a large, field-validated dataset derived from the Flickr photo sharing service and volunteer citizen scientists to show that the phenological match between these ecological and social systems is sensitive to the date that seasonal snowpack disappears. Early snow melts, comparable to conditions predicted in the late 21st century, cause reduced temporal overlap between wildflowers and park visitors (by 17.4 to 48.9 %). In-line with ecological and social theory, we expect social-ecological mismatches in phenology to be common in systems where users of natural resources (i.e. park visitors) have imperfect information about climatic drivers of their resource, and where seasonal shifts in their behavior is constrained by non-climatic factors. Recent dramatic growth in the volume of georeferenced citizen observations coupled with recent advances in machine learning, will soon make it feasible to test these hypotheses at very large spatial scales.

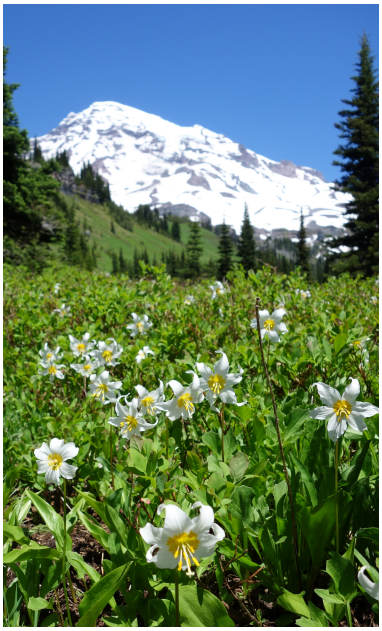

Figure 3.1: The lilies and the lines of the mountain. Avalanche Lily (*Erythronium montanum*) is one of the first wildflowers to bloom after seasonal snowpack disappears in the subalpine zone of Mt. Rainier National Park. This photo was taken from Mildred Point on June 7th, 2015. Credit: National Park Service

3.2 Introduction

When John Muir wrote of his preparations to summit the south side of Mt. Rainier in August of 1888, he unwittingly recorded an important piece of ecological information:"Here we lay all the afternoon, considering the lilies and the lines of the mountain"[128]. The lilies, almost certainly Avalanche Lily (*Erythronium montanum*, Fig. 3.1) and Glacier Lily (*Erythronium grandiflorum*), are among the earliest and most ephemeral wildflowers to emerge after snow disappears in the subalpine ecological zone of the Cascade Mountains [165]. Muir's party was camped near the upper-elevation limit of that zone, the highest elevation where they could find forage for their pack stock. Thus, Muir became one of the first persons to record the state of plant phenology in an ecosystem he described as "the most luxuriant and the most extravagantly beautiful of all the alpine gardens I ever beheld in all my mountain-top

wanderings." [128]

Today the subalpine ecosystem in Mt. Rainier National Park attracts more than a million visitors annually, and many leave geographically referenced digital traces of their visits on social media. Embedded in these digital traces is a surprisingly rich and largely untapped trove of information about how those visitors use the ecosystem for recreation, and how that ecosystem and its human users responds to seasonal and annual variation in climate. Although georeferenced social media data has been recently used to map cultural landscape values [163, 187], visitation rates to natural areas [185, 154], and environmental events such as snowfall [175] and natural disasters [44] this data has seen limited application in environmental science [46]. Despite the increasing emphasis on understanding coupled social-ecological systems [132, 119, 42], we are not aware of any previous work that uses crowd-sourced data to simultaneously track the phenology of these coupled systems or estimate how the spatial and temporal matches between them are affected by changes in climate. The few studies that have examined the effects of climate on the temporal match between people and ecosystem services [169] do so with ethnographic or survey methods with limited spatial and temporal resolution. This contrasts with the large and diverse body of ecological literature that explores how climate affects the timing and intensity of interactions between the non-human components of ecosystems (phenological mismatch) [54, 51]. This study aims to bring high spatial and temporal resolution data derived from social media to bear on the question of whether changes in climate can cause mismatches in space and time between people and the services provided by ecosystems. Specifically, we focus on the effects of changing patterns of snow disappearance on the match between mountain visitors like Muir, and the wildflower displays that captivated him and first popularized Mt. Rainier as a tourist destination.

To measure these relationships between snow, visitors, and wildflowers, we manually classified phases of plant reproductive phenology in 17404 accurately geotagged photos taken in Mt. Rainier's subalpine zone from 2009 to 2015 (Fig. 3.2B). Of these, approximately 11% contain recognizable flowers of ten common wildflower species (Table C.2), which we selected *a priori* because these conspicuous species were also tracked by a citizen-science program that

has operated at Mt. Rainier since 2013 [180]. We demonstrated good agreement between observations of both visitor and flower phenology estimated from photos, and those estimated from other sources, including citizen-science observations and National Park Service visitor records (Fig. C.2, C.3). The Flickr photo sharing service has maintained a relatively stable user base over the time-period of the study, coinciding with the widespread public adoption of cameras and smartphones with embedded GPS technology. The study interval also contains extreme annual climate variation, including years among the latest (2011, Fig. 3.2A) and the earliest (2015, Fig. 3.2B) seasonal snow disappearances in the century-long climate record at Mt. Rainier (Fig. 3.2C). The large inter-annual variation in climate, and the relatively small annual variation in the volume and spatial distribution of Flickr records (Fig. C.4), allowed us to piece together a snapshot of how this contemporary social-ecological system responds to annual variation in climate.

3.3 Methods

3.3.1 Retrieving Photos

We used the Flickr Application Programming Interface (https://www.flickr.com/services/api/) to retrieve metadata on all publicly accessible and accurately geotagged photos (accuracy codes 15 and 16) taken in the subalpine elevation zone (1200 - 2400 m) at Mt. Rainier National Park between January 1st 2011 and December 31st 2015. Records were downloaded on October 26th 2015, and additional records covering the 2015 season were downloaded on January 24th 2016 The resulting database of photos (17403 records) was used to track human visitation and wildflower blooms.

3.3.2 Measuring Park Visitation

As an indicator of park visitation, we counted the number of unique Flickr users per day in our photo database for all days from January 1st 2009 to December 31st 2015. We used the number of unique users instead of the number of photos because it was in closer agreement

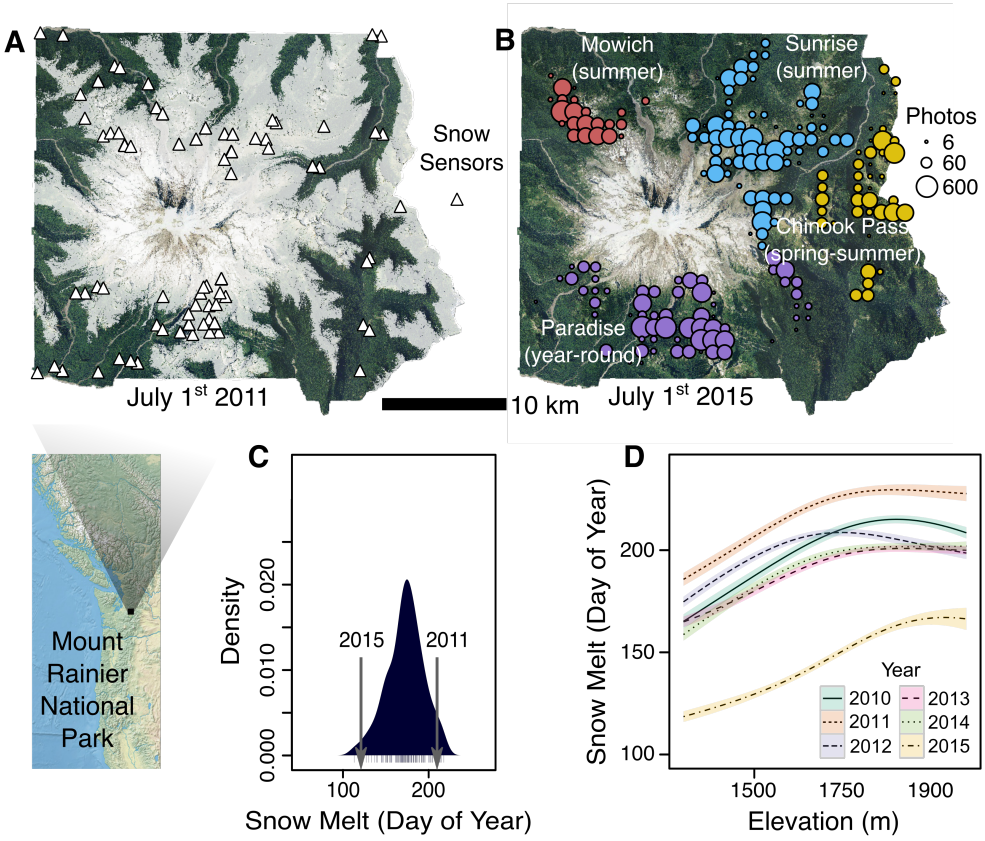

Figure 3.2: **A**. Distribution of snow duration sensors used to estimate the date of snow disappearance for each photo location. There are 3 - 16 sensors installed at each site to account for small-scale heterogeneity in snow accumulation and melt. The sensor locations are overlaid on a map showing predicted snow cover on July 1st 2011. **B**. Distribution of geolocated Flickr photos used in the analysis. The colors correspond to different centers of activity in Mt. Rainier National Park. The photo locations are overlaid on a map of predicted snow cover on July 1st 2015, one of the earliest melts on record. **C**. Distribution of modeled snow disappearance dates in the vicinity of Paradise from 1918 - 2015. **D**. Statistically estimated mean dates of snow disappearance across the lower slopes of Mt. Rainier for different years of the study when other covariates are held at their median values (Table C.1, Fig. C.1). Shading represents 95% confidence bands in the mean fit.

with National Park Service visitor records for the time period (Fig. C.2) and has recently been shown to be a reliable indicator of visitor use across a large network of US National Parks [154]. For the analysis of visitation in different areas of the park, we grouped the photos by which center of access (Paradise, Sunrise, Chinook Pass, Mowich Lake) was closest by geographic distance.

3.3.3 Classifying Photos

In each photo downloaded from Flickr, we manually identified reproductive phenological phases (budding flowers, flowering, ripening fruit, and releasing seeds) of 10 focal wildflower species with conspicuous flowers that are unlikely to be mis-identified (Table C.2). If a photo contained flowers of any of the 10 focal species, it was coded as "focal flowers present", and if it contained none of the focal species it was coded as "focal flowers absent". If a focal species could not be definitively identified in the photo it was recorded as absent.

3.3.4 Estimating Snow Disappearance Dates

We predicted the day of snow melt for each photo location using a linear mixed-effects model fit to data from a network of snow duration sensors maintained at 190 sites across Mt. Rainier's elevation gradient from 2009 to 2015. The sensors, Onset iButton and HOBO Pendant temperature loggers, were installed at the soil surface and retrieved each summer. In Mt. Rainier's maritime climate, the soil surface stays at an equilibrium of 0°C when covered by more than a few inches of insulating snow [69], allowing us to accurately pinpoint the last date of snow cover in each temperature record. The most parsimonious model for predicting snow melt date (Table C.1), incorporated fixed effects of elevation, year, longitude, slope, and relative elevation as well as a random effect of site. The model's fixed-effects explain 91% of the variation in snow melt date, and has an average absolute prediction error of 12.9 days. The residuals from the model were approximately spatially independent (Fig. C.1). Model fitting was done in *R* using the package `lme4`.

3.3.5 Modeling Visitor Phenology

We modeled daily human visitation to the subalpine zone of Mt. Rainier National Park, as indicated by the number of unique Flickr users taking photos, using a Bayesian generalized nonlinear mixed-effects model. Daily visitation in the non-winter season (April - November) was treated as a random variable with a negative binomial distribution. We chose a unimodal, quadratic functional form for the relationship between the mean number of unique users and the day of year (DOY):

$$\log(y) = height + width * (opt - DOY)^2 \tag{3.1}$$

We also allowed the optimum and height of each curve to be linear functions of estimated Snow Disappearance Day (SDD) with characteristic slopes and intercepts according to the following:

$$height = height_{intercept} + height_{slope} * SDD \tag{3.2}$$

$$opt = opt_{intercept} + opt_{slope} * SDD \tag{3.3}$$

Width was modeled as a negative exponential function of SDD:

$$width = -1 * \exp(width_{intercept} + width_{slope} * SDD) \tag{3.4}$$

For the aggregate analysis (Figs. 3.4, C.5, Tables C.3, C.4), we allowed the height of each curve to have a random intercept for each year, day of week, and access point, with all other parameters in common. For the analysis that compared different access points (Fig. 3.5, Table C.3), we also allowed the width and optimum to have fixed intercepts and slopes that varied by access point. In all models, true SDD was represented as a latent (unobserved) random variable with a variance equal to the prediction variance of the snow model to account for uncertainty in snow melt date. Parameters were fit via MCMC in *JAGS* version 4.2 (http://mcmc-jags.sourceforge.net) using diffuse priors (truncated normal

distributions for slopes and intercepts, gamma distributions for random effect variances). Model convergence was confirmed visually, as well as using the Gelman-Rubin statistic (upper CI for all parameters <1.1). Fit parameters for the aggregate visitor model are described in Table C.4.

3.3.6 Modeling Flower Phenology

We took a similar nonlinear approach to modeling wildflower phenology as we used for visitor phenology, but in this analysis we treated the presence or absence of any focal species in a photograph as a Bernoulli distributed random variable. The underlying deterministic form of the model is identical to the model for visitors, except for the use of a logit link function for the response instead of a log link. For the aggregate analysis, we allowed the height of the fit curve to have a fixed intercept, as well as a zero-centered random intercept that varied by user, which allows each Flickr user to have a different intrinsic probability of capturing a flower in a photo. Like in the visitor model, in the aggregate analysis we allowed width and optimum to be related to latent true SDD through either common intercepts and slopes (aggregate analysis), or separate fixed intercepts and slopes by side of the mountain and visitor access restrictions (site-specific analysis). Fit parameters of the aggregate model are described in Table C.4.

3.3.7 Measuring Phenological Mismatch

We measured phenological matching between visitors and wildflowers by numerically computing the area of overlap in the fit phenology functions normalized by the area under each curve. Normalizing each curve to be a density (i.e. integrate to 1) allowed us compare phenological responses of park visitors and wildflowers measured on different scales (i.e. counts for visitors and probabilities for flowers). This normalization is possible because the functional forms we fit are all unimodal and concave-down, and thus have a finite integral. Computing overlaps of normalized phenological curves gives us an estimate of phenological mismatch that varies between zero (complete mismatch) and one (perfect matching) with uncertainty

bounds generated by overlap estimates from each of 1000 posterior MCMC samples of the fit parameters for each model. The computation for this analysis was done in *R* using the function `integrate`. Data and code for this analysis is available on GitHub: (https://github.com/ibreckhe/social_ecological_phenology).

3.4 Results

3.4.1 Social and Ecological Sensitivities to Climate

We found that the phenology of both park visitors and wildflowers was sensitive to the date of snow disappearance (Fig. 3.3). Using a Bayesian non-linear model, we estimated that seasonal peaks of human visitation came approximately 5.5 days earlier for every 10 days earlier snow disappearance (Fig. 3.4, 95% CI 3.86 to 7.08 days), while peaks of wildflower blooms came approximately 7.1 days earlier (Fig. 3.4A, 95% CI 6.56 to 7.83 days). Early melt conditions were accompanied by a lengthened season of human visitation, with the peak period (including 50% of the total season's visitors) lengthening by 4.1 days for every 10 days earlier melt (95% ci 2.63 to 6.12 days). By contrast, every 10 days earlier snow disappearance shortened the period including 50% of the probability density of observing wildflowers by 0.36 days (95% CI 0.28 to 0.52 days). Details of the model structures and model selection procedures can be found in the methods, and further details are described in the supplementary material (Tables C.3, C.4, Figs. C.5, C.6).

3.4.2 Effects of Climate on Phenological Matching

In all, the lengthening visitor season, the shortening wildflower season, and the differing sensitivity of peak visitation and peak flowering to snow disappearance date caused the match between people and wildflower blooms in this system to decrease by 35% in early melt conditions typical in 2015 vs. late melt conditions typical in 2011 (95% ci 17.4 to 48.9%, Figs. 3.4B, 3.4C). This mismatch was accompanied by a decrease in the frequency of observing early-flowering species such as Avalanche Lily and Western Anemone (*Anemone*

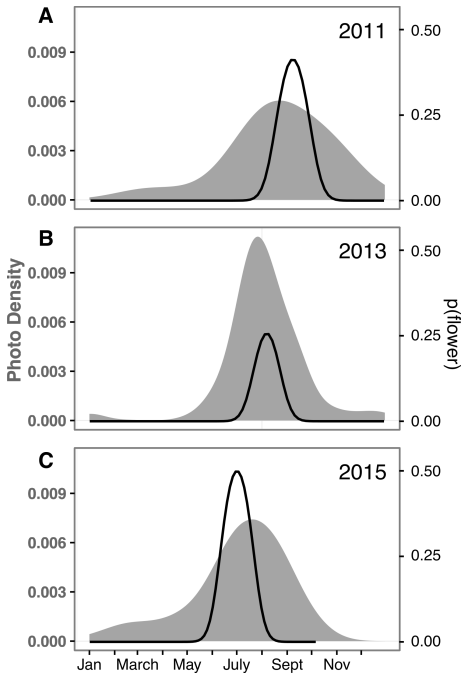

Figure 3.3: Seasonal shifts in the density of photos (grey), and the probability of observing a focal wildflower in a photo (black) in 2011 (**A**, late snow disappearance date), 2013 (**B**, average snow disappearance date), and 2015 (**C**, early snow disappearance date).

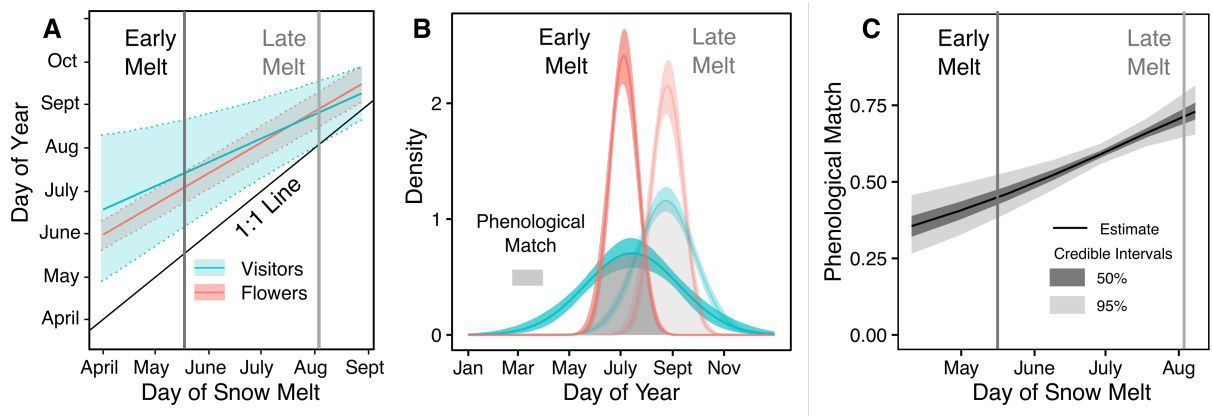

Figure 3.4: **A**. Changes in visitor phenology (blue) and flower phenology (red) driven by changes in snow disappearance date. The shaded regions represent the periods that include 50 percent of seasonal visitors, or 50 percent of the probability density of observing wildflowers in photos. Solid lines indicate the phenological peaks. **B**. Mean predictions (solid lines) and 95% credible intervals (shading) from the fit models when snow disappears on July 28th, typical of conditions in 2011 and May 19th, typical of conditions in 2015. Grey shading represents the phenological overlap discussed in the text. **C**. Changes in phenological matching between people and wildflowers driven by changes in snow disappearance date. Vertical lines indicate snow conditions depicted in panels A and B. Dark and light shading indicate 50% and 95% credible intervals, respectively.

occidentalis) in photos ($\chi^2 = 19.655$, $p < 0.0001$), and a small, marginally non-significant increase in the proportion of late-flowering species Gray's lovage (*Ligusticum grayi*) and American Bistort (*Polygonium bistortoides*) observed in photos ($\chi^2 = 3.2671$, $p = 0.07909$). These results are robust to uncertainties introduced by using estimated, rather than measured snow disappearance dates, and variation in focal species selection (Fig. C.7).

3.4.3 Effects of Visitor Management and Ecological Context

We also found that seasonal constraints on vehicle access, and geographic variation in wildflower sensitivity to climate had strong influences on the ability of visitors to track wildflower blooms (Fig. 3.5). Human activity in the subalpine zone of Mt. Rainier is centered around four points of vehicle access, two of which are open to visitors year-round, and two of which

are open only during the summer (Fig. 3.2B). Access to Paradise, on the southwest slopes of Mt. Rainier, remains open throughout the winter. Chinook Pass, on the east side of Mt. Rainier closes seasonally, but opens early in the spring season (average open date May 6th), and visitors can access the area year-round through the adjacent Crystal Mountain Ski Area. Access to two other subalpine sites, Sunrise and Mowich Lake, is open only during summer (approximately July September). These access restrictions result in larger decreases in phenological matching under early melt conditions in these areas (49.1%, 95% c.i. 35.3 to 61.2%, Figs. 3.5A, 3.5B) compared to areas where visitor use is less seasonally restricted (21%, 95% c.i. 3.3 to 36.9%, Figs. 3.5C, 3.5D). Potential mismatch was also more severe at west-slope locations where wildflower blooms are substantially more sensitive to the date of snow disappearance (Figs. 3.5A, 3.5C).

3.5 Discussion

Ecological theory argues that climate-driven phenological mismatch should be most common when different groups of interacting organisms have access to different sets of phenological cues [141], and are subject to different non-climatic constraints [95]. Both factors appear to mediate the mismatch between visitors and wildflowers we observed at Mt. Rainier in 2015. For example, visitors from out-of-town likely did not access information on seasonal snowpack when they were planning their trips and presumably relied on published typical dates of wildflower blooms, which means they would have arrived 5-6 weeks too late to appreciate peak wildflower displays in 2015. Additionally, the timing of road and facility opening in spring, also determined by typical snow disappearance dates, imposed direct behavioral constraints on park visitors that acted to reduce their exposure to seasonal wildflower displays in 2015, especially at Mowich Lake (Fig. 3.5A), where vehicle access was closed until June 17th in 2015, near the peak of the wildflower season. Over the long-term, our results thus suggest that temporal mismatches between people and wildflower displays could become more common and severe as the climate warms. This would be unfortunate, as it could reduce the status of wildflower meadows as iconic features of Mt. Rainier, affecting the publics

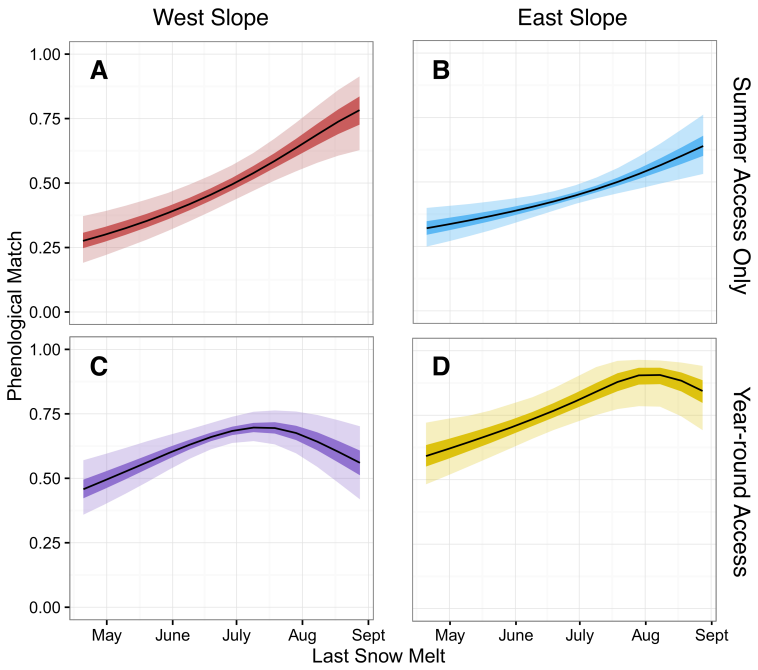

Figure 3.5: Geography and seasonal restrictions on visitor access affect the potential for mismatch between wildflower and visitor phenology at Mount Rainier National Park. The potential for mismatch is greater in two areas where visitor access closes seasonally (**A**, **B**) than in areas where visitors have vehicle access year-round (**C**, **D**). Colors correspond to the geographic areas depicted in Fig. 3.2B. Dark shading indicates 50% credible intervals, and light shading indicates 80% credible intervals.

knowledge of these systems and potential support for conservation measures to preserve them. Although the contribution of wildflower displays, like many other cultural or aesthetic ecosystem services, is difficult to quantify, the stated preferences of citizens indicate that these values are substantial [20].

Fortunately, this study also suggests that some management strategies might mitigate these potential negative outcomes, just as plastic and evolutionary changes can mitigate climate change impacts in ecological systems [94]. For example, shifting road openings of summer-access wildflower meadows to better track snow disappearance and updating visitor materials to reflect current snowpack conditions and peak wildflower bloom timings may reduce the potential for social-ecological mismatch. The feasibility of these strategies depends both on their costs, as well as how closely aligned they are to existing management mandates [36]. Like many studies that use spatial and annual climate variation as a proxy for long-term impacts of anthropogenic climate change [58], our temporal snapshot of climate-driven phenological mismatch does not account for long-term adjustments in the climate responses of either visitors or wildflowers. Our analysis does suggest, however, that social learning and altered visitor management in the social system [62, 168] or plastic and evolutionary change in the ecological system [94] would be necessary to avoid negative social and ecological outcomes in a warming climate. The magnitude or consequences of these outcomes is still unclear. Our major source of visitor data, crowd-sourced photos, does not allow us to directly measure visitors knowledge or appreciation of subalpine meadow ecosystems, or if these factors affect how sensitive visitors are to snow or bloom timings. Previous studies have shown that wildflower displays are a major draw for a large proportion of visitors at Mt. Rainier in mid-summer [113], but there remains a dearth of social-science research on the drivers of visitor phenology at Mt. Rainier and other natural areas [23, 66].

To our knowledge, this study is the first to empirically demonstrate phenological mismatch between coupled social and ecological systems driven by climate. Whether these mismatches are widespread is an interesting and important unanswered question. We believe that passively collected digital records, like the ones we used here, are a promising resource

for monitoring how climate variation affects seasonal cycles in ecosystems and human activity and could be used more widely to detect social ecological mismatches in phenology and other important feedbacks between ecosystem management and social-ecological systems [120, 154]. Recent advances in machine learning and computer vision ("deep learning" [152]) make it possible to train computers to accurately recognize complex objects such as flowers in heterogeneous collections of images [145], and are approaching the performance of trained human observers at recognizing individual species. With automated image classification and high-resolution climate information derived from models and remote-sensing [82, 133] we believe that our approach could be scaled up to understand how climate drives phenological matches and mismatches across a wide variety of social and ecological systems at unprecedented spatial scales.

BIBLIOGRAPHY

[1] John T. Abatzoglou, David E. Rupp, and Philip W. Mote. Seasonal Climate Variability and Change in the Pacific Northwest of the United States. *Journal of Climate*, 27(5):2125–2142, 2013.

[2] John T. Abatzoglou and A. Park Williams. Impact of anthropogenic climate change on wildfire across western US forests. *Proceedings of the National Academy of Sciences*, 113(42):11770–11775, 2016.

[3] Amir AghaKouchak, Linyin Cheng, Omid Mazdiyasni, and Alireza Farahmand. Global warming and changes in risk of concurrent climate extremes: Insights from the 2014 California drought. *Geophysical Research Letters*, 41(24):8847–8852, 2014.

[4] Ramiro Aguilar, Mauricio Quesada, Lorena Ashworth, Yvonne Herrerias-Diego, and Jorge Lobo. Genetic consequences of habitat fragmentation in plant populations: susceptible signals in plant traits and methodological approaches. *Molecular Ecology*, 17(24):5177–5188, 2008.

[5] Leander D. L. Anderegg and Janneke HilleRisLambers. Drought stress limits the geographic ranges of two tree species via different physiological mechanisms. *Global Change Biology*, 22(3):1029–1045, 2016.

[6] B. J. Anderson, H. R. Akakaya, M. B. Arajo, D. A. Fordham, E. Martinez-Meyer, W. Thuiller, and B. W. Brook. Dynamics of range margins for metapopulations under climate change. *Proceedings of the Royal Society of London B: Biological Sciences*, page rspb.2008.1681, 2009.

[7] Amy L. Angert. Demography of Central and Marginal Populations of Monkeyflowers (mimulus cardinalis and M. Lewisii). *Ecology*, 87(8):2014–2025, 2006.

[8] Jonathan B. Armstrong, Gaku Takimoto, Daniel E. Schindler, Matthew M. Hayes, and Matthew J. Kauffman. Resource waves: phenological diversity enhances foraging opportunities for mobile consumers. *Ecology*, 97(5):1099–1112, 2016.

[9] Marie Auger-Mth, Chris Field, Christoffer M. Albertsen, Andrew E. Derocher, Mark A. Lewis, Ian D. Jonsen, and Joanna Mills Flemming. State-space models dirty little secrets: even simple linear Gaussian models can have estimation problems. *Scientific reports*, 6:26677, 2016.

[10] Carol K. Augspurger. Phenology, flowering synchrony, and fruit set of six neotropical shrubs. *Biotropica*, pages 257–267, 1983.

[11] William R. Barker, Guy L. Nesom, Paul M. Beardsley, and Naomi S. Fraga. A taxonomic conspectus of Phrymaceae: a narrowed circumscription for Mimulus, new and resurrected genera, and new names and combinations. *Phytoneuron*, 39:1–60, 2012.

[12] Philip S. Barton, Saul A. Cunningham, Adrian D. Manning, Heloise Gibb, David B. Lindenmayer, and Raphael K. Didham. The spatial scaling of beta diversity. *Global Ecology and Biogeography*, 22(6):639–647, 2013.

[13] Daniel P. Bebber, Mark A. T. Ramotowski, and Sarah J. Gurr. Crop pests and pathogens move polewards in a warming world. *Nature Climate Change*, 3(11):985–988, 2013.

[14] Graham Bell and Andrew Gonzalez. Adaptation and evolutionary rescue in metapopulations experiencing environmental deterioration. *Science*, 332(6035):1327–1330, 2011.

[15] David Biek. Flora of Mount Rainier National Park. *Corvallis, Or.: Oregon State University Press, ISBN*, 2000.

[16] Michael Bode, Nick Outram, and Geoffrey P. Jones. Estimating dispersal kernels using genetic parentage data. *bioRxiv*, page 044305, 2016.

[17] Kjell Bolmgren and Ove Eriksson. Are mismatches the norm? Timing of flowering, fruiting, dispersal and germination and their fitness effects in Frangula alnus (Rhamnaceae). *Oikos*, 124(5):639–648, 2015.

[18] William D. Bowman, Diana R. Nemergut, Diane M. McKnight, Matthew P. Miller, and Mark W. Williams. A slide down a slippery slope alpine ecosystem responses to nitrogen deposition. *Plant Ecology & Diversity*, 8(5-6):727–738, 2015.

[19] Martin F. Breed, K. M. Ottewell, M. G. Gardner, Maria HK Marklund, E. E. Dormontt, and A. J. Lowe. Mating patterns and pollinator mobility are critical traits in forest fragmentation genetics. *Heredity*, 115(2):108–114, 2015.

[20] T. D. Breeze, A. P. Bailey, S. G. Potts, and K. G. Balcombe. A stated preference valuation of the non-market benefits of pollination services in the UK. *Ecological Economics*, 111:76–85, 2015.

[21] Kristin M. Broms, Mevin B. Hooten, Devin S. Johnson, Res Altwegg, and Loveday L. Conquest. Dynamic occupancy models for explicit colonization processes. *Ecology*, 97(1):194–204, 2016.

[22] Waylon Brunette, Mitchell Sundt, Nicola Dell, Rohit Chaudhri, Nathan Breit, and Gaetano Borriello. Open data kit 2.0: expanding and refining information services for developing regions. In *Proceedings of the 14th Workshop on Mobile Computing Systems and Applications*, page 10. ACM, 2013.

[23] Lauren B. Buckley and Madison S. Foushee. Footprints of climate change in US national park visitation. *International Journal of Biometeorology*, 56(6):1173–1177, 2012.

[24] H. K. Burgess, L. B. DeBey, H. E. Froehlich, N. Schmidt, E. J. Theobald, A. K. Ettinger, J. HilleRisLambers, J. Tewksbury, and J. K. Parrish. The science of citizen science: Exploring barriers to use as a primary research tool. *Biological Conservation*, 208:113–120, 2017.

[25] Alex Bush, Karel Mokany, Renee Catullo, Ary Hoffmann, Vanessa Kellermann, Carla Sgr, Shane McEvey, and Simon Ferrier. Incorporating evolutionary adaptation in species distribution modelling reduces projected vulnerability to climate change. *Ecology Letters*, 19(12):1468–1478, 2016.

[26] Bob Carpenter, Andrew Gelman, Matt Hoffman, Daniel Lee, Ben Goodrich, Michael Betancourt, Michael A. Brubaker, Jiqiang Guo, Peter Li, and Allen Riddell. Stan: A probabilistic programming language. *Journal of Statistical Software*, 20:1–37, 2016.

[27] Elisa Casella, Antoine Collin, Daniel Harris, Sebastian Ferse, Sonia Bejarano, Valeriano Parravicini, James L. Hench, and Alessio Rovere. Mapping coral reefs using consumer-grade drones and structure from motion photogrammetry techniques. *Coral Reefs*, 36(1):269–275, 2017.

[28] Hal Caswell. *Matrix population models*. Wiley Online Library, 2001.

[29] T. Trevor Caughlin, Sarah J. Graves, Gregory P. Asner, Michiel van Breugel, Jefferson S. Hall, Roberta E. Martin, Mark S. Ashton, and Stephanie A. Bohlman. A hyperspectral image can predict tropical tree growth rates in single-species stands. *Ecological Applications*, 26(8):2369–2375, 2016.

[30] Guillaume Charrier, Jrme Ngao, Marc Saudreau, and Thierry Amglio. Effects of environmental factors and management practices on microclimate, winter physiology, and frost resistance in trees. *Frontiers in Plant Science*, 6:259–259, 2015.

[31] I.-Ching Chen, Jane K. Hill, Ralf Ohlemller, David B. Roy, and Chris D. Thomas. Rapid range shifts of species associated with high levels of climate warming. *Science*, 333(6045):1024–1026, 2011.

[32] Chester Chiao. *The role of large woody debris and riparian forest in channel avulsion in the Carbon River, Mount Rainier National Park, Washington.* MS Thesis, University of Washington, 2016.

[33] Matthew J. Christmas, Martin F. Breed, and Andrew J. Lowe. Constraints to and conservation implications for climate change adaptation in plants. *Conservation Genetics*, 17(2):305–320, 2016.

[34] Isabelle Chuine and Elisabeth G. Beaubien. Phenology is a major determinant of tree species range. *Ecology Letters*, 4(5):500–510, 2001.

[35] Matthew J. Colloff, Michael D. Doherty, Sandra Lavorel, Michael Dunlop, Russell M. Wise, and Suzanne M. Prober. Adaptation services and pathways for the management of temperate montane forests under transformational climate change. *Climatic change*, 138(1-2):267–282, 2016.

[36] Rita Colwell, Susan Avery, Joel Berger, Gary E. Davis, H. Hamilton, T. Lovejoy, S. Malcom, A. McMullen, M. Novacek, R. J. Roberts, and others. Revisiting Leopold: resource stewardship in the national parks. *National Park System Advisory Board Science Committee, Washington, DC, USA*, 2012.

[37] Benjamin I. Cook, Elizabeth M. Wolkovich, T. Jonathan Davies, Toby R. Ault, Julio L. Betancourt, Jenica M. Allen, Kjell Bolmgren, Elsa E. Cleland, Theresa M. Crimmins, Nathan J. B. Kraft, Lesley T. Lancaster, Susan J. Mazer, Gregory J. McCabe, Brian J. McGill, Camille Parmesan, Stephanie Pau, James Regetz, Nicolas Salamin, Mark D. Schwartz, and Steven E. Travers. Sensitivity of Spring Phenology to Warming Across Temporal and Spatial Climate Gradients in Two Independent Databases. *Ecosystems*, 15(8):1283–1294, 2012.

[38] Eric P. Creeden, Jeffrey A. Hicke, and Polly C. Buotte. Climate, weather, and recent mountain pine beetle outbreaks in the western United States. *Forest Ecology and Management*, 312:239–251, 2014.

[39] Noel Cressie. *Statistics for spatial data*. John Wiley & Sons, 2015.

[40] Shawn M. Crimmins, Solomon Z. Dobrowski, Jonathan A. Greenberg, John T. Abatzoglou, and Alison R. Mynsberge. Changes in climatic water balance drive downhill shifts in plant species optimum elevations. *Science*, 331(6015):324–327, 2011.

[41] Mitchell B. Cruzan, Ben G. Weinstein, Monica R. Grasty, Brendan F. Kohrn, Elizabeth C. Hendrickson, Tina M. Arredondo, and Pamela G. Thompson. Small unmanned aerial vehicles (micro-UAVs, drones) in plant ecology. *Applications in Plant Sciences*, 4(9):1600041, 2016.

[42] Graeme S. Cumming, Craig R. Allen, Natalie C. Ban, Duan Biggs, Harry C. Biggs, David H. M. Cumming, Alta De Vos, Graham Epstein, Michel Etienne, Kristine Maciejewski, and others. Understanding protected area resilience: a multi-scale, social-ecological approach. *Ecological Applications*, 25(2):299–319, 2015.

[43] Christopher Daly, Michael Halbleib, Joseph I. Smith, Wayne P. Gibson, Matthew K. Doggett, George H. Taylor, Jan Curtis, and Phillip P. Pasteris. Physiographically sensitive mapping of climatological temperature and precipitation across the conterminous United States. *International journal of climatology*, 28(15):2031–2064, 2008.

[44] Joao Porto De Albuquerque, Benjamin Herfort, Alexander Brenning, and Alexander Zipf. A geographic approach for combining social media and authoritative data towards identifying useful information for disaster management. *International Journal of Geographical Information Science*, 29(4):667–689, 2015.

[45] J. P. Dedieu, A. Lessard-Fontaine, G. Ravazzani, E. Cremonese, G. Shalpykova, and M. Beniston. Shifting mountain snow patterns in a changing climate from remote sensing retrieval. *Science of The Total Environment*, 493:1267–1279, 2014.

[46] Enrico Di Minin, Henrikki Tenkanen, and Tuuli Toivonen. Prospects and challenges for social media data in conservation science. *Frontiers in Environmental Science*, 3:63, 2015.

[47] Michael C. Dietze. *Ecological Forecasting*. Princeton University Press, 2017.

[48] Jeffrey M. Diez, Ins Ibez, Abraham J. Miller-Rushing, Susan J. Mazer, Theresa M. Crimmins, Michael A. Crimmins, C. David Bertelsen, and David W. Inouye. Forecasting phenology: from species variability to community patterns. *Ecology letters*, 15(6):545–553, 2012.

[49] Daniel F. Doak and William F. Morris. Demographic compensation and tipping points in climate-induced range shifts. *Nature*, 467(7318):959, 2010.

[50] Christopher R. Dolanc, James H. Thorne, and Hugh D. Safford. Widespread shifts in the demographic structure of subalpine forests in the Sierra Nevada, California, 1934 to 2007. *Global Ecology and Biogeography*, 22(3):264–276, 2013.

[51] Alison Donnelly, Amelia Caffarra, and Bridget F. ONeill. A review of climate-driven mismatches between interdependent phenophases in terrestrial and aquatic ecosystems. *International Journal of Biometeorology*, 55(6):805–817, 2011.

[52] Stefan Dullinger, Andreas Gattringer, Wilfried Thuiller, Dietmar Moser, Niklaus E. Zimmermann, Antoine Guisan, Wolfgang Willner, Christoph Plutzar, Michael Leitner, Thomas Mang, and others. Extinction debt of high-mountain plants under twenty-first-century climate change. *Nature Climate Change*, 2(8):619, 2012.

[53] Jennifer A. Dunne, John Harte, and Kevin J. Taylor. Subalpine meadow flowering phenology responses to climate change: integrating experimental and gradient methods. *Ecological Monographs*, 73(1):69–86, 2003.

[54] Martin Edwards and Anthony J. Richardson. Impact of climate change on marine pelagic phenology and trophic mismatch. *Nature*, 430(7002):881–884, 2004.

[55] Jane Elith and John Leathwick. Boosted Regression Trees for ecological modeling. *Retreived on*, 24, 2016.

[56] Jane Elith, John R. Leathwick, and Trevor Hastie. A working guide to boosted regression trees. *Journal of Animal Ecology*, 77(4):802–813, 2008.

[57] ChéM. Elkin and Hugh Possingham. The role of landscape-dependent disturbance and dispersal in metapopulation persistence. *The American Naturalist*, 172(4):563–575, 2008.

[58] Sarah C. Elmendorf, Gregory H. R. Henry, Robert D. Hollister, Anna Maria Fosaa, William A. Gould, Luise Hermanutz, Annika Hofgaard, Ingibjrg S. Jnsdttir, Janet C. Jorgenson, Esther Lvesque, Borgr Magnusson, Ulf Molau, Isla H. Myers-Smith, Steven F. Oberbauer, Christian Rixen, Craig E. Tweedie, and Marilyn D. Walker. Experiment, monitoring, and gradient methods used to infer climate change effects on plant communities yield consistent patterns. *Proceedings of the National Academy of Sciences*, 112(2):448–452, 2015.

[59] Jelmer A. Elzinga, Anne Atlan, Arjen Biere, Luc Gigord, Arthur E. Weis, and Giorgina Bernasconi. Time after time: flowering phenology and biotic interactions. *Trends in Ecology & Evolution*, 22(8):432–439, 2007.

[60] Margaret E. K. Evans, Cory Merow, Sydne Record, Sean M. McMahon, and Brian J. Enquist. Towards process-based range modeling of many species. *Trends in ecology & evolution*, 31(11):860–871, 2016.

[61] S. Fatichi, S. Rimkus, P. Burlando, R. Bordoy, and P. Molnar. High-resolution distributed analysis of climate and anthropogenic changes on the hydrology of an Alpine catchment. *Journal of Hydrology*, 525:362–382, 2015.

[62] Ioan Fazey, John A. Fazey, Joern Fischer, Kate Sherren, John Warren, Reed F. Noss, and Stephen R. Dovers. Adaptive capacity and learning to learn as leverage for social–ecological resilience. *Frontiers in Ecology and the Environment*, 5(7):375–380, 2007.

[63] Songlin Fei, Johanna M. Desprez, Kevin M. Potter, Insu Jo, Jonathan A. Knott, and Christopher M. Oswalt. Divergence of species responses to climate change. *Science Advances*, 3(5):e1603055, 2017.

[64] Kathleen G. Ferris, Laryssa L. Barnett, Benjamin K. Blackman, and John H. Willis. The genetic architecture of local adaptation and reproductive isolation in sympatry within the Mimulus guttatus species complex. *Molecular Ecology*, 26(1):208–224, 2017.

[65] Andrew O. Finley, Sudipto Banerjee, and Alan E. Gelfand. spBayes for large univariate and multivariate point-referenced spatio-temporal data models. *arXiv preprint arXiv:1310.8192*, 2013.

[66] Nicholas A. Fisichelli, Gregor W. Schuurman, William B. Monahan, and Pamela S. Ziesler. Protected Area Tourism in a Changing Climate: Will Visitation at US National Parks Warm Up or Overheat? *PLOS ONE*, 10(6):e0128226, 2015.

[67] Elsa Fogelstrm, Martin Olofsson, Diana Posledovich, Christer Wiklund, Johan P. Dahlgren, and Johan Ehrln. Plant-herbivore synchrony and selection on plant flowering phenology. *Ecology*, 98(3):703–711, 2017.

[68] Jean-Christophe Foltte, Cline Clauzel, and Gilles Vuidel. A software tool dedicated to the modelling of landscape networks. *Environmental Modelling & Software*, 38:316–327, 2012.

[69] Kevin R. Ford, Ailene K. Ettinger, Jessica D. Lundquist, Mark S. Raleigh, and Janneke Hille Ris Lambers. Spatial Heterogeneity in Ecologically Important Climate Variables at Coarse and Fine Scales in a High-Snow Mountain Landscape. *PLOS ONE*, 8(6):e65008, 2013.

[70] Damien A. Fordham, H. Resit Akakaya, Miguel B. Arajo, Jane Elith, David A. Keith, Richard Pearson, Tony D. Auld, Camille Mellin, John W. Morgan, Tracey J. Regan, and others. Plant extinction risk under climate change: are forecast range shifts alone a good indicator of species vulnerability to global warming? *Global Change Biology*, 18(4):1357–1371, 2012.

[71] Jessica R. K. Forrest. Plantpollinator interactions and phenological change: what can we learn about climate impacts from experiments and observations? *Oikos*, 124(1):4–13, 2015.

[72] Austin G. Garner, Amanda M. Kenney, Lila Fishman, and Andrea L. Sweigart. Genetic loci with parent-of-origin effects cause hybrid seed lethality in crosses between Mimulus species. *New Phytologist*, 211(1):319–331, 2016.

[73] L. Gimnez-Benavides, A. Escudero, and J. M. Iriondo. Reproductive limits of a late-flowering high-mountain Mediterranean plant along an elevational climate gradient. *New Phytologist*, 173(2):367–382, 2007.

[74] Nasr H. Gomaa, Alicia Montesinos-Navarro, Carlos Alonso-Blanco, and F. Xavier Pico. Temporal variation in genetic diversity and effective population size of Mediterranean and subalpine Arabidopsis thaliana populations. *Molecular Ecology*, 20(17):3540–3554, 2011.

[75] Simon J. Goring and John W. Williams. Effect of historical land-use and climate change on tree-climate relationships in the upper Midwestern United States. *Ecology Letters*, 20(4):461–470, 2017.

[76] Mountain Research Initiative EDW Working Group and others. Elevation-dependent warming in mountain regions of the world. *Nature Climate Change*, 5(5):424–430, 2015.

[77] Nick M. Haddad, Andrew Gonzalez, Lars A. Brudvig, Melissa A. Burt, Douglas J. Levey, and Ellen I. Damschen. Experimental evidence does not support the Habitat Amount Hypothesis. *Ecography*, 40(1):48–55, 2017.

[78] Ilkka Hanski. Habitat connectivity, habitat continuity, and metapopulations in dynamic landscapes. *Oikos*, pages 209–219, 1999.

[79] Anna L. Hargreaves, Karen E. Samis, and Christopher G. Eckert. Are Species Range Limits Simply Niche Limits Writ Large? A Review of Transplant Experiments beyond the Range. *The American Naturalist*, 183(2):157–173, 2014.

[80] Melanie A. Harsch and Janneke HilleRisLambers. Climate warming and seasonal precipitation change interact to limit species distribution shifts across Western North America. *PloS one*, 11(7):e0159184, 2016.

[81] Melanie A. Harsch, Philip E. Hulme, Matt S. McGlone, and Richard P. Duncan. Are treelines advancing? A global meta-analysis of treeline response to climate warming. *Ecology Letters*, 12(10):1040–1049, 2009.

[82] A. Hedrick, H.-P. Marshall, A. Winstral, K. Elder, S. Yueh, and D. Cline. Independent evaluation of the SNODAS snow depth product using regional-scale lidar-derived measurements. *The Cryosphere*, 9(1):13–23, 2015.

[83] Jan A. Henderson. *Composition, distribution and succession of subalpine meadows in Mount Rainier National Park*. PhD thesis, University of Washington, 1973.

[84] Andrew P. Hendry and Troy Day. Population structure attributable to reproductive time: isolation by time and adaptation by time. *Molecular Ecology*, 14(4):901–916, 2005.

[85] Robert J. Hijmans, Steven Phillips, John Leathwick, Jane Elith, and Maintainer Robert J. Hijmans. Package dismo. *Circles*, 9:1, 2016.

[86] Jane K. Hill, Hannah M. Griffiths, and Chris D. Thomas. Climate change and evolutionary adaptations at species' range margins. *Annual Review of Entomology*, 56:143–159, 2011.

[87] B. J. Hindle, C. L. Kerr, S. A. Richards, and S. G. Willis. Topographical variation reduces phenological mismatch between a butterfly and its nectar source. *Journal of Insect Conservation*, 19(2):227–236, 2014.

[88] Robert D. Holt and Timothy H. Keitt. Alternative causes for range limits: a metapopulation perspective. *Ecology Letters*, 3(1):41–47, 2000.

[89] Chris Hopkinson. The influence of flying altitude, beam divergence, and pulse repetition frequency on laser pulse return intensity and canopy frequency distribution. *Canadian Journal of Remote Sensing*, 33(4):312–324, 2007.

[90] Jeffrey A. Hostetler and Richard B. Chandler. Improved state-space models for inference about spatial and temporal variation in abundance from count data. *Ecology*, 96(6):1713–1723, 2015.

[91] Karl Huelber, Michael Gottfried, Harald Pauli, Karl Reiter, Manuela Winkler, and Georg Grabherr. Phenological responses of snowbed species to snow removal dates in the Central Alps: implications for climate warming. *Arctic, Antarctic, and Alpine Research*, 38(1):99–103, 2006.

[92] Rolf A. Ims. The ecology and evolution of reproductive synchrony. *Trends in Ecology & Evolution*, 5(5):135–140, 1990.

[93] David W. Inouye. Effects of climate change on phenology, frost damage, and floral abundance of montane wildflowers. *Ecology*, 89(2):353–362, 2008.

[94] Jacob Johansson, Nadiah P. Kristensen, Jan-ke Nilsson, and Niclas Jonzn. The eco-evolutionary consequences of interspecific phenological asynchronya theoretical perspective. *Oikos*, 124(1):102–112, 2015.

[95] Peter M. Kappeler, Louise Barrett, Daniel T. Blumstein, and Tim H. Clutton-Brock. Constraints and flexibility in mammalian social behaviour: introduction and synthesis. *Philosophical Transactions of the Royal Society of London B: Biological Sciences*, 368(1618):20120337, 2013.

[96] Yuka Kawai and Gaku Kudo. Local differentiation of flowering phenology in an alpine-snowbed herb Gentiana nipponica. *Botany*, 89(6):361–367, 2011.

[97] Juan E. Keymer, Pablo A. Marquet, Jorge X. Velasco-Hernndez, and Simon A. Levin. Extinction thresholds and metapopulation persistence in dynamic landscapes. *The American Naturalist*, 156(5):478–494, 2000.

[98] Geoffrey Klein, Yann Vitasse, Christian Rixen, Christoph Marty, and Martine Rebetez. Shorter snow cover duration since 1970 in the Swiss Alps due to earlier snowmelt more than to later snow onset. *Climatic Change*, 139(3-4):637–649, 2016.

[99] Walter D. Koenig, Johannes M. H. Knops, William J. Carmen, and Ian S. Pearse. What drives masting? The phenological synchrony hypothesis. *Ecology*, 96(1):184–192, 2015.

[100] David N. Koons, Todd W. Arnold, and Michael Schaub. Understanding the demographic drivers of realized population growth rates. *Ecological Applications*, 27(7):2102–2115, 2017.

[101] Meade Krosby, Joshua Tewksbury, Nick M. Haddad, and Jonathan Hoekstra. Ecological connectivity for a changing climate. *Conservation Biology*, 24(6):1686–1689, 2010.

[102] Alexander Kubisch, Robert D. Holt, Hans-Joachim Poethke, and Emanuel A. Fronhofer. Where am I and why? Synthesizing range biology and the eco-evolutionary dynamics of dispersal. *Oikos*, 123(1):5–22, 2014.

[103] Gaku Kudo. Landscape Structure of Flowering Phenology in Alpine Ecosystems: Significance of PlantPollinator Interactions and Evolutionary Aspects. In Gaku Kudo, editor, *Structure and Function of Mountain Ecosystems in Japan*, Ecological Research Monographs, pages 41–62. Springer Japan, 2016.

[104] Anas Lacoursire-Roussel, Guillaume Ct, Vronique Leclerc, and Louis Bernatchez. Quantifying relative fish abundance with eDNA: a promising tool for fisheries management. *Journal of Applied Ecology*, 53(4):1148–1157, 2016.

[105] Allison M. Lambert, Abraham J. Miller-Rushing, and David W. Inouye. Changes in snowmelt date and summer precipitation affect the flowering phenology of Erythronium

grandiflorum (glacier lily; Liliaceae). *American Journal of Botany*, 97(9):1431–1437, 2010.

[106] Julie A. Lee-Yaw, Heather M. Kharouba, Megan Bontrager, Colin Mahony, Anna Mria Cserg, Annika M.E. Noreen, Qin Li, Richard Schuster, and Amy L. Angert. A synthesis of transplant experiments and ecological niche models suggests that range limits are often niche limits. *Ecology Letters*, 19(6):710–722, 2016.

[107] Jonathan Lenoir, Jean-Claude Ggout, Antoine Guisan, Pascal Vittoz, Thomas Wohlgemuth, Niklaus E. Zimmermann, Stefan Dullinger, Harald Pauli, Wolfgang Willner, and Jens-Christian Svenning. Going against the flow: potential mechanisms for unexpected downslope range shifts in a warming climate. *Ecography*, 33(2):295–303, 2010.

[108] Eric Lonsdorf, Claire Kremen, Taylor Ricketts, Rachael Winfree, Neal Williams, and Sarah Greenleaf. Modelling pollination services across agricultural landscapes. *Annals of Botany*, 103:1589–1600, 2009.

[109] Allison M. Louthan, Daniel F. Doak, and Amy L. Angert. Where and When do Species Interactions Set Range Limits? *Trends in Ecology & Evolution*, 30(12):780–792, 2015.

[110] Hans Lundberg. Effects of weather on foraging-flights of bumblebees (Hymenoptera, Apidae) in a subalpine/alpine area. *Ecography*, 3(2):104–110, 1980.

[111] Jessica D. Lundquist and Brian Huggett. Evergreen trees as inexpensive radiation shields for temperature sensors. *Water Resources Research*, 44(4):W00D04, 2008.

[112] Ilya Maclean, John J. Hopkins, Jonathan Bennie, Callum R. Lawson, and Robert J. Wilson. Microclimates buffer the responses of plant communities to climate change. *Global Ecology and Biogeography*, 24(11):1340–1350, 2015.

[113] M.F. Manni, Y. Li, and S.J. Hollenhorst. *Mt. Rainier National Park Visitor Study: Summer 2012.* Natural Resource Report NPS/NRSS/EQD/NRR2013/736. National Park Service, Fort Collins, Colorado., 2013.

[114] Ricardo O. Manoel, Patrcia F. Alves, Ceclia L. Dourado, Ana P. S. C. Gaino, Miguel L. M. Freitas, Mrio L. T. Moraes, and Alexandre M. Sebbenn. Contemporary pollen flow, mating patterns and effective population size inferred from paternity analysis in a small fragmented population of the Neotropical tree Copaifera langsdorffii Desf. (Leguminosae-Caesalpinioideae). *Conservation Genetics*, 13(3):613–623, 2012.

[115] David C. Marvin, Lian Pin Koh, Antony J. Lynam, Serge Wich, Andrew B. Davies, Ramesh Krishnamurthy, Emma Stokes, Ruth Starkey, and Gregory P. Asner. Integrating technologies for scalable ecology and conservation. *Global Ecology and Conservation*, 7:262–275, 2016.

[116] Suzanna C. Mason, Georgina Palmer, Richard Fox, Simon Gillings, Jane K. Hill, Chris D. Thomas, and Tom H. Oliver. Geographical range margins of many taxonomic groups continue to shift polewards. *Biological Journal of the Linnean Society*, 115(3):586–597, 2015.

[117] Guillaume Mauger, Joseph Casola, Harriet Morgan, Ronda Strauch, Brittany Jones, Beth Curry, Tania Busch Isaksen, Lara Whitely Binder, Meade Krosby, and Amy Snover. State of knowledge: Climate change in Puget Sound. Technical report, University of Washington Climate Impacts Group, 2015.

[118] T. C. McDonnell, S. Belyazid, T. J. Sullivan, H. Sverdrup, W. D. Bowman, and E. M. Porter. Modeled subalpine plant community response to climate change and atmospheric nitrogen deposition in Rocky Mountain National Park, USA. *Environmental Pollution*, 187:55–64, 2014.

[119] Michael D. McGinnis and Elinor Ostrom. Social-ecological system framework: initial changes and continuing challenges. *Ecology and Society*, 19(2):30, 2014.

[120] Marc L. Miller, RW Bill Carter, Stephen J. Walsh, and Sheila Peake. A Conceptual Framework for Studying Global Change, Tourism, and the Sustainability of Iconic National Parks. *George Wright Forum*, 31:256–269, 2014.

[121] Abraham J. Miller-Rushing, Toke Thomas Hye, David W. Inouye, and Eric Post. The effects of phenological mismatches on demography. *Philosophical Transactions of the Royal Society B: Biological Sciences*, 365(1555):3177–3186, 2010.

[122] Emily S. Minor and Dean L. Urban. A Graph-Theory Framework for Evaluating Landscape Connectivity and Conservation Planning. *Conservation Biology*, 22(2):297–307, 2008.

[123] Leonor Patrcia Cerdeira Morellato, Bruna Alberton, Swanni T. Alvarado, Bruno Borges, Elise Buisson, Maria Gabriela G. Camargo, Leonardo F. Cancian, Daniel W. Carstensen, Diego F. E. Escobar, Patrcia T. P. Leite, Irene Mendoza, Nathlia M. W. B. Rocha, Natalia C. Soares, Thiago Sanna Freire Silva, Vanessa G. Staggemeier, Annia Susin Streher, Betnia C. Vargas, and Carlos A. Peres. Linking plant phenology to conservation biology. *Biological Conservation*, 195:60–72, 2016.

[124] Toni Lyn Morelli, Christopher Daly, Solomon Z. Dobrowski, Deanna M. Dulen, Joseph L. Ebersole, Stephen T. Jackson, Jessica D. Lundquist, Constance I. Millar, Sean P. Maher, William B. Monahan, and others. Managing climate change refugia for climate adaptation. *PLoS One*, 11(8):e0159909, 2016.

[125] Craig Moritz, James L. Patton, Chris J. Conroy, Juan L. Parra, Gary C. White, and Steven R. Beissinger. Impact of a Century of Climate Change on Small-Mammal Communities in Yosemite National Park, USA. *Science*, 322(5899):261–264, 2008.

[126] Philip W. Mote. Trends in snow water equivalent in the Pacific Northwest and their climatic causes. *Geophysical Research Letters*, 30(12), 2003.

[127] Philip W. Mote, David E. Rupp, Sihan Li, Darrin J. Sharp, Friederike Otto, Peter F. Uhe, Mu Xiao, Dennis P. Lettenmaier, Heidi Cullen, and Myles R. Allen. Perspectives on the causes of exceptionally low 2015 snowpack in the western United States. *Geophysical Research Letters*, 43(20), 2016.

[128] John Muir. *Steep trails*. University of California Press, 1918.

[129] G. L. Nesom. New distribution records for Erythranthe (Phrymaceae). *Phytoneuron*, 67:1–15, 2013.

[130] Markus Neteler and Helena Mitasova. *Open source GIS: a GRASS GIS approach*, volume 689. Springer Science & Business Media, 2013.

[131] Ola Olsson, Arvid Bolin, Henrik G. Smith, and Eric V. Lonsdorf. Modeling pollinating bee visitation rates in heterogeneous landscapes from foraging theory. *Ecological Modelling*, 316:133–143, 2015.

[132] Elinor Ostrom. A general framework for analyzing sustainability of social–ecological systems. *Science*, 325(5939):419–422, 2009.

[133] Thomas H. Painter, Daniel F. Berisford, Joseph W. Boardman, Kathryn J. Bormann, Jeffrey S. Deems, Frank Gehrke, Andrew Hedrick, Michael Joyce, Ross Laidlaw, Danny Marks, and others. The Airborne Snow Observatory: Fusion of scanning lidar, imaging spectrometer, and physically-based modeling for mapping snow water equivalent and snow albedo. *Remote Sensing of Environment*, 184:139–152, 2016.

[134] Gretta T. Pecl, Miguel B. Arajo, Johann D. Bell, Julia Blanchard, Timothy C. Bonebrake, I.-Ching Chen, Timothy D. Clark, Robert K. Colwell, Finn Danielsen, Birgitta Evengrd, Lorena Falconi, Simon Ferrier, Stewart Frusher, Raquel A. Garcia, Roger B. Griffis, Alistair J. Hobday, Charlene Janion-Scheepers, Marta A. Jarzyna,

Sarah Jennings, Jonathan Lenoir, Hlif I. Linnetved, Victoria Y. Martin, Phillipa C. McCormack, Jan McDonald, Nicola J. Mitchell, Tero Mustonen, John M. Pandolfi, Nathalie Pettorelli, Ekaterina Popova, Sharon A. Robinson, Brett R. Scheffers, Justine D. Shaw, Cascade J. B. Sorte, Jan M. Strugnell, Jennifer M. Sunday, Mao-Ning Tuanmu, Adriana Vergs, Cecilia Villanueva, Thomas Wernberg, Erik Wapstra, and Stephen E. Williams. Biodiversity redistribution under climate change: Impacts on ecosystems and human well-being. *Science*, 355(6332):eaai9214, 2017.

[135] Malin L. Pinsky. Marine Taxa Track Local Climate Velocities. *Journal of Glaciology*, 58:1227–1244, 2012.

[136] Samuel Pironon, Guillaume Papuga, Jess Villellas, Amy L. Angert, Mara B. Garca, and John D. Thompson. Geographic variation in genetic and demographic performance: new insights from an old biogeographical paradigm. *Biological Reviews*, 92:1877–1909, 2016.

[137] Martyn Plummer and others. JAGS: A program for analysis of Bayesian graphical models using Gibbs sampling. In *Proceedings of the 3rd international workshop on distributed statistical computing*, volume 124, page 125. Vienna, Austria, 2003.

[138] Jean-Nicolas Pradervand, Anne Dubuis, Loc Pellissier, Antoine Guisan, and Christophe Randin. Very high resolution environmental predictors in species distribution models Moving beyond topography? *Progress in Physical Geography*, 38(1):79–96, 2014.

[139] Graham H. Pyke, David W. Inouye, and James D. Thomson. Activity and abundance of bumble bees near Crested Butte, Colorado: diel, seasonal, and elevation effects. *Ecological Entomology*, 36(4):511–521, 2011.

[140] Shenhua Qian, Waka Saito, Makiko Mimura, Shingo Kaneko, Yuji Isagi, Eri Mizumachi, and Akira S. Mori. Asymmetric gene flow and the distribution of genetic diversity in morphologically distinct Abies mariesii populations in contrasting eco-habitats. *Plant Ecology*, 215(12):1385–1397, 2014.

[141] Nicole E. Rafferty, Paul J. CaraDonna, and Judith L. Bronstein. Phenological shifts and the fate of mutualisms. *Oikos*, 124(1):14–21, 2015.

[142] Mark S. Raleigh, Karl Rittger, Courtney E. Moore, Brian Henn, James A. Lutz, and Jessica D. Lundquist. Ground-based testing of MODIS fractional snow cover in subalpine meadows and forests of the Sierra Nevada. *Remote Sensing of Environment*, 128:44–57, 2013.

[143] Sailesh Ranjitkar, Eike Luedeling, Krishna Kumar Shrestha, Kaiyun Guan, and Jianchu Xu. Flowering phenology of tree rhododendron along an elevation gradient in two sites in the Eastern Himalayas. *International Journal of Biometeorology*, 57(2):225–240, 2013.

[144] Christopher PO Reyer, Sebastian Leuzinger, Anja Rammig, Annett Wolf, Ruud P. Bartholomeus, Antonello Bonfante, Francesca de Lorenzi, Marie Dury, Philipp Gloning, Rene Abou Jaoud, and others. A plant's perspective of extremes: terrestrial plant responses to changing climatic variability. *Global change biology*, 19(1):75–89, 2013.

[145] Angie K. Reyes, Juan C. Caicedo, and Jorge E. Camargo. Fine-tuning deep convolutional networks for plant recognition. In *Working notes of CLEF 2015 conference*, 2015.

[146] Mark E. Ritchie and Han Olff. Spatial scaling laws yield a synthetic theory of biodiversity. *Nature*, 400(6744):557–560, 1999.

[147] Kermit Ritland. Genetic differentiation, diversity, and inbreeding in the mountain monkeyflower (Mimulus caespitosus) of the Washington Cascades. *Canadian Journal of Botany*, 67(7):2017–2024, 1989.

[148] Regina M. Rochefort and David L. Peterson. Temporal and spatial distribution of trees in subalpine meadows of Mount Rainier National Park, Washington, USA. *Arctic and Alpine Research*, 28(1):52–59, 1996.

[149] J. Andrew Royle and Marc Kry. A Bayesian state-space formulation of dynamic occupancy models. *Ecology*, 88(7):1813–1823, 2007.

[150] Roy A. Sanderson, Louis A. Goffe, and Carlo Leifert. Time-series models to quantify short-term effects of meteorological conditions on bumblebee forager activity in agricultural landscapes. *Agricultural and Forest Entomology*, 17(3):270–276, 2015.

[151] Jason Scalzitti, Courtenay Strong, and Adam Kochanski. Climate change impact on the roles of temperature and precipitation in western U.S. snowpack variability. *Geophysical Research Letters*, 43(10):2016GL068798, 2016.

[152] Jrgen Schmidhuber. Deep learning in neural networks: An overview. *Neural Networks*, 61:85–117, 2015.

[153] Josep M. Serra-Diaz, Robert M. Scheller, Alexandra D. Syphard, and Janet Franklin. Disturbance and climate microrefugia mediate tree range shifts during climate change. *Landscape Ecology*, 30(6):1039–1053, 2015.

[154] Carrie Sessions, Spencer A. Wood, Sergey Rabotyagov, and David M. Fisher. Measuring recreational visitation at US National Parks with crowd-sourced photographs. *Journal of Environmental Management*, 183:703–711, 2016.

[155] Jason P. Sexton, Patrick J. McIntyre, Amy L. Angert, and Kevin J. Rice. Evolution and ecology of species range limits. *Annual Review of Ecology, Evolution, and Systematics*, 40:415–436, 2009.

[156] Seema Nayan Sheth and Amy Lauren Angert. Demographic compensation does not rescue populations at a trailing range edge. *bioRxiv*, page 117606, 2017.

[157] Seema Nayan Sheth, Amy Lauren Angert, Mark Vellend, and Yannis Michalakis. Artificial selection reveals high genetic variation in phenology at the trailing edge of a species range. *The American Naturalist*, 187(2):182–193, 2016.

[158] Michael C. Singer and Camille Parmesan. Phenological asynchrony between herbivorous insects and their hosts: signal of climate change or pre-existing adaptive strategy? *Philosophical Transactions of the Royal Society of London B: Biological Sciences*, 365(1555):3161–3176, 2010.

[159] T. W. Sisson, J. E. Robinson, and D. D. Swinney. Whole-edifice ice volume change AD 1970 to 2007/2008 at Mount Rainier, Washington, based on LiDAR surveying. *Geology*, 39(7):639–642, 2011.

[160] Christian Steger, Sven Kotlarski, Tobias Jonas, and Christoph Schr. Alpine snow cover in a changing climate: a regional climate model perspective. *Climate Dynamics*, 41(3-4):735–754, 2013.

[161] Chris Stubben, Brook Milligan, and others. Estimating and analyzing demographic models using the popbio package in R. *Journal of Statistical Software*, 22(11):1–23, 2007.

[162] C. S. Sutherland, D. A. Elston, and X. Lambin. A demographic, spatially explicit patch occupancy model of metapopulation dynamics and persistence. *Ecology*, 95(11):3149–3160, 2014.

[163] Patrizia Tenerelli, Urka Demar, and Sandra Luque. Crowdsourcing indicators for cultural ecosystem services: A geographically weighted approach for mountain landscapes. *Ecological Indicators*, 64:237–248, 2016.

[164] Elli J. Theobald, Ian K. Breckheimer, and Janneke HilleRisLambers. Climate Drives Phenological Reassembly of a Mountain Wildflower Meadow Community. *Ecology*, 98(11):2799–2812, 2017.

[165] Elli J. Theobald, Hrach Gabrielyan, and Janneke HilleRisLambers. Lilies at the limit: Variation in plant-pollinator interactions across an elevational range. *American journal of botany*, 103(2):189–197, 2016.

[166] Ingrid M. Tohver, Alan F. Hamlet, and Se-Yeun Lee. Impacts of 21st-Century Climate Change on Hydrologic Extremes in the Pacific Northwest Region of North America. *JAWRA Journal of the American Water Resources Association*, 50(6):1461–1476, 2014.

[167] Justin M. J. Travis, Maria Delgado, Greta Bocedi, Michel Baguette, Kamil Barto, Dries Bonte, Isabelle Boulangeat, Jenny A. Hodgson, Alexander Kubisch, Vincenzo Penteriani, Marjo Saastamoinen, Virginie M. Stevens, and James M. Bullock. Dispersal and species responses to climate change. *Oikos*, 122(11):1532–1540, 2013.

[168] Petra Tschakert and Kathleen Ann Dietrich. Anticipatory learning for climate change adaptation and resilience. *Ecology and Society*, 15(2):11, 2010.

[169] N. J. C. Tyler, J. M. Turi, M. A. Sundset, K. Strm Bull, M. N. Sara, E. Reinert, N. Oskal, C. Nellemann, J. J. McCarthy, S. D. Mathiesen, and others. Saami reindeer pastoralism under climate change: applying a generalized framework for vulnerability studies to a sub-arctic socialecological system. *Global Environmental Change*, 17(2):191–206, 2007.

[170] Christopher Ulrey, Pedro F. Quintana-Ascencio, Gary Kauffman, Adam B. Smith, and Eric S. Menges. Life at the top: Long-term demography, microclimatic refugia, and responses to climate change for a high-elevation southern Appalachian endemic plant. *Biological Conservation*, 200:80–92, 2016.

[171] Mark C. Urban. Accelerating extinction risk from climate change. *Science*, 348(6234):571–573, 2015.

[172] Mark C. Vanderwel and Drew W. Purves. How do disturbances and environmental heterogeneity affect the pace of forest distribution shifts under climate change? *Ecography*, 37(1):10–20, 2014.

[173] Jess Villellas, Daniel F. Doak, Mara B. Garca, and William F. Morris. Demographic compensation among populations: what is it, how does it arise and what are its implications? *Ecology Letters*, 18(11):1139–1152, 2015.

[174] Sverine Vuilleumier, Chris Wilcox, Benjamin J. Cairns, and Hugh P. Possingham. How patch configuration affects the impact of disturbances on metapopulation persistence. *Theoretical Population Biology*, 72(1):77–85, 2007.

[175] Jingya Wang, Mohammed Korayem, Saul Blanco, and David J. Crandall. Tracking natural events through social media and computer vision. In *Proceedings of the 2016 ACM on Multimedia Conference*, pages 1097–1101. ACM, 2016.

[176] Shiping Wang, Changshun Wang, Jichuang Duan, Xiaoxue Zhu, Guangping Xu, Caiyun Luo, Zhenhua Zhang, Fandong Meng, Yingnian Li, and Mingyuan Du. Timing and duration of phenological sequences of alpine plants along an elevation gradient on the Tibetan plateau. *Agricultural and Forest Meteorology*, 189190:220–228, 2014.

[177] Nickolas M. Waser. Competition for pollination and the evolution of flowering time. *The American Naturalist*, 185(6):iii–v, 2015.

[178] Julia A. Wheeler, Andres J. Corts, Janosch Sedlacek, Sophie Karrenberg, Mark van Kleunen, Sonja Wipf, Guenter Hoch, Oliver Bossdorf, and Christian Rixen. The snow and the willows: earlier spring snowmelt reduces performance in the low-lying alpine shrub Salix herbacea. *Journal of Ecology*, 104(4):1041–1050, 2016.

[179] Adam M. Wilson and John A. Silander. Estimating uncertainty in daily weather interpolations: a Bayesian framework for developing climate surfaces. *International Journal of Climatology*, 34(8):2573–2584, 2014.

[180] Anna Wilson, Kevin Bacher, Ian Breckheimer, Jessica Lundquist, Regina Rochefort, Elli Theobald, Lou Whiteaker, and Janneke HilleRisLambers. Monitoring wildflower phenology using traditional science, citizen science, and crowdsourcing approaches. *Park Science*, 33(1):17–26, 2017.

[181] M. S. Wisz, R. J. Hijmans, J. Li, A. T. Peterson, C. H. Graham, A. Guisan, and NCEAS Predicting Species Distributions Working Group. Effects of sample size on the performance of species distribution models. *Diversity and Distributions*, 14(5):763–773, 2008.

[182] Elizabeth M. Wolkovich, Benjamin I. Cook, Jenica M. Allen, Theresa M. Crimmins, Julio L. Betancourt, Steven E. Travers, Stephanie Pau, James Regetz, T. Jonathan Davies, Nathan JB Kraft, and others. Warming experiments underpredict plant phenological responses to climate change. *Nature*, 485(7399):494–497, 2012.

[183] S. Wood and F. Scheipl. *gamm4: Generalized additive mixed models using mgcv and lme4*. R package version 0.2-2, URL http://CRAN. R-project. org/package= gamm4, 2013.

[184] Simon N. Wood. *Generalized additive models: an introduction with R*. CRC press, 2017.

[185] Spencer A. Wood, Anne D. Guerry, Jessica M. Silver, and Martin Lacayo. Using social media to quantify nature-based tourism and recreation. *Scientific Reports*, 3:2976, 2013.

[186] Andrew Young, Tim Boyle, and Tony Brown. The population genetic consequences of habitat fragmentation for plants. *Trends in Ecology & Evolution*, 11(10):413–418, 1996.

[187] Boris T. van Zanten, Derek B. Van Berkel, Ross K. Meentemeyer, Jordan W. Smith, Koen F. Tieskens, and Peter H. Verburg. Continental-scale quantification of landscape values using social media data. *Proceedings of the National Academy of Sciences*, 113(46):12974–12979, 2016.

[188] Chiara Ziello, Nicole Estrella, Mariya Kostova, Elisabeth Koch, and Annette Menzel. Influence of altitude on phenology of selected plant species in the Alpine region (19712000). *Climate Research*, 39(3):227–234, 2009.

[189] Niklaus E. Zimmermann, Nigel G. Yoccoz, Thomas C. Edwards, Eliane S. Meier, Wilfried Thuiller, Antoine Guisan, Dirk R. Schmatz, and Peter B. Pearman. Climatic extremes improve predictions of spatial patterns of tree species. *Proceedings of the National Academy of Sciences*, 106(Supplement 2):19723–19728, 2009.

Appendix A

SUPPLEMENTARY MATERIAL FOR CHAPTER 1

A.1 Transplant Experiment Details

We propagated seedlings of both species for the transplant study on standard potting mix (Sunshine #4) in the Botany Greenhouse at the University of Washington. In August 2014 (*E. caespitosa*) or August 2015 (*E. guttata*), we transferred 3 week old seedlings to 5.25 in diameter pots filled with homogenized alluvial soil taken from the channel of the Nisqually River (46.7289N, -121.8698W). After hardening-off outside for approximately 5 days, we buried each pot to the rim in the substrate at each site in 8 blocks of 42 individuals per species at each transolant site. Plantings of the two species were separated by approximately 50 m at each site to reduce the potential for reproductive interference. During the growing season (May - October) we sub-irrigated each pot with a drip system that kept soil in and outside the pots saturated. We weeded pots and 10 cm surrounding each pot approximately weekly during the growing season to suppress competing plants. We assessed survival and plant size in late September of the planting year, and for the following two growing seasons, with each census corresponding to the peak of local flowering. We collected all mature fruits from each individual in each growing season, and measured seed production by distributing seeds on white paper, photographing them, and counting particles using the Analyze Particles function in *ImageJ*(Version 1.2). To assess germination and seedling survival, we installed four 5.25 in pots in the center of each transplant block filled with the same homogenized soil used for the transplant study. In late August 2015, we distributed 25 seeds on the surface of each pot, tracking germination and seedling survival every two weeks during September and October 2015, and in May through July of 2016.

Seed sources for both the transplant and the germination study came from a known

pedigree based on extensive field collections in Mt. Rainier National Park. In the summer of 2013, we collected cuttings from individuals of both species at 20 sites distributed across Mt. Rainier, and propagated these individuals in the Botany Greenhouse at the University of Washington. For each of 9 (*E. caespitosa*) or 6 (*E. guttata*) source populations, we crossed each collected individual with a randomly selected individual from the same source population, and a randomly-selected individual from a single, large, population located near the range center. For the transplant study, we randomly selected seed from 30 half-sib families of each species, evenly split between low-elevation, and high-elevation dams, and within-population and other-population sires. Each experiment block of 42 plants contained individuals from identical maternal families. This design allowed us to track aggregate demographic performance as well as understand how that performance could be modified by local adaptation and pollen dispersal, but in this study we focus on aggregate demographic performance, and do not examine performance differences between populations or maternal families, except to treat them as grouping factors (random effects) when estimating vital rates.

Figure A.1: Site photos of the transplant experiment. **A**. Blocks 1-3 at Nisqually Vista, the high-elevation transplant site, showing the arrangement of plants and black tubing for the drip irrigation system. **B**. Close-up of a single *E. caespitosa*, showing how pots were buried in the substrate. Drip tubing is visible at the top of the photo.

A.2 Interpolating Microclimate Conditions

We measured air temperature, snow duration, and soil surface temperatures at each transplant site and each population survey site using Onset HOBO pendant data loggers. Air temperature sensors were suspended 4 m above the ground surface (above the level of the seasonal snowpack) and were protected from direct insolation by 10 cm diameter white plastic funnels and conifer vegetation. Soil temperature sensors, from which snow duration measurements can also be extracted[142], were buried 5 cm deep in stream banks within 2 m of the stream channel, and were secured to trees and adjacent riparian vegetation using aluminum or stainless steel wire. Two air temperature sensors were installed at each population survey site along with three soil temperatures sensors. Microclimate conditions (mean growing season temperatures, snow-free soil growing degree days) were estimated for each 27 m grid cell in each year of the study. We produced these maps using a three stage procedure based on Bayesian regression kriging[179]. First, we used topographic and vegetation structure covariates to predict the linear relationship (slope and intercept) that links daily local conditions recorded at the microclimate sensor location to regional average conditions, calculated as the mean of 4 km resolution PRISM[43] data within 50 km of the boundary of Mt. Rainier National Park. Because the local microclimate measurements were centered to have a mean of zero, the intercept of this relationship represents how cold or warm a local site is on a typical day relative to the seasonal average, and the slope represents how sensitive conditions at a site are to changes in the regional average. We allowed these relationships, and our geostatistical predictions of the coefficients linking local and regional temperatures, to vary seasonally by separately estimating these quantities for each site in each season (DJF, MAM, JJA, SON), and then extrapolating them across the landscape using GAMMs with structures similar to those used to estimate SDD. The regional PRISM daily time-series was then combined with the GAMM estimates of the local-regional temperature relationship to derive high-resolution gridded estimates of expected temperatures for each day. Residual variation from each site was approximately zero-centered and showed dramatically reduced

temporal autocorrelation and much smoother patterns of spatial autocorrelation than the raw data. Finally, we interpolated geographic patterns of daily residual temperature variation using Bayesian kriging. This spatial model, fit with the `SpLM` function in the *R* package `SpBayes`[65], incorporated elevation, latitude, and longitude as predictors of the daily trend, and had an exponential covariance function. We chose a Bayesian approach here instead of traditional kriging because some days had relatively few measurements, which caused a traditional kriging estimator to perform poorly, a behavior that could be minimized in the Bayesian analysis by imposing a mildly informative prior on the parameters defining the spatial covariance function ($\phi \sim Unif(0.1, 300)$,$\sigma^2 \sim IG(2, 2)$,$\tau^2 \sim IG(2, 0.1)$). Our geostatistical estimates of daily microclimate perform well when measured against data held-out for testing (RMSE 0.74°C). Finally, we used these daily high-resolution grids of average air temperature to compute early growing-season (March - August) average air temperatures temperature, as well as temperature sums (the sum of temperatures above 0°C) in the 100 days after snow disappeared at each 27 m raster cell.

A.3 Population Model Details

In the model, initial abundance $N_{t=1}$ in grid cell j on year $t = 1$ is taken to be a discrete random variable with a Negative Binomial distribution (mean λ_j, reciprocal dispersion α_{init}). In subsequent years ($t = 2 - n_t$) the expected number of individuals μ in grid cell j on year t, (μ_{jt}) , is

$$\mu_{jt} = N_{t-1} * exp(r_{j,t-1}(1 - \frac{\log(N_{t-1} + 1)}{\log(K + 1)})) * \rho_{j,t-1} + \iota_{j,t-1} \tag{A.1}$$

This is an extension of the Gompertz formulation of the classical logistic population growth curve, where $r_{j,t-1}$ represents the expected population growth rate of cell j, and the carrying capacity, K, is assumed to be a constant for every cell. $\rho_{j,t-1}$ is a discrete random variable indicating whether local extinction has occurred ($\rho = 0$ represents population-replacing disturbance), and $\iota_{j,t-1}$ represents the number of immigrants to cell j. Actual abundance in other years N_t, is also treated as Negative Binomially distributed with a mean

u_{jt} and dispersion α. The disturbance process is Bernoulli distributed with a catastrophe probability ϕ.

$$(1 - \rho_{j,t-1}) \sim Bernoulli(\phi_{j,t-1}) \tag{A.2}$$

Environmental covariates are allowed to modify initial expected population size λ, growth rate r, catastrophe probability ϕ, and immigration rate ι according to the following regression equations

$$\log(\lambda_j) = \lambda_0 + \lambda_{site} + \lambda_{Clim} M_{j,t=1} + \lambda_{Dist} D_{j,t=1} + \lambda_{Stream} S_j + \lambda_{Stream^2} S_j^2 + \lambda_{Canopy} C_j + \lambda_{Canopy^2} C_j^2 \tag{A.3}$$

$$r_{j,t} = r_{0+} r_{Clim} M_{j,t} + r_{Dist} D_{j,t} + r_{Stream} S_j + r_{Canopy} C_j \tag{A.4}$$

$$logit(\phi_{j,t}) = \phi_0 + \phi_{Clim} M_{j,t} + \phi_{Dist} D_{j,t} + \phi_{Clim:Dist} M_{j,t} D_{j,t} \tag{A.5}$$

$$\log(\iota_{j,t}) = \iota_0 + \iota_{Site} + \iota_{Clim} M_j + \iota_{Dist} D_{j,t} + \iota_{Stream} S_j + \iota_{Stream^2} S_j^2 + \iota_{Canopy} C_j + \iota_{Canopy^2} C_j^2 + \iota_{Neighbor} B_{j,t-1} \tag{A.6}$$

where the subscripted terms for λ, r, ϕ, and ι represent slopes and intercepts of the regression equations, and capitalized terms represent covariates. M_{jt} is the value of the the growing-season air temperature at site$j$ in year t, D_{jt} is the value of the flood disturbance index, S_j is the logit-transformed proportion of stream habitat at site j, C_j is the canopy cover at site j. Unmeasured environmental effects on initial abundance and colonization are subsumed into zero-centered site-level random effects λ_{site} and ι_{Site}. Local dispersal is accounted for with a simple neighbor effect, where the covariate $B_{j,t-1}$ is an index of abundance in neighboring cells with

$$B_{jt-1} = \sum_{j=1}^{n_k} N_{j,t-1} + 0.72 \sum_{j=1}^{n_q} N_{j,t-1} \tag{A.7}$$

where n_k and n_q represent the number of kings-case and queens-case (diagonal) neighboring cells. All covariates (except for neighbor abundance) were standardized to a mean of zero and standard deviation of one to facilitate computation.

The model was implemented separately for each focal species, with vague priors and hyperpriors (zero-centered, normally distributed priors with a precision of 0.1 for regression slopes, intercepts and random effects) with two exceptions. First we incorporated information about climate's effects on local population growth rates from the transplant experiment by imposing an informative prior for the slope representing the relationship between local population growth rate and growing season temperature (r_{Clim}). The prior mean and precision for this parameter was taken from our posterior estimate of the difference in r between the high-elevation and low-elevation transplant sites for each species, divided by the difference in measured growing season temperatures between the sites. Because we standardized non-climatic differences between the two sites (insolation, soils, site water status), we contend that the differences in performance are primarily due to climatic factors, making the choice of prior information appropriate. We did not consider the transplant experiment to be informative for the intercept, r_0, because the transplant experiment conditions are likely considerably more favorable to the focal species than a typical wild site.This is reflected in extremely high estimated population growth rates at the two transplant sites (see Results). Our second informative prior was for the patch carrying capacity, K. Our initial model fit without this informative prior revealed that K was poorly constrained by the data, and posterior estimates were strongly correlated with estimates of r. This is a common problem with population models fit using this general approach[9], and so we chose a moderately informative prior for K (mean 200, precision 0.001) that constrained maximum posterior estimates of predicted population sizes to roughly match the maxima observed in our dataset. The model was implemented in *JAGS* version 4.2[137], which estimates posterior samples

with Markov Chain Monte-Carlo (MCMC) using Gibbs Sampling. The model converged rapidly but mixed slowly, so we estimated parameters using three chains of 50,000 MCMC iterations, throwing away 10,000 iterations for burn-in, and thinning chains to yield 1,000 posterior samples for each chain.

A.4 Model Validation

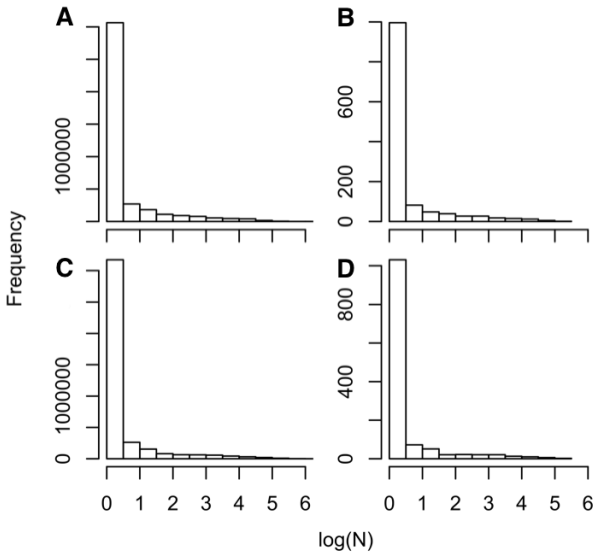

Figure A.2: Our spatial population model accounts for the extremely skewed statistical distributions of abundance that we observed in our population survey. Predicted (**A**,**C**) distributions of population size closely match observations (**B**, **D**) for both E. guttata (**A**, **B**), and E. caespitosa (**C** ,**D**). Y-axis scales are strikingly different between predicted and observed plots because the predicted plots use counts from from 50 years of simulated values.

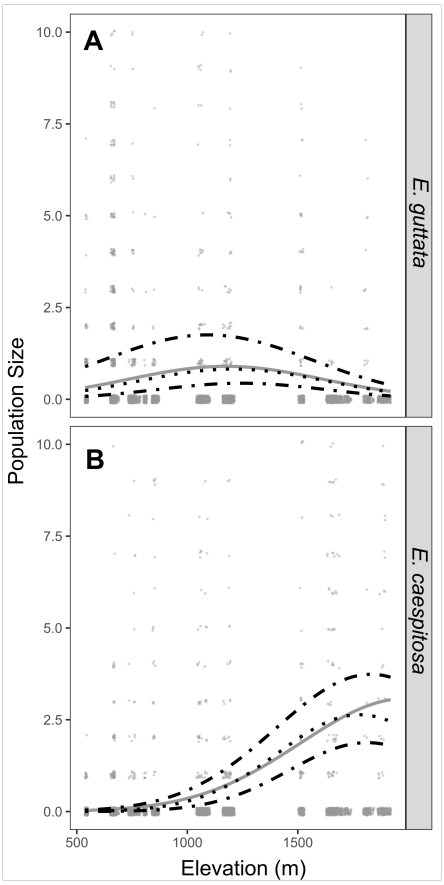

Figure A.3: Our spatial population model faithfully reproduces patterns of occupancy and population size across Mt. Rainier's environmental gradient for both *E. guttata* (**A**) and *E. caespitosa* (**B**). Grey dots represent measured population sizes in each 27 m grid cell across all years of the study (2013 to 2016), and solid gray line represents a second-order polynomial fit to the data assuming a negative binomial error distribution using the `glm.nb` function in the *R* package `MASS`. Black dotted line represents the same statistic fit to (one step ahead) predicted counts from the spatial population model. Dot-dashed black lines represent 80% posterior credible intervals of the predicted relationship between elevation and population size.

Appendix B

SUPPLEMENTARY MATERIAL FOR CHAPTER 2

B.1 Mapping Meadow Extents

Both large-scale and small-scale climatic and habitat heterogeneity produce distinctive patterns of plant distributions at Mt. Rainier. We mapped subalpine and alpine meadow environments using a simple threshold-based classification of vegetation structure and spectral characteristics derived from a high-density discrete-return LiDAR dataset collected at Mt. Rainier in 2007 and 2008[159]. This collection produced precise, high-resolution (1 m) digital elevation models and canopy surface models as well as estimates of first-return intensity that are directly related to near-infrared (1064 nm) surface reflectance, and thus, to green vegetation abundance or density[89]. In this study, we considered areas to be meadow if they had vegetation canopies less-than or equal to 3m in height with a reflectance greater than 0.568, and they were between the elevations of 1400 m and 2200 m. This raster-based map of meadow extents was converted to a vector map, and small areas (< 0.01 ha) were removed, leaving 4621 individual meadows with a total area of 4723 ha. We used a simple threshold-based classification, rather than a more elaborate vegetation mapping method because our goal was to simply circumscribe the study areas, and using our vegetation composition data to both define the study area as well as to estimate the distributions of meadow-associated species was deemed circular. Despite using a simple classification method, our meadow map (Fig. 2.2A) aligns well with existing larger-scale vegetation maps, and adequately captures meadow extents for field-accessible sites (*pers. obs.*). All of the computation involved in meadow mapping was performed in GRASS GIS (Version 7.0.5)[130].

B.2 Interpolating Snow Disappearance

We measured the disappearance of seasonal snowpack at Mt. Rainier by examining daily variation in soil surface temperatures measured using Thermochron iButton or Onset HOBO pendant temperature loggers installed at 520 sites across Mt. Rainier National Park. These sensors, recording temperature every 2-4 hours, can accurately pinpoint the timing of snow disappearance because the soil surface in the study area stays at a thermal equilibrium near 0°C in the ablation season when the sensors are covered by even a few inches of insulating snow[142]. We defined the snow disappearance date (SDD) as the day of year after the last day that average soil temperatures were between -2 and 2°C and the diurnal range in soil surface temperature was less than 1°C. All time-series of measurements were visually inspected to ensure that the selected threshold produced reliable estimates. We extrapolated point estimates of SDD to the landscape scale using topographic and vegetation structure covariates and a Generalized Additive Mixed Model (GAMM) fit with the R package GAMM4[183]. The best-fitting model explained over 90% of the variation in SDD in our dataset, and had an average absolute error on held-out data of 8.3 days. Despite the good fit, a visual assessment of the residual variogram indicated that the prediction was too spatially smooth: small-scale spatial autocorrelation remained in model residuals over distances <45 m. Because our estimates of intra-specific phenological mismatch might be sensitive to small-scale heterogeneity in climatic drivers (Fig. C.1A), we fit an exponential variogram model to the residuals of the GAMM using the *R* package *gstat* and then used that fit model to produce a kriging prediction with spatially autocorrelated noise using Gaussian geostatistical simulation[39] (Fig. C.1B). Adding the spatially autocorrelated noise to the GAMM prediction of SDD produced maps that accurately reproduce overall spatial patterns driven by topographic and vegetation heterogeneity as well as small-scale heterogeneity associated with unmeasured features of the environment (Fig. B.1C).

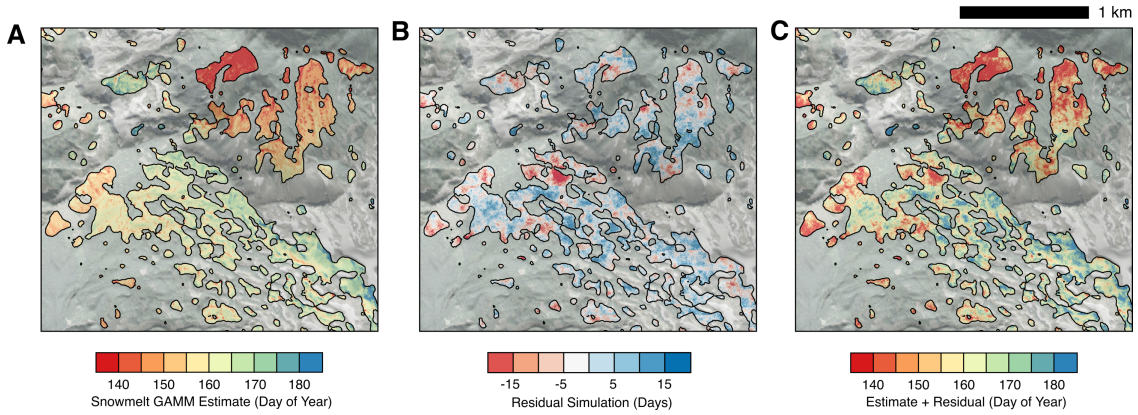

Figure B.1: Predicted snow disappearance day (SDD) in the vicinity of Spray Park in 2015. **A** GAMM Prediction. **B** Geostatistical simulation of kriged residuals. **C** Final prediction of SDD used for analysis of intraspecific phenological mismatch.

B.3 Interpolating Air Temperature Microclimates

We measured air temperature microclimates at 8 weather stations and 111 other sites distributed throughout Mt. Rainier National Park that we instrumented with Thermochron iButton or Onset HOBO data logging temperature sensors. Sensors were hung from conifer trees at 3-5 m above the ground (above the level of the seasonal snowpack), and recorded air temperature every two hours on odd hours (i.e. 1pm). Sensors were placed under 5cm diameter inverted white plastic funnels, and were situated so that they received radiation shielding from conifer branches both above and below the sensor. This technique has been shown to produce measurements indistinguishable from sensors outfitted with more elaborate radiation shields[111]. Because our phenology model relied on a measure of seasonal warmth accumulation derived from daily air temperature data, we produced geostatistical estimates of daily average air temperatures for each day of the growing season (April 1st - October 31st) from 2009 to 2015. We produced these maps using a three stage procedure based on Bayesian regression kriging[179]. First, we used topographic and vegetation structure covariates to predict the linear relationship (slope and intercept) that links daily local conditions recorded at the microclimate sensor location to regional average conditions, cal-

culated as the mean of 4km-resolution PRISM[43] data within 50km of the boundary of Mt. Rainier National Park. Because the local microclimate measurements were centered to have a mean of zero, the intercept of this relationship represents how cold or warm a local site is on a typical day relative to the seasonal average, and the slope represents how sensitive conditions at a site are to changes in the regional average. We allowed these relationships, and our geostatistical predictions of the coefficients linking local and regional temperatures, to vary seasonally by separately estimating these quantities for each site in each season (DJF, MAM, JJA, SON), and then extrapolating them across the landscape using GAMMs with structures similar to those used to estimate SDD. The regional PRISM daily time-series was then combined with the GAMM estimates of the local-regional temperature relationship to derive high-resolution gridded estimates of expected temperatures for each day. Residual variation from each site was approximately zero-centered and showed dramatically reduced temporal autocorrelation and much smoother patterns of spatial autocorrelation than the raw data. Finally, we interpolated geographic patterns of daily residual temperature variation using Bayesian kriging. This spatial model, fit with the `SpLM` function in the *R* package textttSpBayes[65], incorporated elevation, latitude, and longitude as predictors of the daily trend, and had an exponential covariance function. We chose a Bayesian approach here instead of traditional kriging because some days had relatively few measurements, which caused a traditional Kriging estimator to perform poorly, a behavior that could be minimized in the Bayesian analysis by imposing a mildly informative prior on the parameters defining the covariance function ($\phi \sim Unif(0.1, 300)$,$\sigma^2 \sim IG(2, 2)$,$\tau^2 \sim IG(2, 0.1)$). Our geostatistical estimates of daily microclimate perform well when measured against data held-out for testing (RMSE 0.74°C, Fig. B.2). Finally, we used these daily high-resolution grids of average air temperature to compute temperature sums (the sum of temperatures above 0°C) in the 50 days after snow disappeared at each 3m raster cell located in the subalpine zone.

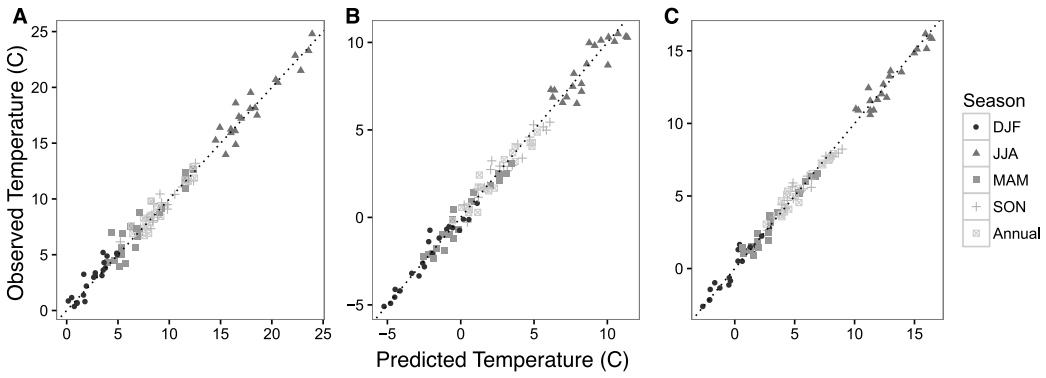

Figure B.2: Comparison between observed and geostatistically modeled air temperatures for 20 sites where data was withheld from model fitting. **A** Average daily maximum temperatures. **B** Average daily minimum temperatures. **C** Average daily temperatures.

B.4 Validating Landscape Phenology

In order to independently validate our meadow-scale estimates of flowering phenology, we compared our predictions to observations of flowering made by volunteers in a citizen science program (MeadoWatch, http://www.meadowatch.org) that we have operated at Mt. Rainier since 2013. MeadoWatch volunteers collected observations at 24 sites distributed across two areas of Mt. Rainier National Park, Mazama Ridge, located on the southwestern slope of Mt. Rainier, and Glacier Basin, located 5km northeast of the summit, where monitoring was initiated in 2015. For each species (8 of 16) and year (2013-2015) in which we had both meadow-scale model predictions and citizen-science observations, we calculated the proportion of volunteer observations indicating open flowers that fell within the interval that spans 80% of the highest predicted area in flower for meadows within 300 m of the monitoring plots. We considered this agreement good if $> 95\%$ of the volunteer observations fell within this interval (Fig. B.3)

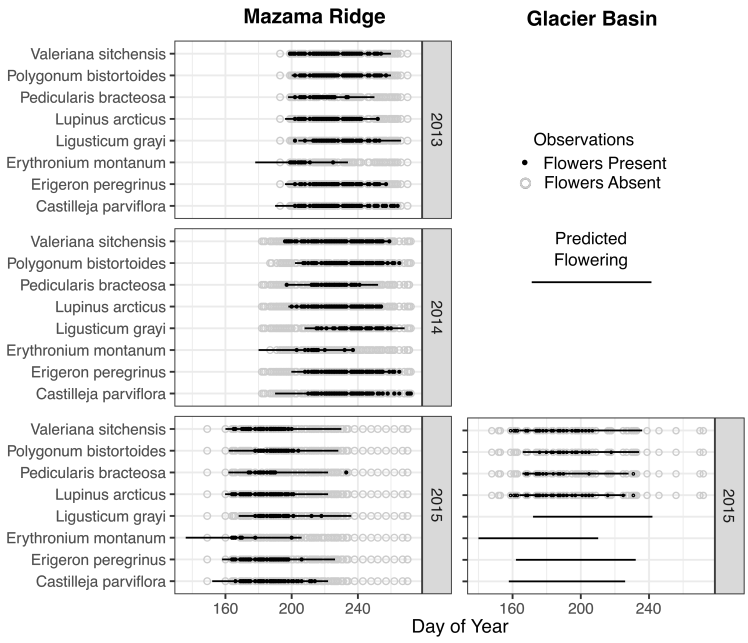

Figure B.3: Comparison between meadow-scale predictions of flowering phenology and MeadoWatch citizen scientist observations collected between 2013 and 2015. Black line represents the period containing 80% of the total flowering area for each species in meadows within 300 m of the MeadoWatch sites. Closed black circles represent volunteer observations of flowering, and grey open circles represent observations without flowering.

Appendix C

SUPPLEMENTARY MATERIAL FOR CHAPTER 3

C.1 Supplementary Figures and Tables

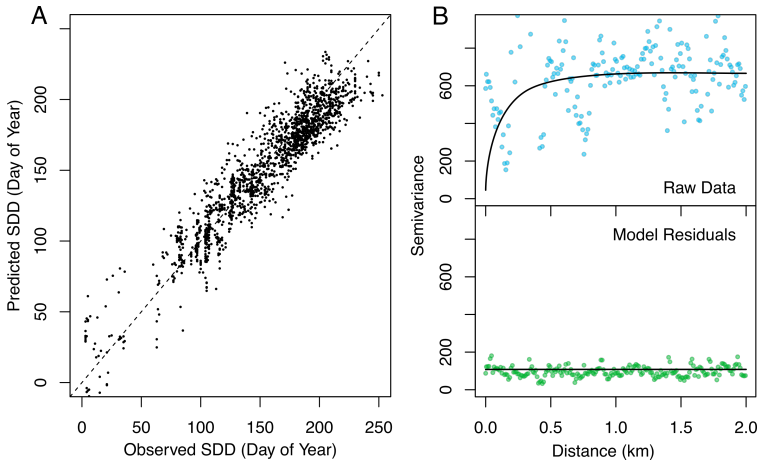

Figure C.1: **A**. Observed vs. predicted values for the statistical model of snow disappearance day (SDD) that was used as a predictor of wildflower and visitor phenology. Predictions use only the fixed effects from the model. Dotted line is the 1:1 line. **B**. Empirical semivariograms of the binned raw data (top) and model residuals (bottom) demonstrating that the model adequately deals with spatial autocorrelation in SDD. Distance bins were 50 m wide. Solid lines are spherical spatial covariance models fit with the function `variofit` in the *R* package `geoR`.

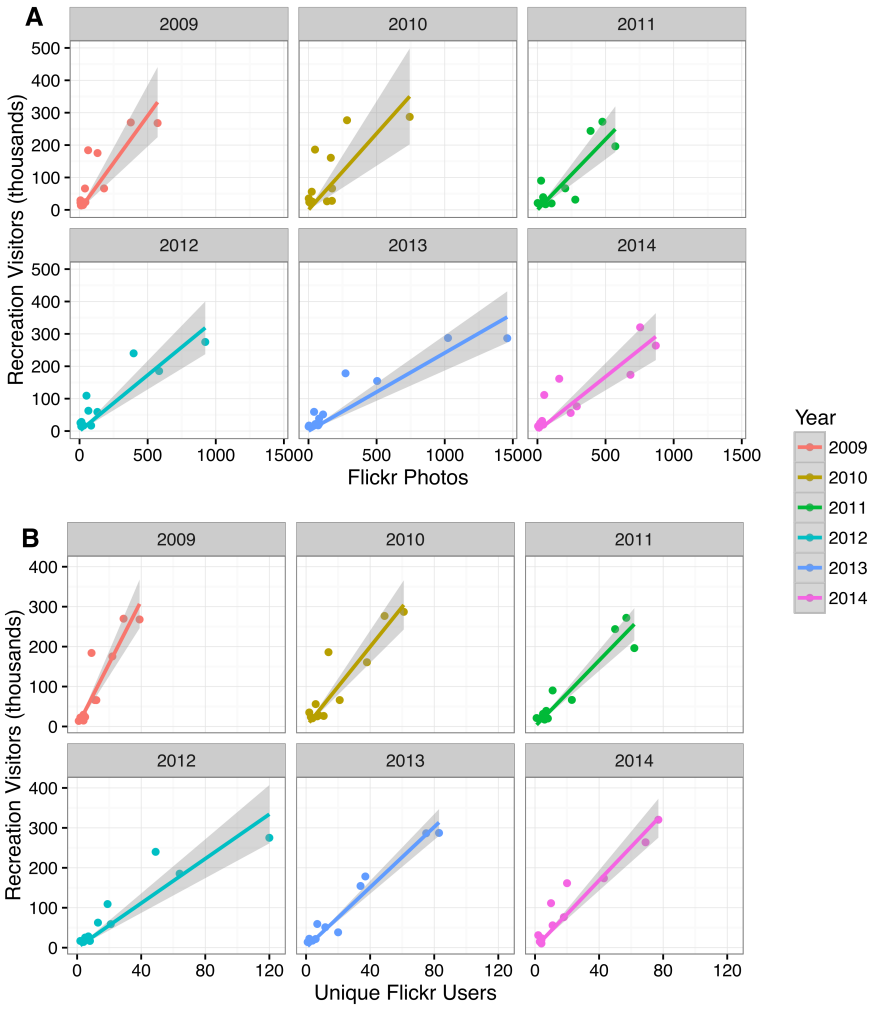

Figure C.2: The number of Flickr photos (**A**) and unique users (**B**) is strongly related to the number of recreation visitors recorded monthly at Mt. Rainier National Park. A linear model with the number of Flickr photos and year (lines) explains 84% of the variation in NPS monthly recreation visitor counts. A linear model using the number of unique users (**B**) and year explains 93% of the variation in recreation visitors recorded at the gates. NPS visitor data from 2015 was not available at the time of preparation. Data was downloaded on November 5th, 2015 from (https://irma.nps.gov/Stats/Reports/Park/MORA).

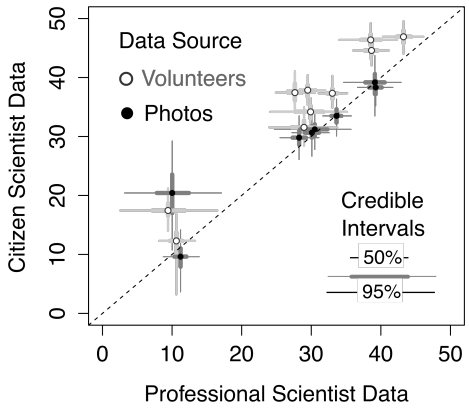

Figure C.3: Both citizen-science volunteer observations (gray) and crowd-sourced data from photos (black) provide reliable estimates of the timing of peak flowering for the 10 focal species. The two data sources where compared to structured observations of phenology by professional scientists in 70 1 m^2 quadrats in the vicinity of Paradise. Parameters shown are derived from data in 2013. The X and Y axes in the figure represent days since snow disappearance. Figure modified from [180].

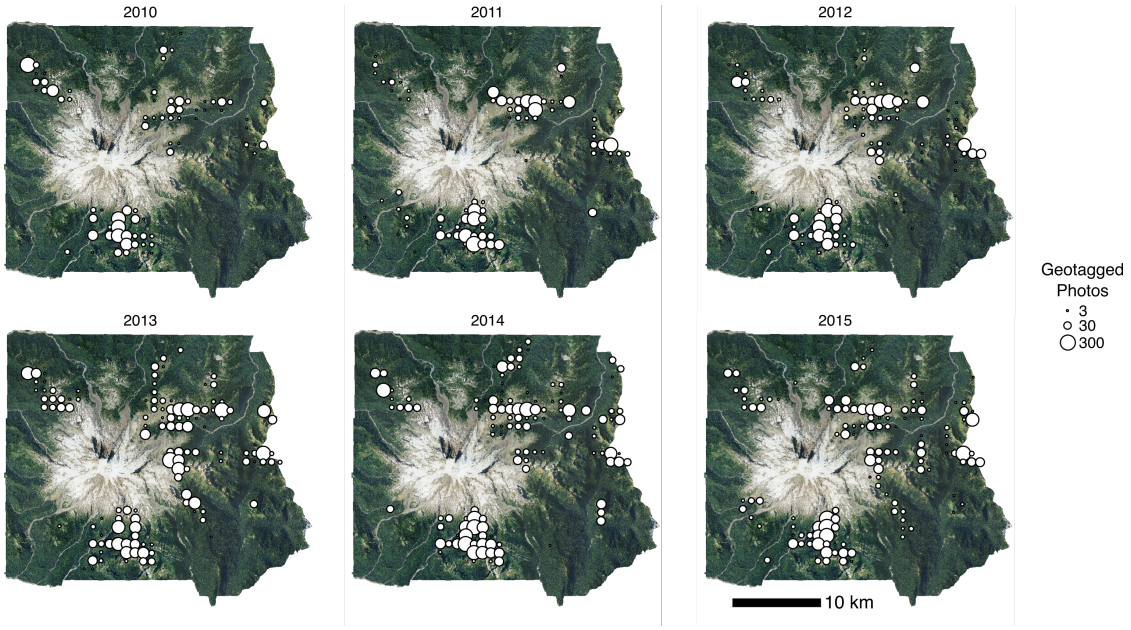

Figure C.4: Maps showing the spatial distribution of Flickr photos used in this analysis in each year from 2010 to 2015. Photos where accurately geotagged, and from locations between 1200 and 2400 m elevation. The size of the symbol is proportional to the number of photos in 500 m resolution spatial bins.

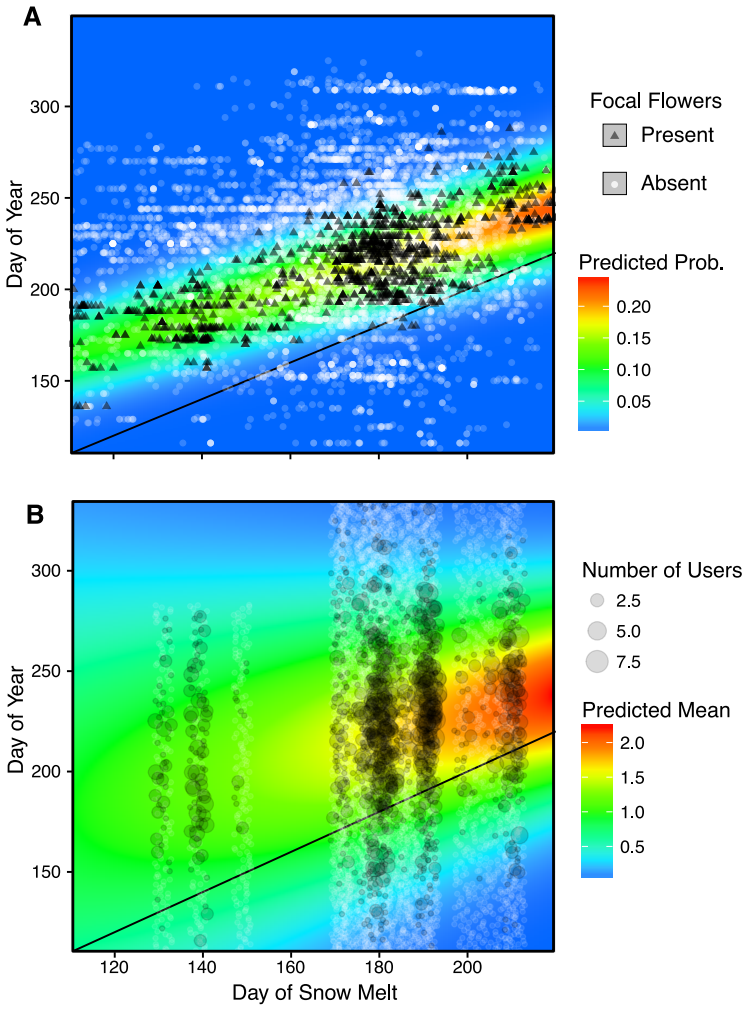

Figure C.5: Data and fit curves from the best aggregate visitor phenology model (**A**) and wildflower phenology model (**B**). In A., black triangles represent photos that contain recognizable flowers of at least 1 focal species, and white circles represent photos without focal species. The colored background represents the fit probability of at least one focal species being present in a photo. In B., circle size represents the number of unique Flickr users on each day of the study, with days where there are no users uploading photos represented as white circles. The colored background represents the predicted mean number of Flickr users uploading photos.

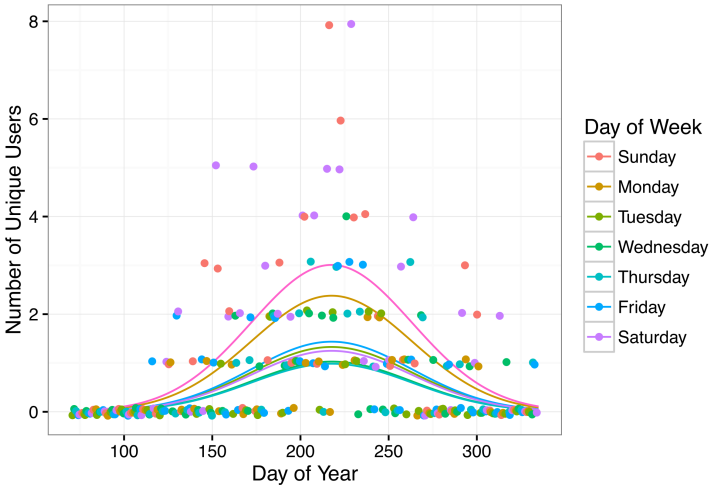

Figure C.6: Scatter plot of unique Flickr users by day of year, and day of the week for subalpine sites in the vicinity of Paradise in 2013. Lines represent median predictions for Paradise from model V4 (Table C.3).

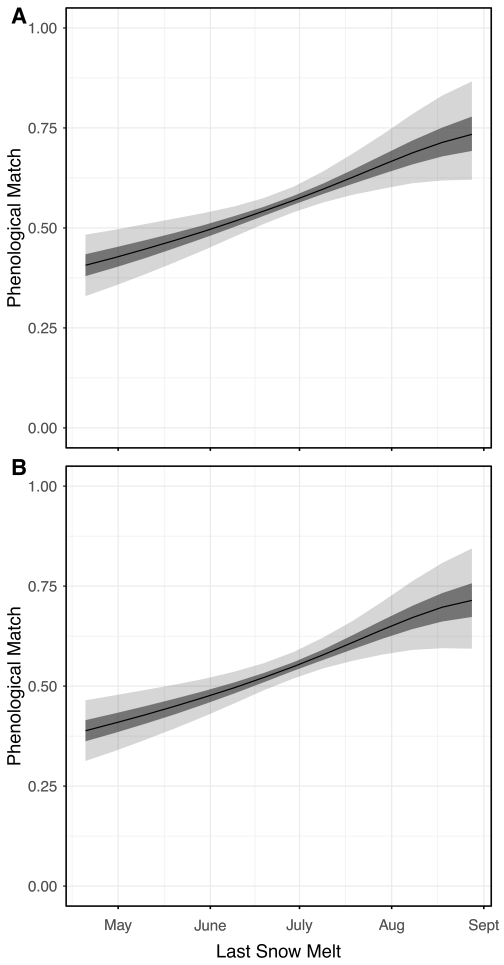

Figure C.7: Phenological match as a function of snow melt when the most common wildflower species (arctic lupine) is excluded from the dataset (**A**) and when assumed snow model errors are doubled from their estimated values (**B**).

Table C.1: Parameter estimates from the mixed-effects model used to predict snow melt date. Parameter confidence intervals were computed with a parametric bootstrap procedure implemented in the function `bootMer` in the *R* package `lme4`. Coordinates are in the reference system NAD83 UTM Zone 10N.

Predictor	Predictor Unit	Estimate	Lower 95%c.i.	Upper 95% c.i.
Predictor	Predictor Unit	Estimate	Lower 95% c.i.	Upper 95% c.i.
Intercept	unitless	63.581	-328.171	449.74
Elevation	meters	0.1648	0.0915	0.2393
Year 2010	factor	429.001	111.484	793.695
Year 2011	factor	-126.634	-435.71	200.334
Year 2012	factor	-77.335	-378.308	253.158
Year 2013	factor	181.759	-125.708	508.063
Year 2014	factor	120.653	-207.57	456.08
Year 2015	factor	876.564	545.96	1212.064
Elevation	meters	-4.24E-05	-7.02E-05	-1.65E-05
UTM Easting (NAD Zone 10N)	km	-0.058	-0.693	0.596
Canopy Cover	Proportion	-6.061	-8.057	-4.149
Slope	Degrees	-0.399	-0.51	-0.284
Relative Elevation (30m window)	Elev. ASL (m)	10.246	7.509	13.118
Average daily solar Radiation	Wh/m2	-0.522	-0.8985	-0.1321
Elevation:Year 2010	meters	-0.0676	-0.1376	0.0005
Elevation:Year 2011	meters	0.068	0.007	0.1266
Elevation:Year 2012	meters	0.0333	-0.027	0.0912
Elevation:Year 2013	meters	-0.035	-0.0938	0.023
Elevation:Year 2014	meters	0.0178	-0.0431	0.0759
Elevation:Year 2015	meters	0.0779	0.0155	0.1375
Elevation2: Year 2010	meters	3.87E-05	1.15E-05	6.63E-05
Elevation2: Year 2011	meters	-1.31E-05	-3.61E-05	1.00E-05
Elevation2: Year 2012	meters	-2.73E-06	-2.43E-05	2.05E-05
Elevation2: Year 2013	meters	1.80E-05	-3.22E-06	4.10E-05
Elevation2: Year 2014	meters	5.98E-06	-1.56E-05	2.95E-05
Elevation2: Year 2015	meters	-1.34E-05	-3.52E-05	1.02E-05
UTM Easting : Water Year 2010	km	-0.6908	-1.2907	-0.1832
UTM Easting : Water Year 2011	km	0.1364	-0.4006	0.6584
UTM Easting : Water Year 2012	km	0.0701	-0.4815	0.5736
UTM Easting : Water Year 2013	km	-0.2876	-0.8227	0.207
UTM Easting : Water Year 2014	km	-0.2766	-0.8573	0.2669
UTM Easting : Water Year 2015	km)	-1.6902	-2.23	-1.1741
Elevation : Relative Elevation	Elev. ASL (m)	-0.0078	-0.0094	-0.0063

Table C.2: Focal wildflower species identified in crowd-sourced photos.

Species	Taxonomic Reference	# Flower Photos
Anemone occidentalis	S. Watson	73
Castilleja parviflora	Bong.	453
Erigeron peregrinus	Banks ex Pursh	290
Erythronium montanum	S. Watson	103
Ligusticum grayi	J.M. Coult. & Rose	99
Lupinus arcticus	S. Watson	868
Nothocalais alpestris	(A. Gray) K.L. Chambers	23
Pedicularis bracteosa var. latifolia	(Pennell) Cronquist	71
Polygonum bistortoides	(Pursh) Small	449
Valeriana sitchensis	Bong.	323
No focal species	-	13530
Total Photos	-	17403

Table C.3: Model selection for visitor and wildflower models

Wildflower Models

Model	Form	DIC	Delta-DIC
W1	Common opt, width, height, parameters	-17704	166
W2	Common opt, width, site-specific height intercept.	-17830	39
W3	Common width, site-specific opt and height intercept.	-17821	48
W4	Site-specific width, opt, and height intercept.	-17812	57
W5	Site-specific width, opt, and height intercept. Side-specific opt slope (east vs. west slope).	-17869	-

Visitor Models

Model	Form	DIC	Delta-DIC
V1	Common opt, width, height, parameters	4713	1016
V2	Common opt and width intercepts and slopes, site- and year-specific height intercept.	5729	101
V3	Common width intercepts and slopes, year and site-specific opt and height intercept.	5612	4
V4	Site-specific width, opt, and height intercept. Access-specific opt slope.	5608	-

Table C.4: Estimated parameters for visitor and wildflower models used in the aggregate analysis.

	Wildflower model (W2)		
Parameter	Estimate	Lower 95% c.i.	Upper 95% c.i.
Height Intercept	0.05	-0.806	0.77
Height Slope	3.064	2.576	3.583
Opt Intercept	0.322	0.304	0.339
Opt Slope	0.659	0.603	0.716
Width Intercept	2.638	2.525	2.745
	Visitor Model (V2)		
Parameter	Estimate	Lower 95% c.i.	Upper 95% c.i.
Height Intercept	0.453	0.056	0.824
Height Slope	0.494	-0.485	1.381
Opt Intercept	0.276	0.249	0.302
Opt Slope	0.491	0.348	0.638
Width Intercept	1.095	0.967	1.236
Width Slope	0.312	0.914	1.624